Empennage Wake Filling using Steady Chord-wise Blowing for Propulsive Fuselage Concept

APPU Configuration

S. Garg

Technische Universiteit Delft

TU Delft Delft University of Technology

Challenge the future

EMPENNAGE WAKE FILLING USING STEADY CHORD-WISE BLOWING FOR PROPULSIVE FUSELAGE CONCEPT

APPU CONFIGURATION

by

S. Garg

in partial fulfillment of the requirements for the degree of

Master of Science
in Aerospace Engineering(Flight Performance and Propulsion)

at the Delft University of Technology,
to be defended publicly on Thursday April 14, 2022 at 09:15 AM.

Student number:	5061326	
Supervisor:	Prof. dr. ir. L.L.M. (Leo) Veldhuis	
	Ir. Martijn van Sluis, PhD.	
Thesis committee:	Prof. dr. ir. L.L.M. (Leo) Veldhuis,	Chair
	Dr. ir. A. (Arvind) Gangoli Rao,	Examiner
	Dr. ir. AH. (Alexander) van Zuijlen,	Examiner

An electronic version of this thesis is available at http://repository.tudelft.nl/.

TU Delft Delft University of Technology

APPU Auxiliary Propulsion and Power Unit

ABSTRACT

Aviation is a growing industry and contributes to 5% of the total anthropogenic emissions causing global warming. It is the need of the hour to focus research and development towards curbing these emission. Technological advancements in efficient airframe, engines and new energy sources are one way to go in order to limit the emissions from the aviation industry. Boundary layer Ingesting(BLI) propellers for development of propulsive fuselage concept(PFC) aircraft is one such technological investment aimed at reducing the fuel flow and achieving a higher propulsive efficiency. This forms the basis for the APPU project(Advanced Propulsion and Power Unit) which aims towards utilizing hydrogen as an alternative energy source in order to power an auxiliary propulsion system, in form of a BLI propeller, attached on the aft fuselage behind the empennage in pusher configuration. However, the concept is not without its challenges. Operating a propeller in the wake of the empennage leads to unsteady blade loading which is detrimental to the propeller, specifically in terms of noise penalties. Empennage wake mitigation using flow control technique like chord-wise wake blowing to fill the empennage wake, is one potential solution for this problem.

It is the aim of this research to provide an insight into the proficiency of chord-wise wake blowing system in filling the empennage wake in order to mitigate the detrimental effects of the wake on the inflow of the aft mounted BLI propeller. A geometry, with a fuselage and vertical tail combination, was used in 3D RANS simulations to achieve this goal. Wake blowing system was analysed for two configurations, fan-off and fan-on, where the difference is the respective absence and presence of a propeller which is modeled as an actuator disk.

Empennage wake measurements showed that using the empennage wake blowing system, an almost 100% mitigation of the velocity deficit could be achieved, within the confines of the chosen mesh and solver. For the right combination of blowing slot height and the blowing momentum coefficient, a near complete wake filling was observed for both fan-off and fan-on configurations as compared to the unblown configuration. The slot height of h_{slot}/c = 0.001 and a blowing momentum coefficient of C_μ = 0.012 for a propeller inflow plane located almost 1m behind the empennage-fuselage trailing edge junction yielded a wake uniformity coefficient(W) of 0.997. Meaning a 99.7% uniformity was achieved in the velocity profiles for the filled empennage wake. The chosen wake blowing system parameters provided good amount of mixing of the blown jet with the low momentum boundary layer and yielded close to none secondary minimas in the wake velocity profiles. The uniformity achieved at the propeller inflow was reciprocated in the total pressure coefficient and dynamic pressure loading plots. However, it was found out that a complete filling of the wake might not be desirable for a uniform dynamic pressure loading of a blade section going around the propeller plane. A complete filling of the empennage wake leads to an overshoot in the dynamic pressure loading of the 0.75R propeller section at the 90° azimuth which is located right behind the empennage.

The wake blowing system had some negative impact on the inflow angles obtained at the propeller inflow plane, specifically towards the upper fuselage section near the hub where angles up to ±6° were introduced. On the other hand, fan-on configuration showed a favorable effect due to the propeller by reducing the inflow angles at the hub region towards the lower fuselage. The drag analysis of the system showed that the addition to the overall aircraft drag due to the wake blowing system was less than 4 drag counts and was largely contributed by the viscous drag component. Finally a mass flow rate analysis of the wake blowing system showed that a mass flow rate of 1.82-2.46Kg/s would be needed in blown cases depending on the blowing slot height. This is a point of consideration that needs to be addressed in future research since this requirement will be difficult to meet with the engine bleed and thus requires alternative solutions.

PREFACE

This thesis is part of the graduation project to fulfil the requirements for the MSc degree for the Flight Performance and Propulsion Track(FPP) in Aerospace Engineering at Delft University of Technology. The past year involved a lot of hard work and patience which has finally resulted in this report, to which I can look back with joy and a sense of achievement. Now, I would like to take the time to express my gratitude to the people without whose support and guidance this achievement would not have been possible.

First, I would like to thank Leo, who's constant support, guidance and unparalleled critical analysis skills have helped me to ask the right questions to reach my final goal. I would like to thank Martijn, for his guidance through all the phases of my thesis, from problems with meshing to discussion on interesting results. I express my gratitude to Arvind and Alexander for accepting to be a part of the graduation committee. I would also like to thank Tomas, George and the rest of the Propeller Research Group for their immensely valuable feedback and suggestions.

Also, I would like to express my gratitude to the academic counsellor, Yinneke, for her time and patience through the troubled times of my studies. I thank the ICT tech support for their quick action in resolving the hardware and software related issues.
A big part of my masters has been the groups and teams that I have been a part of. So, to my colleagues who I worked with in JIP, AeroDelft, Master Mentor group and AWEP Society, I thank you for the invaluable experiences and knowledge I gained from working with you.

They say a man is rich if he has many friends. Well, I feel like the richest person on earth. I would like to extend my gratitude to all my friends, old and new, for their encouraging words and laughs that made this journey fun. My special thanks to Antony, whose help and support in the past couple of months have played a big role in the completion of my masters. Also, to Francisco, Ravi, Vivek and the 'Desis', I would like to thank you for being my family away from home. A special mention to my friend Corona, for teaching me patience and the immense value of plans B to Z.

Lastly, and most importantly, I would like to 'namaskar' my parents and my sister for their blessings, love, patience and support. I would not be here without them. My family would not be complete without the mention of the newest addition, my niece Ivy, meeting whom has been the best and biggest motivation I have ever had for a task.

S. Garg
Delft, April 2022

CONTENTS

NOMENCLATURE

LIST OF SYMBOLS

Symbol	Name	Unit
$c_{\dot{m}}$	Blowing coefficient	[-]
h_{slot}	Blowing slot height	m
v_j	Blown flow velocity through the jet	m/s
F	Body forces	N
ρ	Density of fluid	Kg/m^3
C_D	Drag coefficient	[-]
C_q	Dynamic pressure coefficient	[-]
M_{a_∞}	Far-field mach number	[-]
V_∞, U_∞	Freestream velocity	m/s
u_τ	Friction velocity	m/s
η_p	Froude propulsive efficiency	[-]
m	Harmonic number	m
n	Harmonic number in the frequency domain	[-]
Q	Heat energy	J
ϕ	Inflow angles	degrees
e	Internal energy per unit mass	J/Kg
κ, B	Karman constants	[-]
C_L	Lift coefficient	[-]
U_e	Local undisturbed velocity	m/s
$\dot{m}$	Mass flow rate through the propulsor	Kg/s
P_k	Mechanical energy inflow rate	W
P_M	Mechanical power	W
U_{min}, U_{max}	Minimum and maximum wake velocities	m/s
μ	Molecular viscosity	Ns/m^2
B	Number of blades	[-]
$W_{\dot{h}}$	Potential energy inflow rate	W
P_{loss}	Power loss	W
p	Pressure	Pa
P_v	Pressure-volume power	W
$\dot{E}_p$	Pressure-work deposition rate	W
J	Propeller advance ratio	[-]
c	Pylon chord	n
W	Pylon wake uniformity criterion	m/s
P_s	Shaft power	N/s
C_μ	Blowing Momentum Coefficient	[-]
$\dot{E}_a$	Streamwise kinetic energy deposition rate	W
k	Therman conductivity	W/m K
T	Thrust	N

Symbol	Name	Unit
C_T	Thrust Coefficient	[-]
C_{P_T}	Total Pressure Coefficient	[-]
$\dot{E}_v$	Transverse kinetic energy deposition rate	W
ΔV	Velocity increase in the streamtube	m/s
u'	Velocity Perturbation	m/s
ψ	Viscous dissipation rate	W
l_v	Viscous Length Scale	m
τ	Viscous Stress Tensor	N/m^2
t_v	Viscous Time Scale	s
k	Wave number	[-]
y^+	Wall Units	[-]
$\dot{E_w}$	Wave-pressure work	W
A_r	Wake Area Ratio	[-]
W	Wake Uniformity Coefficient	[-]
δ	Wake Velocity Deviation Coefficient	[-]

LIST OF ACRONYMS

ACARE Advisory Council for Aeronautics Research in Europe

AFC Aft Fuselage Configuration

APPU Auxiliary Propulsion and Power Unit

ATAG Air Transport Action Group

BLI Boundary Layer Ingestion

BPF Blade Passing Frequency

BPR By-Pass Ratio

BWB Blended Wing Body

CAD Computer Aided Design

CFD Computational Fluid Dynamics

CV Control Volume

DLR German Aerospace Centre

DNS Direct Numerical Simulation

DNW German-Dutch Wind Tunnels

ERA Environmentally Responsible Aviation project

FAA Federal Aviation Administration

FSP Free-stream Propeller

IATA International Air Transport Association

K.E. Kinetic Energy

LES Large Eddy Simulations

LEVM Linear Eddy Viscosity Models

LLF Large Low-Speed Facility

MAC Mean Aerodynamic Chord

NACRE New Aircraft Concepts REsearch

NASA National Aeronautics and Space Administration

PBM Power Balance Method

PFC Propulsive Fuselage Concept

QWA Quantitative Wake Analysis

RANS Reynolds Averaged Navier Stokes equations

SFW Subsonic Fixed Wing

SPL Sound Pressure Level

UN United Nations

VTP Vertical Tail Plane

List of Figures

List of Tables

1

INTRODUCTION

Sustainable aviation has become a necessity due to the growing concern about the environmental impact of aviation in general. Emissions like CO_2, CO, NO_x, soot and unburnt hydrocarbons, that come from the combustion of kerosene, are major contributors towards the global issue of climate change[20]. Currently, aviation is responsible for about 5% of the total anthropogenic emissions causing global warming[20]. It is estimated that by 2050 aviation would become one of the most used mode of transportation(in terms of passenger-km)[1], second only to automobiles, as shown in Figure 1.1

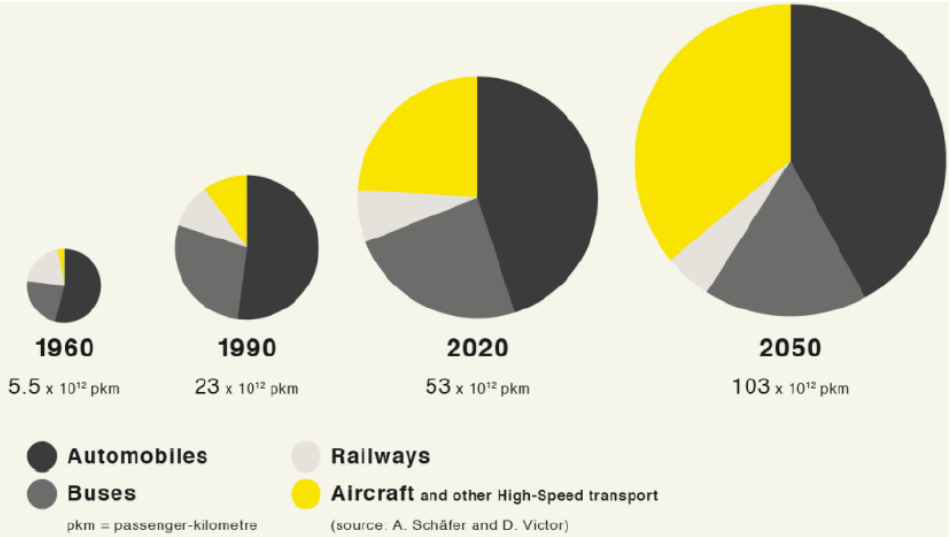

Figure 1.1: Growth of aviation industry and projected estimate for 2050(in passenger-km)[1]

UN's Glasgow Climate Change Summit reaffirmed the necessity to act towards achieving carbon neutrality by 2050[21]. The goal was first established as part of the Paris Agreement which was signed in December of 2015 to keep the global temperature rise of this century below 2^oC and strive to even further restrict it to 1.5^oC[22]. In an attempt to deal with impact of climate change and reduce green house gas(GHG) emission, organizations like NASA, IATA, ATAG and ACARE have adopted climate resilient pathways. Consequently, FlightPath 2050 goals were established by ACARE to motivate revolutionary technological solutions and enhance sustainable energy supplies. These goals include a 75% reduction in CO_2 emissions per passenger kilometer, a 90% decrease in NO_x and a 65% reduction in perceived noise emissions, all relative to a typical aircraft from the year 2000[23]. In order to achieve the emission goals by 2050, the design and development of new aircraft needs to start now due to the fact that developing a new aircraft requires time of up to 15 years to realise[2].

Technological advancements are an important part of the mission to achieve emissions reduction. One of the pillars of the four pillar strategy laid out by IATA stresses on technological investments into more efficient

airframe, engines and equipment, sustainable biofuels and new energy sources[2]. The projected emissions trend for the next 30 years, keeping mind the effects of technological developments on carbon emissions, is shown in Figure 1.2. It is clear that not taking any action is not a choice if a sustainable future for the environment and for aviation, is to be achieved.

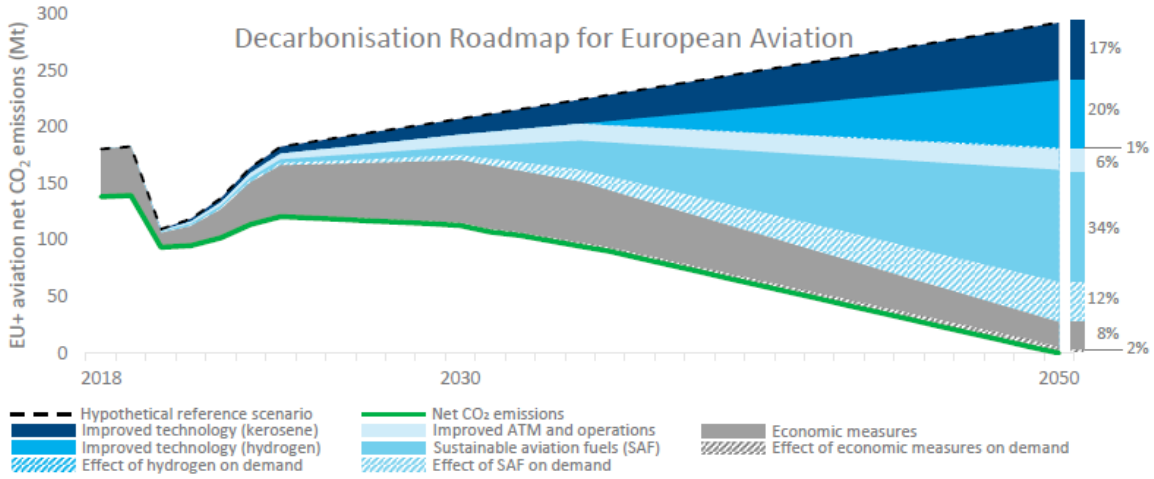

Figure 1.2: CO_2 Emission projections up to 2050 corresponding to different measures which could help in achieving carbon neutral growth in aviation[2]

One such potential technological advancement is the use of boundary layer ingesting(BLI) propellers in development of propulsive fuselage concepts(PFC). Boundary Layer Ingestion is an integrated propulsion concept in which a propulsor operates in a boundary layer flow instead of the freestream flow. The intention behind this is to reduce the fuel flow for a given operating condition by utilizing the lower speed inflow. It is seen as an alternative to increasing the BPR of a propulsor in order to get a higher propulsive efficiency. The propulsive efficiency for BLI propellers will be discussed in more detail in chapter 2.

BLI is not a new concept. Past works account for effects of BLI on aspects such as noise reduction, weight saving and increasing fuel efficiency[24, 25]. All of these being relevant for emissions reduction. Increasing propulsive efficiency by using the slower moving boundary layer is a common study in the field of marine propulsion. For aircraft propulsion, BLI appears less beneficial since the wake is spread more by the wings and due to the reduced density and total pressure properties of air compared to water[26]. However, it has been researched that BLI can reduce the fuel consumption in cruise by up to 10%[24].

In a step towards achieving sustainable aviation, a joint initiative between SAFRAN group, Airbus and Delft University of Technology was setup where one of the objectives is to utilize the benefits of BLI propellers. This initiative is called Project APPU(Advanced Propulsion and Power Unit). A schematic of the proposed APPU configuration is presented in Figure 1.3.

The aim of the APPU project is to accelerate the utilization of an “Energy Mix” in aviation by using hydrogen as an alternative energy source in order to power an auxiliary propulsion system, in form of an open BLI propeller, attached on the aft fuselage behind the empennage in pusher configuration. This concept is proposed to reduce the aircraft’s CO2 emissions in cruise conditions by 20% and the emissions of air pollutants during take-off and landing by half[27]. Hydrogen would be used to drive the BLI propulsion unit located at the aft fuselage. Thus, providing at least 10-15% of required thrust in all phases and enabling emission optimisation of the entire mission. As mentioned, the blend of BLI with a hydrogen powered unit is a novel approach with the potential to reduce the CO_2 emission by around 20% and make a major impact in reduction of local airport emissions. Due to the possibility of the propulsion unit being incorporated in the existing aircraft architecture, the enter into service time for APPU concept is reduced. This is expected to act as a stepping stone towards a CO_2 neutral aviation industry for the future.

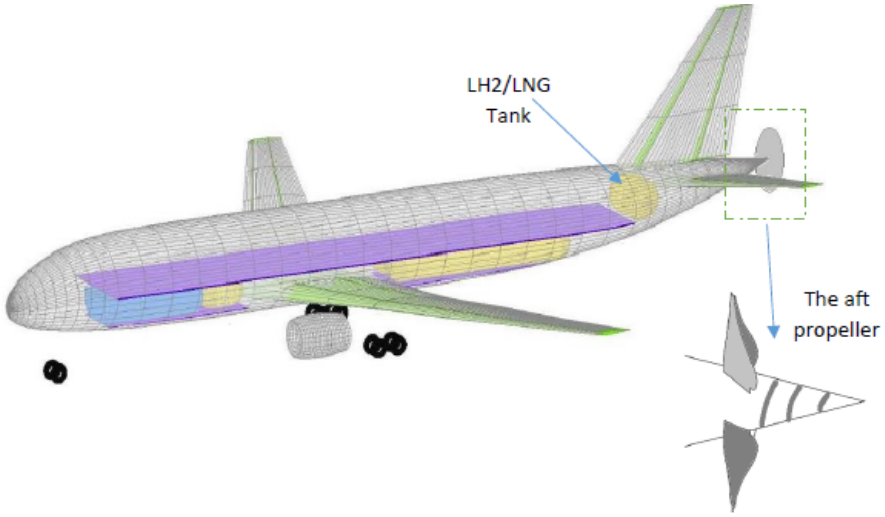

Figure 1.3: Schematic for the proposed APPU concept involving a propulsive fuselage using a BLI propeller, for a single aisle aircraft like A320 family [3].

Although, the benefits of boundary layer ingestion are well established, its use in PFCs is not without limitations. Studies show that the presence of an upstream body leads to detrimental effect on the BLI propeller's performance in terms of noise and efficiency[12]. Especially for BLI concepts involving open rotors, the absence of a shroud leads to greater tonal noise penalties as compared to turbofan engines due to the fact that the nacelle in a turbofan engine shields the blade tonal noise emissions. Advancements in open rotor technology have led to acceptably quieter open rotor engines, however, they still fall behind when compared to turbofan engines. The broadband noise that creeps in due to installation of the propeller, is also becoming more and more important as its dominance increases when the tonal noise is reduced[28–31].

Similar challenges will be faced by the BLI propeller in the APPU configuration despite its benefits in fuel burn reduction. Since the BLI propeller will be installed behind the empennage the interaction of the empennage wake with the downstream propeller will lead to detrimental effects on propeller noise performance[12]. The wake flow behind the empennage impinges on the on the BLI propeller leading to unsteady blade loading. This can lead to higher tonal noise penalties [28, 29, 32–35]. Figure 1.4 gives a representation of the empennage wake profile. It can be seen how the velocity deficit in turn will lead to a non uniform blade loading. Recovering this velocity deficit is the main solution which can help in alleviating these detrimental effects.

One possible way to reduce the detrimental effects of the upstream empennage can be to employ the flow control technique of wake blowing for filling the wake of the empennage[36]. Wake blowing, as an active technique, shows potential in reducing the detrimental effects of empennage-propulsor interaction, based on the studies in literature on pylon-propulsor interactions[8, 35]. Out of the different wake blowing techniques(see chapter 2), chord-wise blowing of air at the empennage surface along the airfoil chord provides a more uniform post blowing wake velocity profile. This is due to the fact that the blown flow has a longer length to merge and settle to the external flow conditions[16].

To that end, the purpose of this thesis is to study the affect of chord-wise blowing in filling the empennage wake in order to provide a more uniform loading for the aft propeller. This will potentially reduce the noise penalties that arise due to the non uniformity of the propeller inflow and also have a positive effect on the propulsive efficiency of the propeller. To give a clear idea of how the air will be blown chord-wise along the empennage surface to fill the empennage wake ahead of the BLI propeller, a conceptual description is shown in Figure 1.5.

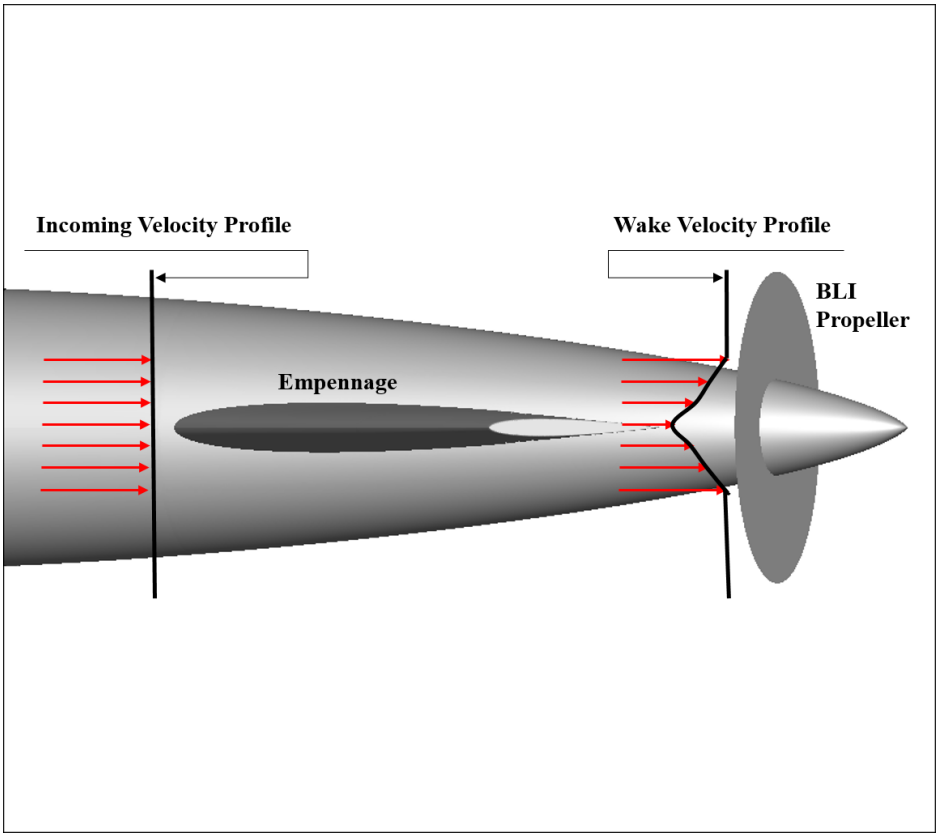

Figure 1.4: Change in the incoming velocity profile due to the presence of the empennage resulting in a non-uniform wake profile impinging on the BLI propeller

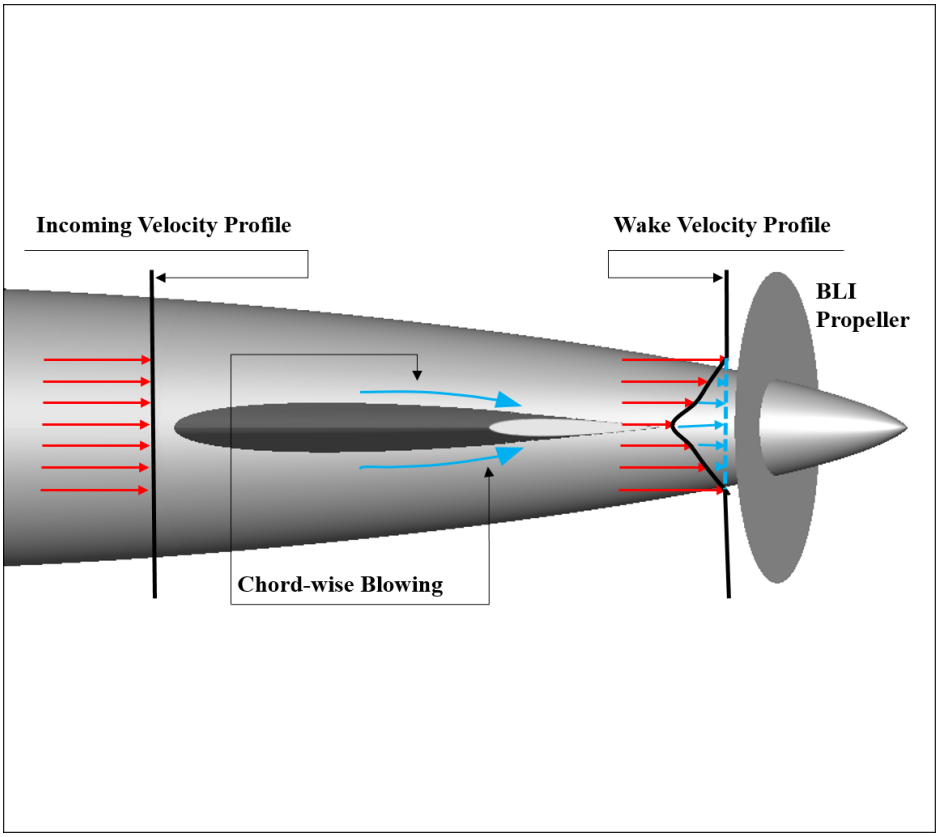

Figure 1.5: A conceptual representation of how the air will be blown in chord-wise direction over the empennage in order to fill the empennage wake to provide a uniform inflow profile to the BLI propeller

chapter 2 will provide an in depth review of the literature available on the concepts of BLI and wake blowing, followed by a description of the research objectives and questions, which will be addressed over the course of this thesis, in chapter 3. Some relevant design specifications chosen for the current work will be laid down in chapter 4, followed by chapter 5 which will provide a description of the Computational setup and meshing technique. The results for the wake blowing analysis for the fan-off and fan-on configurations will be discussed in chapter 6 and 7 respectively, followed a comparison between the two, based on the physical implications of adopting the wake blowing system on the fan and on the aircraft in general. Lastly, the major conclusions along with some recommendations for future work will be mentioned in chapter 9.

2

THEORETICAL BACKGROUND

Since the APPU concept is based on the utilization of the propulsive efficiency benefits of a BLI propeller, it is prudent to go deep into the concept to familiarise with the literature available on the topic. This would be followed by a literature review of the wake blowing techniques available that can be employed in order to mitigate the adverse effects of the empennage wake on the BLI propeller inflow, which is the main aim of this research.

2.1. BOUNDARY LAYER INGESTION (BLI)

BLI is a concept where the boundary layer generated over an upstream body is ingested by a propulsion unit operating downstream which in the case of the APPU project is an unshrouded propeller. The interest in BLI propellers arises due the higher propulsive efficiency associated with them. A basic comparison can be made between a BLI propulsor versus free-stream propulsor to study the increase in efficiency due to BLI(see Figure 2.1).

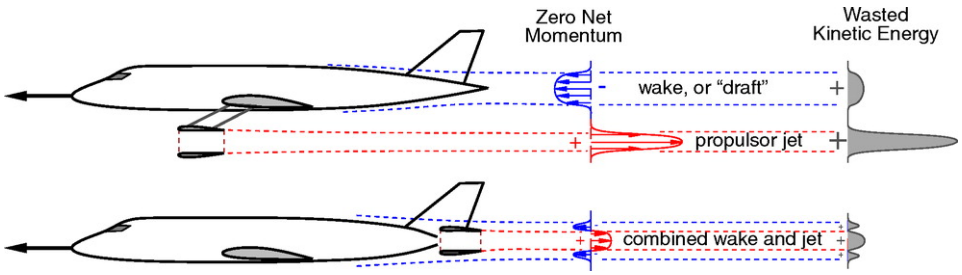

Figure 2.1: Illustration of power-saving benefit of (bottom) boundary layer ingestion compared with (top) a conventional aircraft. Lower wake velocities of combined wake and jet result in a reduction in wasted kinetic energy. [4]

Figure 2.1 shows how immersing the propulsor in the wake balances the momentum deficit in the flow. To further understand the effect of BLI on an open rotor's performance, it is important to understand how the propulsive efficiency of an open rotor can be defined. For simplicity, assume an open rotor to be similar to a very high by-pass ratio(BPR) turbofan where the jet part becomes small enough to be ignored. So, same theory of increase in propulsion efficiency of turbofan engines with increasing BPR can be assumed to extend to open rotors. The propulsive efficiency, as given by Froude[37], is the ratio of thrust power(TV_∞) to the added mechanical power(P_M). Power loss(P_{loss}) in the rotor is also important here. The corresponding expressions for each are given as follows:

$$T = \dot{m}\Delta V \tag{2.1}$$

$$P_M = \frac{1}{2}\dot{m}((V_\infty + \Delta V)^2 - V_\infty^2) \tag{2.2}$$

$$P_{loss} = \frac{1}{2}\dot{m}\Delta V^2 \tag{2.3}$$

$$\eta_p = \frac{TV_\infty}{P_M} = \frac{\dot{m}\Delta V V_\infty}{\frac{1}{2}\dot{m}((V_\infty + \Delta V)^2 - V_\infty^2)} = \frac{2}{2 + \frac{\Delta V}{V_\infty}} \tag{2.4}$$

where $\dot{m}$ is the mass flow rate through the propulsor and ΔV is the velocity difference between the inlet and exit velocities, making $V_\infty + \Delta V$ the exit velocity. A control volume analysis for an actuator disk model, as seen Figure 2.2, shows the depiction of the velocities at the inlet, exit and propeller locations. A higher exit velocity (thus a higher momentum) increases the thrust of the engine, but also the power loss. So to increase the thrust without increasing the losses, the solution is to increase the mass flow rate of the bypass or in other words, increasing the BPR and lowering the fan pressure ratio at the same time. As the contribution of the core thrust to the total thrust generated reduces, the propulsive efficiency increases[38]. Since open rotors have large blade radii, this increases the mass flow and the thrust produced. This also means that the fan pressure ratio needs to be lowered accordingly.

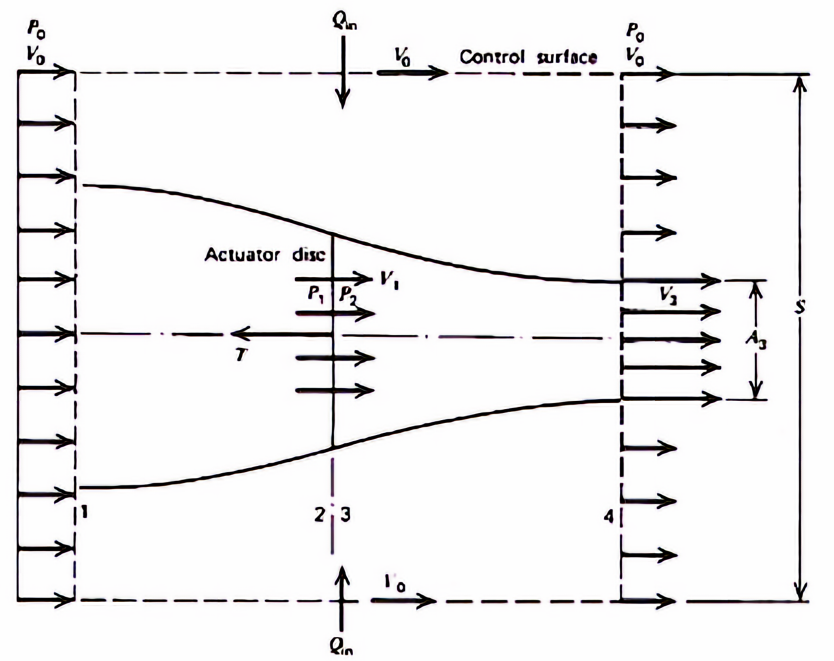

Figure 2.2: Propeller streamtube with velocity description at the inlet, outlet and the actuator disk location within the streamtube[5]

Applying the same concept in case of BLI open rotors, it can be noted from Equation 2.4 that a positive thrust means that the value of ΔV is positive which yields a propulsive efficiency value of less than unity. Also, from the same expression it is evident that smaller the ΔV higher would be the efficiency. Now, due to the presence of fuselage boundary layer, the propeller encounters a lower inlet velocity. This means that less energy is needed to achieve the same thrust.[25], thus leading to a reduction in fuel burn. Also, apart from this, an allied positive effect of BLI concept for PFC is that it is a more favorable configuration in terms of drag. Since the engine is now behind the fuselage, therefore it does not contribute as much to the frontal area of the aircraft, thus reducing the drag. This could potentially have a domino effect in reducing the fuel burn.

The field of marine propulsion is a good source for applications of BLI propellers. Propulsion of submerged bodies such as torpedoes have been discussed by Wislicenus and Smith (1952)[39], Wislicenus (1960)[40], Gearhart and Henderson (1966)[41] and Bruce et al. (1974)[42]. Although, for aircraft propulsion, BLI effect is less pronounced due to the reduced density and total pressure properties of air[26], still studies as back as in 1940's showed a reduction in fuel consumption for an engine which ingests BL[24]. Experiments were conducted which resulted in the conclusion that BL ingesting engines reduced fuel consumption as compared to a turbojet engine propelling the same configuration[25].

Betz [43] explains that by ingesting lower velocity flow, the power expended can actually be less than the product of the forward speed and aircraft drag. This has also been referred to in the works of Drela[44] and

Peijian[6] as the drag-power. Betz also concluded that the required power of the wake ingesting propeller is reduced as the energy left in the wake is used by the engine, thus reducing the excess energy in the propeller slipstream.

Plas(2006)[25] also mentions a study in which BL ingesting and non-ingesting case were compared by means of keeping the relative velocity increment given by the engine to the flight speed constant. It was found that BLI is beneficial because the kinetic energy of both the wake and jet is reduced. Douglass(1970)[45] calculated that a maximum propulsive efficiency of 16% is possible assuming no losses in the engine inlet.

In a research done by NASA[46] on Ultra Efficient Technology Program - Propulsion Airframe Integration Project, an investigation was made to understand the potential propulsion airframe integration improvements using BLI propellers with aft fuselage configuration (AFC). A Blended Wing Body (BWB) aircraft was used for the study with a turbofan engine mounted atop the aft end of the fuselage. A potential benefit of up to a 10% reduction in fuel burn was found to be possibly achievable if the AFC was used for boundary layer control, enabling a short offset BLI inlet.

Hardin et al.[47] carried out a study in which fuel burn benefits associated with BLI for generation-after-next (N+2) aircraft and propulsion system concepts are identified. It was concluded that a 3-5% BLI fuel burn benefit could be achieved for N+2 aircraft relative to baseline high-performance, pylon mounted ultra high bypass propulsion system.

Furthermore, a study on the D8 aircraft[48] shows the BLI benefit for a BWB configuration. Wind-tunnel experiments were performed at the NASA Langley Subsonic Wind Tunnel. The comparison is made using the propulsive power required to produce a given net stream-wise force on the entire aircraft. Note, that although the D8 aircraft utilises the benefits of BLI, it uses a ducted propeller. This means that the nacelle is present which slow the high subsonic flow of Mach 0.72 to a lower Mach of 0.6 for better performance of the BLI propeller. Studies with open BLI propellers, like the experiments done by Hartuc[49], showed that BLI propulsors require 6% less electrical power at the simulated cruise point. However, it should be noted, that most of the open BLI propeller studies are conducted at low subsonic velocities. For example, the experiments by Hartuc were conducted at a maximum wind tunnel speed of 26m/s. The reason that unducted BLI propeller studies are not common for high subsonic Mach numbers is due to the fact that for most propeller types, a speed of larger than Mach 0.6 leads to local supersonic flow which can cause stalled flow over the blade and thus have a penalty on the thrust production. Therefore, most of the experiments discussed might not relate to APPU configuration's high subsonic cruise Mach number regime(M = 0.78). However, benefits of unducted propellers in terms of reduced weight and possibility of achieving high operable subsonic Mach numbers by employing specific propeller configurations, make a valid case for unducted BLI propeller studies. This point will be further addressed in more detail later in this section.

Peijian[6] in his work focused on understanding the physics behind the BLI in a more absolute sense. It was aimed at overcoming the discrepancies in past works related to the benefits offered by BLI in terms of power consumption. A physical model based on the power conversion analysis utilizing the Power Balance Method(PBM) was used to carry out the theoretical analysis, validated by experimental and numerical studies. The analysis yielded that for an aircraft to adopt the BLI capabilities, the design process should aim at minimising the total power consumption rather than the drag. Steady case simulations were carried out for 2D flows and complex flows such as turbulent or compressible flows were not considered to keep the cases simple. It turned out although the use of BLI could lead to added profile drag but the overall power consumption is found to be reduced. These findings were then validated through experiments .

Experiments at the TU Delft wind tunnel facilities have shown that the propulsive efficiency of a propeller mounted at the end of the fuselage can benefit significantly from wake/boundary layer ingestion[6]. Figure 2.3 shows how the propulsive efficiency is improved due to the aft-mounted BLI propeller. It is clear that the BLI case has higher propulsive efficiency than the conventional propeller case where the propeller is placed in the uniform free stream flow. Same is true after the system characteristics are modified with corrections for the incoming velocity profile since the energy of the wake is now not wasted.

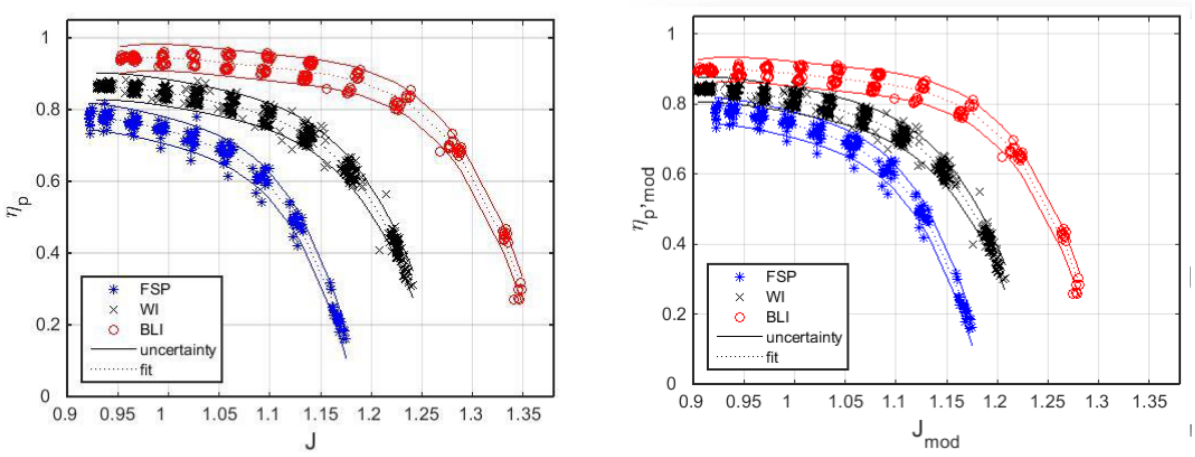

Figure 2.3: Propulsive Efficiency versus advance ratio for different propeller configuration based (L) on free stream velocity and (R) on the average inlet velocity of the propeller[6]

Preliminary simulations using the NASA Common Research Model in which a BLI propeller at the end of the fuselage is modelled as an actuator disk have shown that the required power can be reduced by more than 8% as well as a reduction of the aircraft drag by 12 counts [50].

Even though vast research has been performed in the past advocating the benefits of BLI propellers, for the case of BLI propeller proposed within the APPU configuration, it should be noted that the advantage of improved efficiency is constrained by the design Mach number of the aircraft. At higher cruise Mach numbers, the flow reaches supersonic velocities over the blades of the propeller which lead to shock formation and consequently leads to flow separation[7]. This creates a huge impact on the propulsive efficiency of the propeller. Thus a 'PropFan'[51] type of open rotor would be more suitable for the APPU project. The propfan involves a highly loaded, multi-bladed, unducted propulsor, with highly swept blades to avoid shock losses at transonic or supersonic speeds. It was shown to consume 20% less fuel as compared to modern turbofans[51]. Further developments lead to the start of the Advanced Turboprop Project(ATP) with initial focus on the single propeller and which later shifted to contra-rotating propellers[52]. Figure 2.4 shows NASA's propfan from their Propfan Test Assessment (PTA) program in 1987 and a recent development made by Safran with the use of contra-rotating open rotor engines. A comparison of efficiency profiles with cruise Mach numbers is shown in Figure 2.5

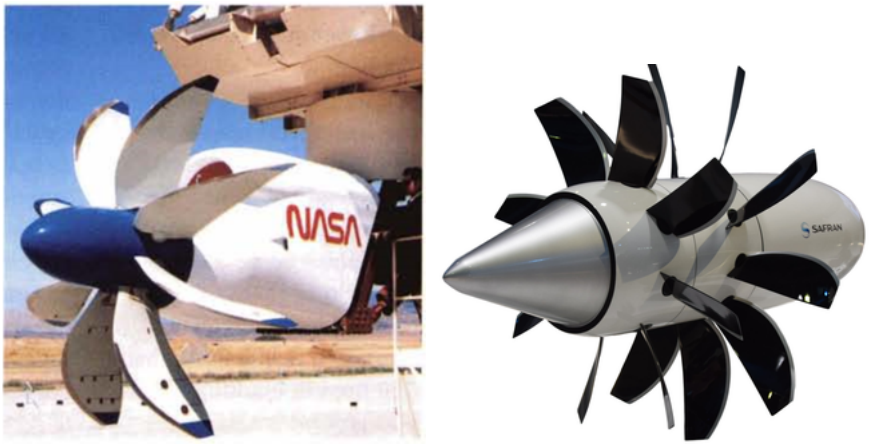

(a) NASA Propfan (1987)[53] (b) Safran Open Rotor mockup (2017)[54]

Figure 2.4: Past and recent examples of highly loaded, multi-bladed, unducted PropFan engines

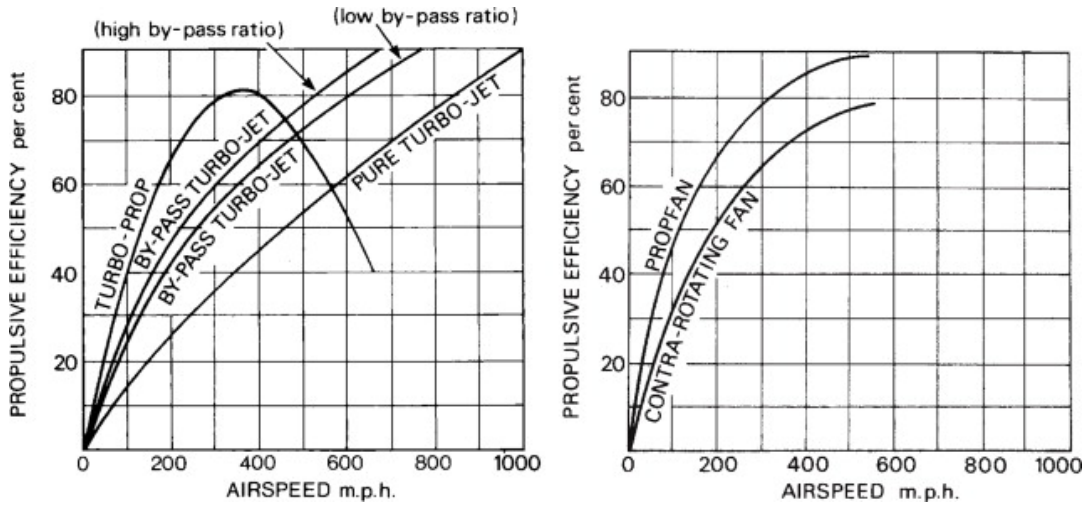

Figure 2.5: Variation of efficiencies for different engine configuration with cruise airspeeds[7]

However, the limit on operable Mach number is not the only challenge for the BLI open rotors. Another challenge is the integration of the BLI propeller engine in the aircraft frame. The large diameter of the propeller governs certain design parameters like the location of the propeller on the aircraft while adhering to the ground clearance requirements. Another related issue is that there is no nacelle or fan case, therefore, the certification requirements make it essential to prove that the probability of blade release is within the set limit [12].

Another prime issue related to BLI concepts involving open rotors is of noise penalty. The absence of a shroud leads to greater tonal noise penalties as compared to turbofan engines. Although, advancements have led to quieter propeller engines, however, the difference in tonal noise emissions between the turbofan and open rotor BLI engine still remains. Also, as the tonal noise contribution reduce, the dominance of broadband noise, which is generated due to the addition of the propeller to the aircraft frame, increases[28–31]. This effect is further aggravated due to the non-uniformity induced by the empenage wake for the aft mounted propeller configurations. Addressing this non-uniformity due to the presence of the empennage will be the focus of this thesis and therefore, needs to be addressed in more detail.

2.2. WAKE FILLING- A SOLUTION FOR WAKE INDUCED ADVERSE EFFECTS

A BLI propeller in pusher configuration poses a major challenge despite its benefits in fuel burn reduction and also drag reduction[6, 48, 55]. This challenge arises due to the interaction of the empennage or pylon wake with the installed downstream propeller. The wake flow behind the empennage impinges on the propeller leading to unsteady blade loading. This can prove detrimental for propeller noise performance [28, 29, 32–35]. In other words, the velocity deficit in the empennage wake leads to a non uniform blade loading at the propeller which can lead to tonal noise penalties. Another important aspect to be taken into account is the angle of attack of the incoming air. It can be shown the at a higher angle of attach these penalties become larger due to a more distorted or deficit wake[16, 28–31]. Care needs to be taken when dealing with cases involving angle of attack variations as the incoming air is no longer symmetric and hence neither is the wake. Recovering the velocity deficit is the main solution which can help alleviate these detrimental effects. One of the methods available in literature is of filling this wake by blowing air. This forms the basis for the wake blowing techniques employed in the current work. Although, studying the effect of angle of attack on the wake blowing mechanism is beyond the scope of this thesis.

PENALTY ON NOISE LEVELS

The velocity deficit due to the upstream pylon effects the propeller noise but has almost no effect on the interaction noise tones [16, 28–31]. The APPU configuration is proposed to have either a T-tail empennage configuration or a crucifix empennage configuration in order to avoid the interaction of the horizontal tail plane with the aft propeller. This means that for the analysis only the wake of the vertical tail plane(VTP) needs to be considered. This can be extended to a more complex empennage configuration in future itera-

tions where there is a wake due to more than one empennage structure. This stationary single empennage wake has been shown to interact with the propeller to generate acoustic modes of the form $m = k - nB$ at the frequencies nB and its multiples. Thus the wake-propeller interaction noise consists of acoustic mode at each harmonic of the Blade Passing Frequency(BPF). Same can be observed in Figure 2.6. This figure also shows high installation noise penalties as compared to the isolated configuration. This shoot in SPL level at BPF tones can be attributed unsteady loading noise at the propeller.

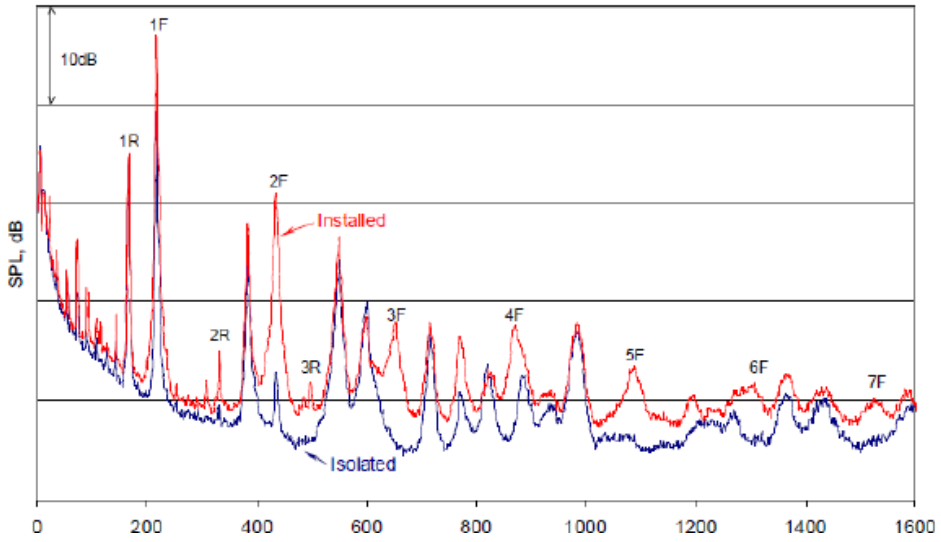

Figure 2.6: Noise penalty for isolated and installed propeller configuration [8].

POTENTIAL SOLUTIONS

The FAA CLEEN Program specifies some of the ways to reduce these installation effects which can be easily extended to the empennage-propulsor interaction under question in this study[36]. These are:

- Empennage wake mitigation
- Reduced disk loading
- Varying pylon-to-propeller spacing
- Aeroacoustic blade design/geometry
- Increased blade counts

Past works have shown that out of the above methods, wake mitigation shows a high potential in reducing the interaction effects, specially interaction noise [11, 13, 28, 56].

The various flow control techniques to remove these detrimental effects, can be mainly divided into active and passive techniques. It has been found out that active techniques such as wake blowing are more effective in reducing the detrimental effects of empennage-propulsor interaction[8, 11, 13, 28, 30, 35]. Most of these works have been performed looking at the engine pylon but they can be easily be extended to the empennage as well. The most common outlet positions for the blowing system is at the trailing edge of the pylon or along the chord at the aft part of the pylon, or the empennage in the current case. Figure 2.7 shows the difference between the two types of wake blowing techniques in terms of their location of implementation and the direction in which the air is usually blown. Organisations like DLR, Airbus and Boeing have found the trailing edge blowing approach allows for a much easier integration of the blowing outlet in the structural model[8, 28, 35]. This has also been experimentally investigated by NASA [11]. However, blowing air at the surface along the chord provides a more uniform post blowing wake velocity profile which is due to the fact the blown flow has a longer length to merge and settle to the external flow conditions. This has been mentioned in the works of Jindal[16] and in the works of ONERA [13].

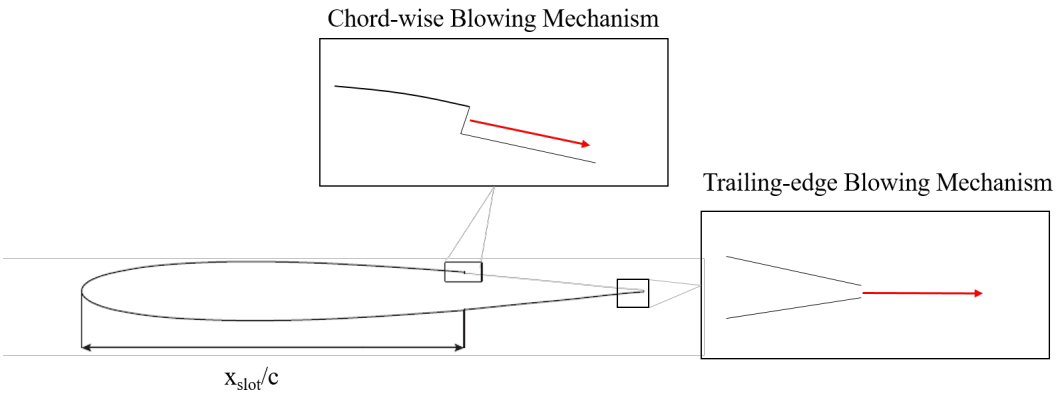

Figure 2.7: Conceptual difference between trailing edge blowing mechanism and the chord-wise blowing mechanism in terms of location of application and the blown air direction

Trailing edge blowing

As mentioned, this method has been studied extensively by Airbus, Boeing and DLR [8, 28, 35]. Experimental investigations have also been performed in the low speed facility (LLF) of the German-Dutch wind tunnels (DNW) to study the effects of tailing edge blowing on the pusher propeller performance and noise emissions, reported by Sinnige [10].

Figure 2.8 gives the corresponding wake velocity profiles. It can easily be noticed that applying the pylon trailing edge blowing leads to a reduction in the velocity deficit.

About 80% reduction in integrated wake velocity deficit, in comparison to the unblown configuration, was achieved by using a blowing coefficient of $c_{\dot{m}} = 1.62$. It is important to note however, that a reduction in total wake width could not be achieved. The effect of wake filling, on the noise emission penalties that are incurred due to interaction of the wake with the propeller, were also studied. Figure 2.9 gives the noise emissions for the isolated, installed, and blown ($c_{\dot{m}} = 1.60$) configuration.

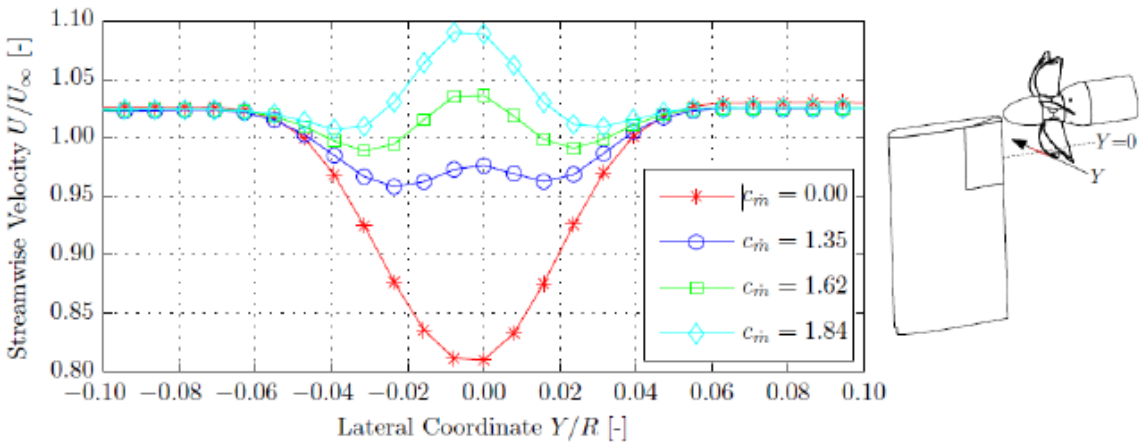

Figure 2.8: Wake velocity profiles for different blowing momentum rates [9]

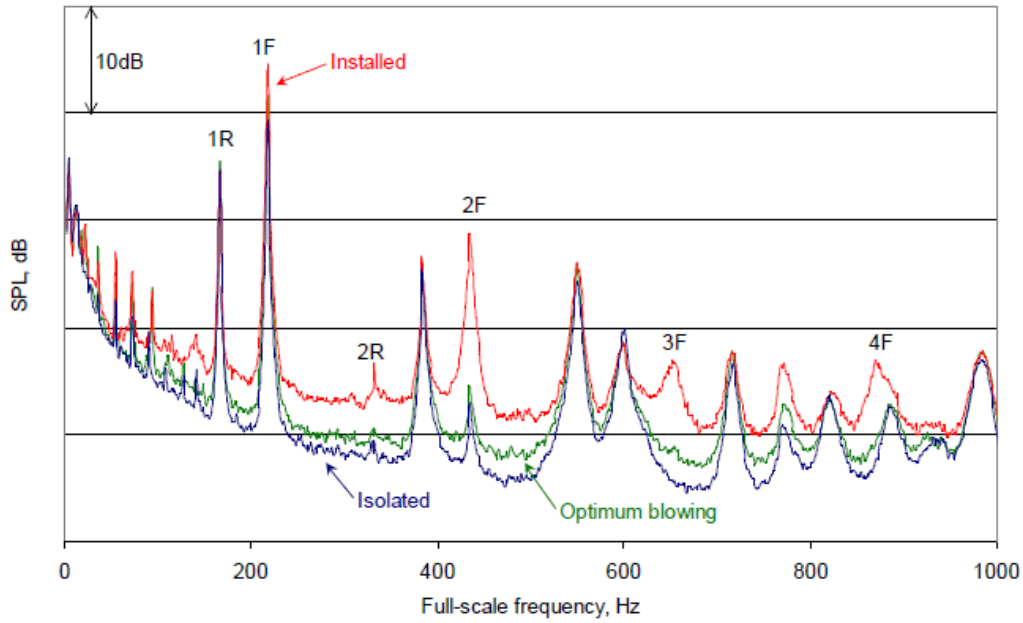

Figure 2.9: Total SPL versus propeller frequency for isolated, installed, and blown configurations [8]

Figure 2.9 depicts how filling the wake velocity deficit, using a trailing edge blowing system, affects the propeller noise emissions. It also shows the reduction in sound pressure level, especially for the lower frequencies. The pylon played a big part in the noise emissions that were observed. First two tones for the isolated propeller case are differentiable from the background noise levels whereas for the case with unblown pylon, the higher harmonics are also distinguishably visible. A noise increase of 5 dB was reported in the measurement of the fundamental tone while it increased by 8 dB for the 2^{nd} BPF. The analysis of noise penalty for unblown and blown cases yielded the plots in Figure 2.10

The fact that a noise penalty is associated with pylon installation is firmly established by the Figure 2.10. This penalty is almost fully mitigated by employing trailing edge blowing, the effect of which on the performance of the propeller is given in Figure 2.11

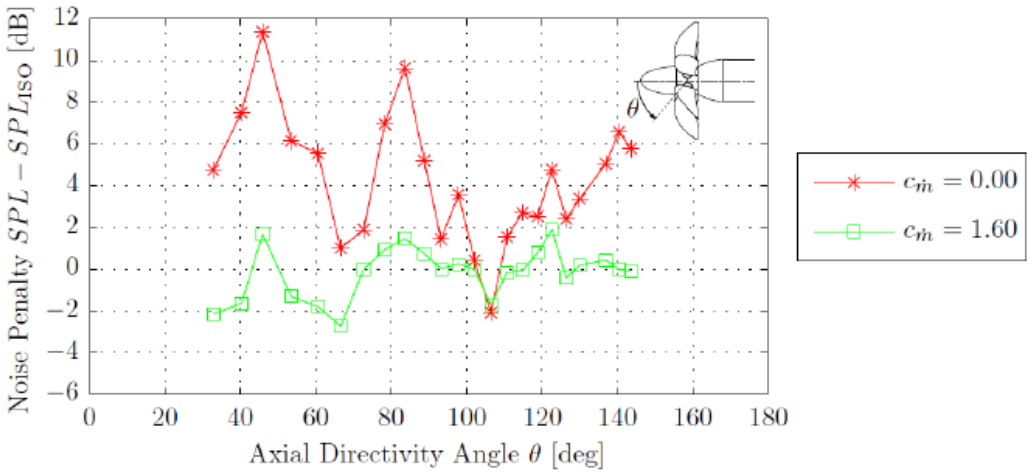

Figure 2.10: Variation of the noise penalty with the axial directivity angle for unblown and blown pylon cases at an advance ratio of 1.40 [10]

It can be inferred from Figure 2.11 that the thrust coefficient increased by less than 2% for advance ratio, J≤1.4 due to installation effects. A peak-to-peak variation of up to 4% was observed in the time-accurate thrust and torque for the same range of advance ratios. Although, similar effects were shown for the blowing configuration case, the peak-to-peak variations only reached a maximum of 2%, depicting that propeller performance is further reduced due to the presence of pylon.

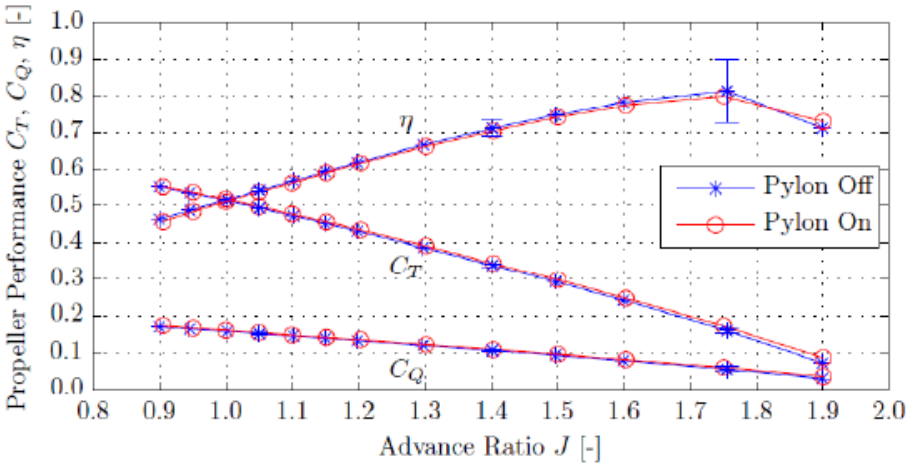

Figure 2.11: Propeller performance in terms of C_T(Thrust Coefficient), C_Q(Torque Coefficient) and η(Propeller Efficiency) for isolated(pylon off) and installed(pylon on) propeller configurations, U_∞=19m/s, 0.9 ≤ J ≤ 1.9[10]

Similar studies were conduced by NASA as well[11]. Their investigation on reduction of pylon wake velocity deficit through the application of pylon blowing is a well established reference to study the effects of pylon blowing on the propeller performance. This can be seen in their results as shown in the Figure 2.12.

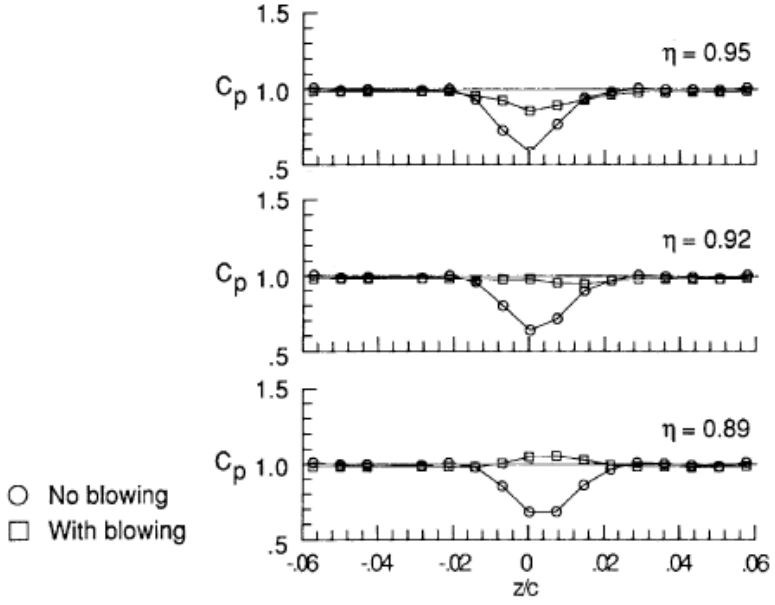

Figure 2.12: Pylon wake profiles with and without blowing with blowing slot at 0.8c. Reproduced from [11] by [12]

Figure 2.12 shows the successful use of pylon blowing to fill up the wake. For the value of η = 0.92, almost uniform wake filling was achieved compared to the unblown case. The propeller performance was also measured in the isolated, installed, and blown configurations using a time-averaged thrust coefficient as a function of

the advance ratio as shown in Figure 2.13.

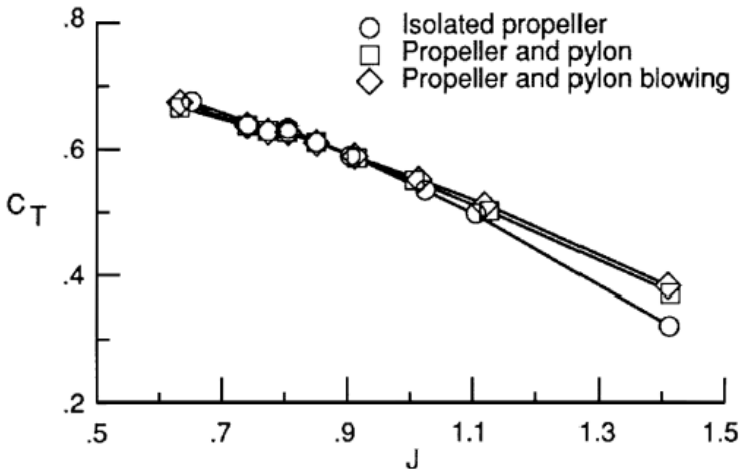

Figure 2.13: Thrust coefficient(C_T) versus advance ratio(J) for isolated, installed, and blown propeller configurations. Reproduced from [11] by [12]

It is evident from Figure 2.13 that the steady state effects dominate the time averaged propeller performance due to the fact that the installation effects were found to be rather small for the advance ratio values of less than 1. However, considerable differences were observed for the cases with advance ratios greater than 1. The highest thrust output is observed with the propeller in the blown configuration, whereas the isolated propeller case generated lowest thrust. This behavior seems unexpected. Taking into account the velocity profiles depicted in the Figure 2.12, the expected behavior would have been the thrust of the blown propeller falling in between the ones measured for the isolated and installed configurations, due to the fact that the velocity deficit in the blown pylon wake is reduced as compared to the unblown case. However, no concrete explanation for the observed behavior could be given.

Chord-wise Blowing

In chord wise blowing configurations, holes for blowing air are introduced on the pylon surface ahead of the trailing edge. If more than one hole are to be added then they are arranged in a system along the pylon chord. This provides additional length to the freestream flow and the blowing jets, on the pylon surface itself, to follow a more uniform pattern of mixing, resulting in a wake which is much more uniform than the trailing edge blowing configuration. This has been established by ONERA in their numerical works in 2012 [13].

The variation in wake deficit for various mass flow rate of the blown air for different blowing configurations is given in Figure 2.14. Three configurations were taken into account, first trailing edge blowing (INJA), second single lateral-injection chord-wise blowing (INJB1; injection position localized at 5% pylon chord upstream of the trailing edge) and lastly, double lateral-injections chord-wise blowing (INJB12; injection position localized at 5% pylon chord upstream of the trailing edge).

To specify the wake deficit criterion, an absolute integrated area is defined around the far-field Mach number(M_{a_∞}) of 0.23. It was found out that the deficit in the wake for the unblown case corresponded to a confined azimuthal angle of 8^o and reduction of Mach number from 0.23 to 0.05. Corroborating the results of the experimental investigation of Sinnige[9], the trailing edge blowing depicted a deficit in velocity without any reduction in the wake width for the local region ($\sim 2^o$). Looking at the single lateral injection next, it was shown that a 50% reduction in wake width was achieved while the deficit area was also smaller as compared to trailing edge blowing case. However, a 40% higher Mach number was attained with respect to the reference Mach number of 0.23. Lastly, the double lateral injection case improved the velocity deficit from 78% to 28% while maintaining the same wake width as in case of single lateral blowing.

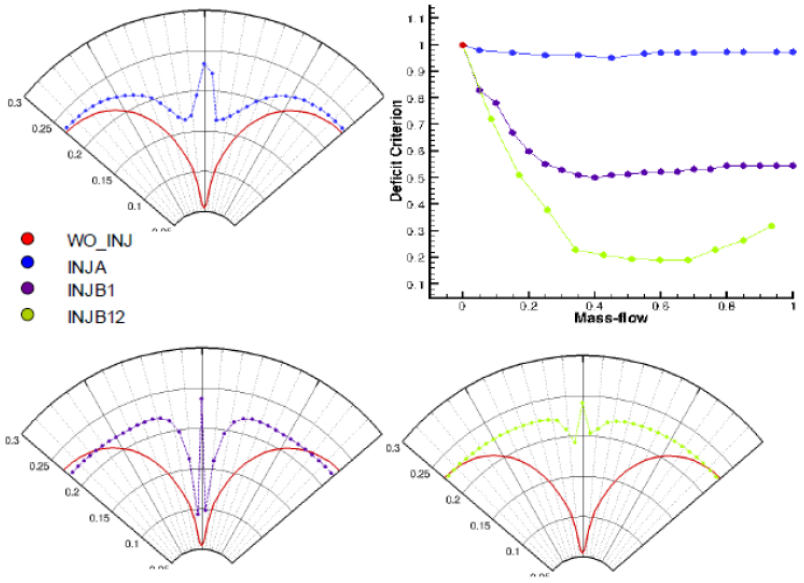

Figure 2.14: Depiction of velocity deficit at optimal mass flow for each injection type ('WO_INJ' = no blowng, 'INJA' = simple trailing-edge blowing, 'INJB1' = single lateral injection from lower surface at 95% pylon chord, 'INJB12' = double lateral injection from upper and lower surface at 95% pylon chord). [13]

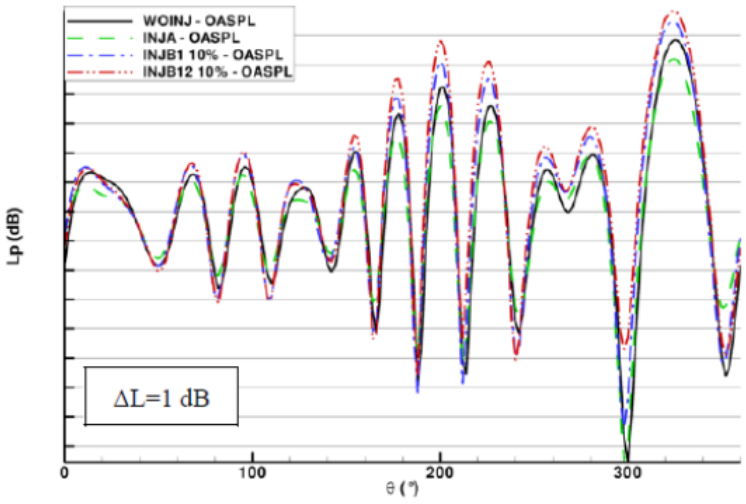

Figure 2.15: Overall sound pressure level directives comparison for all four flow injection cases(WO_INJ, INJA, INJB1 and INJB12) showing an increase in sound level of up to 1dB[13]

INJB12 case showed to have a minimum while plotting variation of deficit criterion with the blown mass flow rate, which is not present in any of the other two configurations. Even though no concrete justification could be found, this behaviour might find basis in the fact that the difference between $M_{a_{min}}$ and $M_{a_{max}}$ as seen in the profiles is much lesser for INJB12 case than the other two configurations. This difference makes the area under the velocity deficit curve much more sensitive to change in the shape of the profile itself, especially when it goes beyond the undisturbed Mach number value. For the other cases this difference in Mach numbers seems more significant. Additionally, Figure 2.15 gives the effect of the said blowing techniques on the propeller noise emission performance. The sound level was increased by $\sim 0.7dB$ and $\sim 1dB$ for the single and double lateral injection cases, respectively, while for the trailing edge blowing case, a reduction by $\sim 0.5dB$ was observed.

A detailed study establishing the superiority of the chord-wise blowing technique was conducted by Jindal[14] who also investigated some major physical parameters having an influence over the wake profile. Jindal used a steady state RANS model to carry out the numerical investigation of the use of pylon blowing systems to mitigate the effects of pylon wake impingement over the open pusher propeller located at the rear end of the fuselage. He studied the effect on the uniformity of the blown pylon wake for varying blowing-slot geometry and blowing momentum coefficient. The study establishes the superiority of chord-wise blowing over trailing edge blowing with the reasoning that trailing edge blowing has to deal with two major disadvantages. First, that the boundary layer is much bigger as compared to that encountered by chord-wise blowing case, at their respective operation locations. This leads to the requirement of a higher blowing coefficient. Due to thicker boundary layer, the flow mixing also takes longer to yield a comparatively more uniform profile. This brings the discussion to the second disadvantage of trailing edge blowing, that a smaller length is available for proper mixing of the blown flow with the external flow. A theoretical maximum reduction of about 99.7% in the wake non-uniformity was found to be possible with the use of chord-wise blowing at the optimal location x/c = 0.7[14] and blowing blowing coefficient of 0.0123.

Certain design parameters which are crucial for the chord-wise blowing system are the location of blowing slot, their heights and the slot blowing coefficient. The slot blowing coefficient is defined as the follows:

$$C_\mu = 2\frac{h_{slot}}{c}\frac{U_j^2}{U_\infty^2} \tag{2.5}$$

where c was the pylon chord, h_{slot} is the slot height, U_j is the velocity of the blown flow through the jet and U_∞ is the freestream velocity. However, to measure the uniformity of the pylon wake after blowing, a new criterion was introduced called the J-criterion which can be defined as follows[14]:

$$J = A(\frac{U_{max} - U_{min}}{U_e}) \tag{2.6}$$

where U_{min} and U_{max} are the minimum and maximum velocities encountered in the wake, U_e is the local undisturbed velocity, and A is the absolute area under the non-dimensionalized wake velocity curve which gives the integral wake velocity deficit[14].

The slot height itself shows very less influence on uniformity of the blown wake but its effect is already included in the blowing coefficient. Figure 2.16 gives the contour of J-criterion as a function of chord-wise slot location and blowing momentum coefficient, obtained at a plane located at a chord-wise location of x/c = 1.25[14]

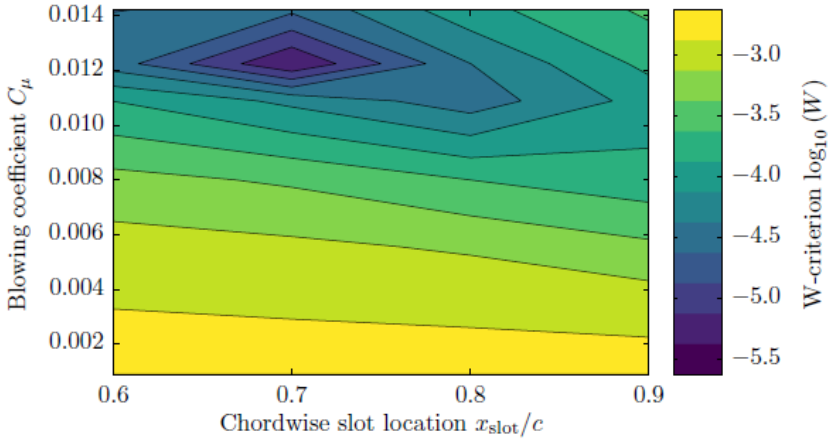

Figure 2.16: Wake uniformity versus chord-wise slot location and blowing coefficient at x/c = 1.25, $h_{slot}/c = 10^{-3}$[14]

Figure 2.16 shows the optimal slot location and blowing coefficient as mentioned earlier. It was found out that for lower blowing coefficient the upstream chord-wise location are not as efficient. However, better results

were obtained on moving the slots downstream towards the trailing edge. Lower the blowing coefficients, higher the rearward shift required for improved results. At higher blowing coefficient values, however, require a longer mixing distance for the blown flow to mix with the external flow. Thus, a more upstream location for slot are preferred for these cases. Another observation is that the wake uniformity first increases with increasing blowing coefficient but then decrease after a certain level, while keeping the slot location constant. This is because the high blown flow generated a strong overcompensation in the velocity deficit. This overshoots the wake velocity profile and leads to ever filling.These observations can also be devised from Figure 2.17. The change in value of the J-criterion grows more steep as the optimum blown value is reached. It was also shown using Figure 2.17 that local velocities for the optimal case remained within the margin of 1.5% of the external flow.

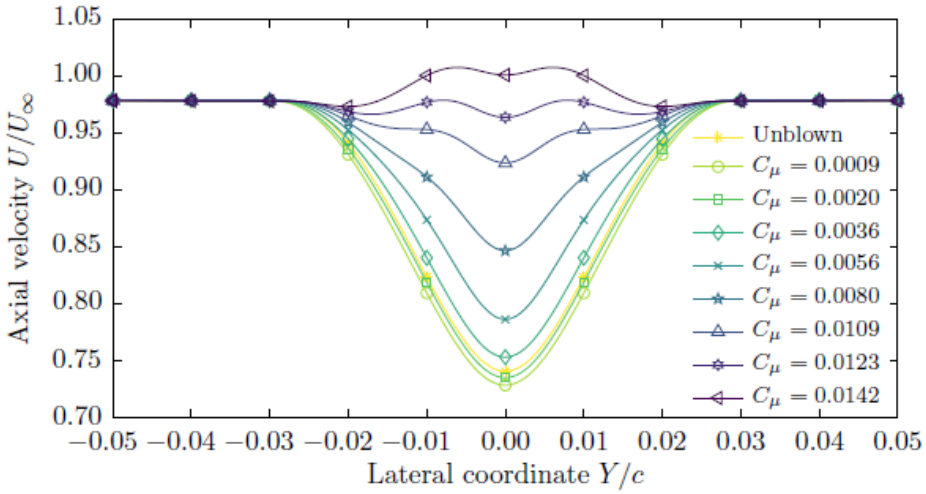

Figure 2.17: Velocity profiles in the blown pylon wake at x/c = 1.25, $x_{slot}/c = 0.7$, $h_{slot}/c = 10^{-3}$ [14]

The theoretical background discussed in this chapter would by now have given the reader an indication of the detrimental effects that an empennage wake can have on the performance of a BLI propeller along with the understanding of ways to mitigate it. From this section it can be concluded that the chosen chord-wise wake blowing technique shows great potential in mitigating these detrimental effect, however, the research done on the topic is highly limited and largely focused on two dimensional cases. This leaves a gap in knowledge over its applicability in a 3D setting and the influence of the propeller on the wake blowing mechanism itself. This leads to the objective of the current research which is laid down in the following chapter.

3

PROJECT DESCRIPTION

A few points have been established by now, firstly, the presence of the emennage will lead to a non-uniform flow in it's wake which would serve as the inflow for the BLI propeller on the upper fuselage side. Secondly, this non-uniform inflow will lead to potential negative impact on the propeller's noise performance. Thirdly, the potential of filling this wake using active flow control techniques is high. And lastly, the chord-wise wake blowing method seems to be the most promising in achieving a uniform wake profile and mitigating the negative impact of the non-uniform wake. The last point is where the research available is limited and where the research gap lies in terms of the applicability of chord-wise wake blowing in a 3D setting and in presence of a propeller and its capability of filling the empennage wake with high uniformity. This chapter will focus on defining the research goals and objectives for the current topic based on the literature studied in the previous chapter and the research gap thereof.

3.1. RESEARCH GOALS AND OBJECTIVES

The project APPU aims at investigating the design of a novel tail-based propulsion system that combines an adapted hydrogen powered turboshaft engine (APU) with a BLI propeller. The presence of the empennage wake would induce changes in the blade angles and the local dynamic pressure loading for a propeller which will be installed downstream of the empennage. As seen from the literature[8, 11, 28, 30, 32, 35], the resultant unwanted detrimental effects can manifest in the form of propulsive efficiency losses and noise production. Although, presence of wings and other upstream aircraft components are also expected to influence the performance of the aft propeller, quantifying this influence is out of the scope of this thesis. To that end, the present work aims to *understand the interaction between the empennage and the aft propeller inflow and analyse the effect of the wake blowing system, installed chord-wise over the empennage, on the propeller inflow and vice verse. It would be determined whether flow control techniques like wake blowing can be used to improve the uniformity of the inflow seen by the propeller in an attempt to mitigate the empennage wake effects*

RESEARCH OBJECTIVES

To study the empennage-propulsor interaction for an aft mounted propeller with respect to the effect of empennage wake on propeller inflow and use flow control technique of chord-wise wake blowing in order to mitigate the empennage wake effects, investigated using numerical simulations.

Fulfilling these objectives will help to derive possible design guidelines for the APPU project. Certain goals have been set to meet the aforementioned objective and are discussed in this paragraph. In order to analyze the empennage-propulsor system, a high fidelity CFD analysis will be performed to capture the flow physics. Since one of the main aims of the APPU project is to reduce the emissions in ground operation and assist in landing and take-off in an attempt to reduce the ground emissions, the simulations will be carried for take-off conditions of Mach 0.23. The quality of simulations will depend on the mesh quality, the turbulence model and discretization schemes used during the CFD analysis. An off the shelf CFD software, like Ansys Fluent[57] will be used for the simulations. A RANS(Reynolds-Averaged Navier Stokes equations) model will be chosen for the current research(see chapter 5) due to its proficiency in resolving flow phenomena like boundary

layers and body wake flows at a much lesser computational cost as compared to the more accurate yet computationally intensive methods like DNS(Direct Numerical Simulation) or LES(Large Eddy Simulation).
The first goal of the project would be to understand the wake and it's progression behind the empennage in order to quantify the amount of wake velocity deficit that needs to be overcome using the wake blowing analysis. The next step would be to apply the wake blowing technique on the empennage structure to attain a more uniform wake velocity profile at the propeller. Subsequently, detailed wake blowing analysis will be carried out for the configurations without and with the propeller model. Finally, the difference in the flow physical quantities will be investigated to understand the effect of wake blowing in propeller on and off cases as well as the effect of propeller on the flow with and without the implementation of wake blowing. This would lead to a proper understanding of the individual and combined effects of wake blowing and BLI techniques on the propeller performance. In order to achieve these goals, a set of research questions have been formulated which are discussed in the following section.

RESEARCH QUESTIONS

The main question to be addressed is as follows:

What are the effects of filling the wake of the empennage, by means of chord-wise wake blowing, on the non-uniformity of the inflow of a BLI propulsor, like the one in APPU configuration?

Certain associated sub-questions need to answered in order to achieve satisfactory reply to the main question:

1. How does empennage wake effect the inflow velocity profile of the BLI propeller?
2. What level of uniformity can be achieved using the wake blowing analysis in cases with and without the presence of the propeller?
3. What is the effect of the wake blowing technique on the inflow angles seen by the propeller?
4. What are some aircraft level implication of installation of the said flow control technique? How do the key forces and loads change due to wake blowing?
5. What are the major constraints and requirements on the mass flow rates needed for the wake blowing system?

These questions will form the base of this research. Successfully understanding and answering these questions will give significant insight to the flow physics associated with the APPU propulsor concept. This knowledge will help in determining the necessary design modification and guidelines, which will bring the project a step closer towards commercial induction.

3.2. SCOPE OF THESIS

Although, the concept of wake blowing is not novel, it's application to assist in improving the performance of BLI propeller used in propulsive fuselage concepts, is. TU Delft has been at the forefront of the research related to this concept owing to the works of Sinnige[12] and Jindal[16]. The topic still requires further research and therefore, provides opportunity for researchers with interests in novel propulsion techniques and aerodynamics. It is this fact that makes the definition of the scope for this thesis all the more important. It is important to address the areas that will form of the present study while laying out the equally important and interesting areas which are beyond the scope of this masters thesis.

The main focus of this research is to achieve a good degree of uniform propeller inflow using the wake blowing technique. Along with this, the physical properties of the flow will also be studied. However, even though the efforts of this research are aimed towards mitigating the detrimental effects of the empennage on the aft propeller, it is beyond the scope of this thesis to actually perform performance and noise analysis for the aft propeller. This point is further supported by the fact that the project is in its initial phases and the design of the actual aft aircraft geometry and that of the APPU propeller still remains to be developed. A performance related study will be more prudent at a time when these designs have been decided upon. Thus, the propeller for this research is modelled using an inbuilt actuator disk model of fluent which will be described in more detail in the later section. section 7.1 provides the design parameters which were used to model the BLI

propeller in the CFD analysis. These parameters will remain fixed for the scope of this thesis, but are prudent for future propeller analysis focusing on the sensitivity of the these parameters. Furthermore, since the APPU concept is primarily aimed to target the A320 fleet of Airbus, the current fuselage and empennage geometries are based on the A320 dimensions. This means that the cross-section of the fuselage where the propeller will be potentially placed, is not circular. Some initial thought was given into modifying the fuselage geometry, however, that would have required the shift in focus of this thesis to quantify the effect of the modification on the local flow field. This process would had diverged the research away from the current objective and was therefore, not pursued further but still remains as one of the prominent recommendations for future research. Note, that lifting surfaces like the wings and horizontal stabilizers are also not included. Presence of such aircraft components upstream of the propeller, are also expected to influence the performance of the APPU propulsor but quantifying this influence is out of the scope of this thesis. The present study would limit itself to the investigation of the effects of the wake blowing system on the aft propeller inflow and focus on filling the said wake, in order to eliminate the non-uniformity in the inflow that is experience by the propeller.

3.3. METHODOLOGY AND THESIS OUTLINE

This section will provide a concise break down of the various steps involved in the current thesis. Some software specifications will be mentioned. The relevance and mindset behind each step will be discussed to provide an overview of what and how the goals of the thesis have been tried to achieve. Consequently, these phases will be addressed in different chapters of this thesis.
The whole thesis project can be divided in to the following phases:

1. **Aircraft Geometry Design Phase:** The first and foremost decision that needed to be made was the choice of the geometry. The fuselage and the vertical tail plane(VTP) will be constructed based on the the A320 dimensions. Software like OpenVSP[58] and Catia V5[59] were used in the construction of the geometry. These steps will be discussed in chapter 4. As the logical next step is to mesh the geometry and prepare it for simulations, part of this phase will also include the construction and convergence analysis of the mesh, described in chapter 5

2. **APPU propeller Dimension and Location Choice:** This phase has been under modification and is carried along on the side with phase 1 and 3 until a final decision was made which led to the commencing of phase 4. This phase involves fixing specifications and configuration for the BLI propeller to be modeled. A preliminary propeller diameter was selected based on the tail strike requirements of the A320. A further discussion and detailed specification of the propeller are mentioned in section 4.3. Ansys Fluent v2019R3[57] software package was used for the simulation. It's in-built Fan boundary condition was used to model the APPU propeller as an actuator disk.

3. **Wake Blowing Analysis- Fan Off Case:** Since all the specifications regarding the geometry had been fixed, the step was made towards performing the actual simulations. This phase included a detailed wake analysis study of the system and a complete set of simulations for the variation in the specified system design parameters. The relevance of this case is to understand the physics associated with the implementation of the wake blowing mechanism and how it fairs in a three dimensional setting as compared to the past studies done in 2D. This part of the analysis will be instrumental in delivering a flow profile which the propeller will see in idealing state. Since the idea behind the study is also to provide information which will help in designing of the APPU propeller, this section will form a crucial part of it. It will also give an estimate on the system settings which will be required for the blowing system when operated with the APPU propeller. This part is included in chapter 6.

4. **Wake Blowing Analysis- Fan On Case:** This chapter consists of the second part of the 3D wake blowing analysis which includes the application of the actuator disk model in order to simulate the propeller. The relevance of this case is to understand the implication of the addition of the APPU propeller on the wake blowing mechanism in terms of its capability to fill the empennage wake. This phase is the most important part of the study since it will not only help in understanding how the wake blowing mechanism effects the propeller inflow while in operation but will also provide information on how the addition of a propeller in the flow effects the blowing parameters required to obtain a uniform flow. This phase is included in chapter 7.

5. **Comparison of Flow Properties: Fan-Off vs Fan-On:** This last phase will deal with drawing a comparison between the fan-off and fan-on configurations which will provide information on the effect of wake

blowing on the propeller slipstream and vise-verse. This part will also address the more fundamental physical flow properties in order to give a better understanding of how the flow physics is effected. The mass flow rate and drag studies will form a part of this phase. This phase is included in chapter 8.

Finally, some of the most stimulating conclusions are highlighted in chapter 9 along with some relevant recommendations for future work.

4

GEOMETRY SPECIFICATIONS AND DESIGN

It is essential that the geometric decisions be taken with caution and while taking into consideration all possible obstacles. Two references[15, 16] were used from literature to set up the existing geometry. Since the APPU configuration is proposed for A320 family for initial induction, emphasis is on keeping the geometry as close to A320 as possible. For this purpose the geometry specifications were taken from the A320 aircraft maintenance manual[15]. There was no official reference geometry available for the A320. Nevertheless, some geometries could be found online but with very low or no freedom of easy modification. The time required to modify the off the shelf geometries was better spent developing basic geometries in the software OpenVSP which makes tracing diagrams easy. At the same time, it is important to note that an attempt is made to keep the geometry as simple as possible in order to focus more on the physics of the flow and minimise the effect of multiple geometric complexities. To this end, only a fuselage-vertical tail combination is chosen for this study. The second reference is the work done by Aman Jindal[16]. In his research, Jindal used a simple NACA0010 airfoil of unit chord length. To keep the problem simple, the same symmetric airfoil is used in the vertical tail design. This is also done in the anticipation that this will lead to reduced differences in the qualitative findings. Now, for the cases where the BLI propeller needs to be modeled for the APPU configuration, the location and specifications were needed. These were decided in collaboration with the data obtained inhouse from the System Design and Integration team working on the project. Each of these three aspects is further addressed in more detail separately.

4.1. FUSELAGE DESIGN CONSIDERATIONS

The software OpenVSP[58] is used to make the initial design of the fuselage. Table 4.1 shows the basic dimensions of the A320 fuselage which have been traced using the official renders in OpenVSP. This section will further focus on the key details of the fuselage which will be of prime importance in later stages of the work.

Parameter	Value	Unit
Length	37.57	m
Diameter	3.95	m
Fineness Ratio	4.14	-

Table 4.1: Fuselage geometry specifications[19]

The front, side and top view of the A320 (as shown in Figure 4.1) were taken from the Airbus maintenance manual[15] and were used to make a close enough render of the A320 fuselage. It should to be noted of course that the fuselage is not identical to the A320 fuselage but is a good representation in terms of the fuselage length, diameter and the aft-fuselage upsweep, which are the most important parameters with regards to the current work. For the top, front and side view of the CAD model, the reader is referred to Appendix C

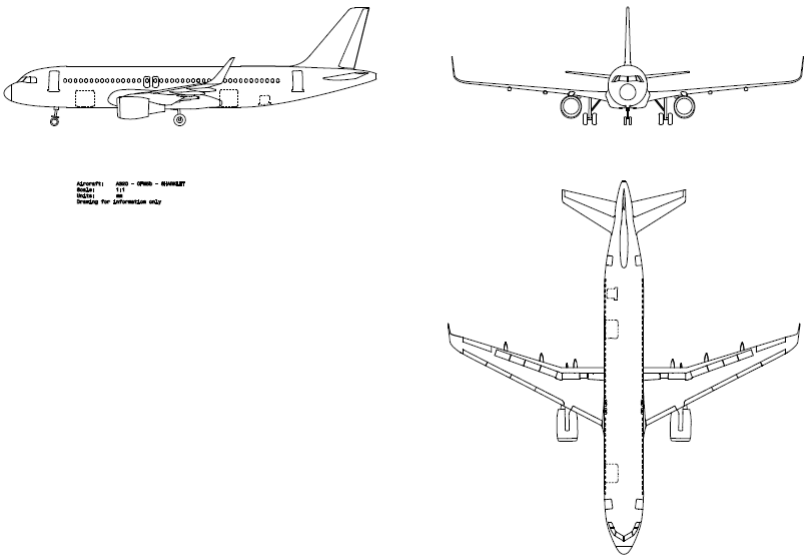

Figure 4.1: A320 side, front and top views(clockwise) used to model the fuselage in OpenVSP[15]

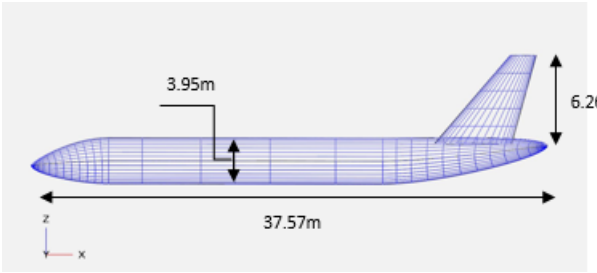

Figure 4.2: Resultant visual of the fuselage and empennage modeled in OpenVSP using official A320 dimensions

It can be seen from Figure 4.2 that the fuselage is not axis-symmetric. Past projects have extensively investigated axis-symmetric fuselage in combination with boundary layer ingesting propellers in pusher configuration. The propulsive fuselage concept discussed in Centreline project[60] is an example of such projects. There are two features of the fuselage in question that need to be addressed.

Firstly, the upsweep of the aft fuselage and the potential effect it will have on the pusher propeller and the flow in general, should be addressed. It was seen in the Centreline project[60] that the fuselage upsweep prevents the vortex that stems from the wing-fuselage junction to impinge on the propeller nacelle which could be beneficial for the propulsor, as the distortion of the inflow is thereby reduced. A similar benefit should occur for the APPU project as well for any vortices stemming from the wings or engine nacelles but as the wings have not been modeled for the current thesis, this effect will remain a mere speculation. The other flow properties on the upper fuselage, which is the focus area of the research, are not much effected by the fuselage upsweep(for more information, see [60, 61]). However, in literature the horse shoe vortex, stemming from the empennage leading edge junction, was found to be slightly further outboard due to the less conical contraction of the upper aft-fuselage body[61]. One observation which will be clearly visible in the results section is that the asymmetry of the fuselage will lead to a considerable variation in the inflow patters for the propulsor. It is also seen in literature that the upsweep in the fuselage has a negative effect on the overall drag of the aircraft. Nonetheless, the benefit of the fuselage upsweep with respect to ground clearance and preventing tail strike during landing and takeoff, makes it a common feature in the modern conventional aircraft.

Secondly, due to the fuselage being closer in design to a commercial aircraft, the aft fuselage cross-section behind the empennage is not axis-symmetric. This means that the hub of the actuator disk, used to model the

APPU propeller, is not circular but of a more vertical 'oval' configuration, as shown on the right in Figure 4.3. Since the propeller is modeled using the fan boundary condition which uses a fixed pressure jump value, it does not adversely effect the flow physics and does not hinder the flow convergence of the solver. However, it is important to keep in mind the implications it might have to the current work. The first and foremost effect will be on the local flow at the hub. As discussed, due to the fuselage upsweep, the flow will diverge from the fuselage underbelly to the aft fuselage sides, inducing a cross flow component along the fuselage circumference. This velocity component direction is shown using the arrows in the figure. Likewise, a small downward diverging flow will be generated on the upper fuselage due to the slight convergence of the upper surface of the fuselage cone. Due to the interaction of these flows, there will be a point on the fuselage sides where the tangential component of velocity becomes zero, leaving only the axial component. The asymmetry of the aft fuselage can lead to an upward shift in the location of these points. Another implication of the same phenomenon might be seen in the inflow angles that the propeller blades will encounter at different azimuths. This arises from the same reasoning that the asymmetry of the propeller disk hub might lead to difference in tangential/circumferential velocities, which will manifest in terms of a difference in the inflow angles that the propeller blades will experience.

Another point to be noted is that, in case a propeller is attached to this asymmetric hub, it will likely have a circular hub within the confines of the outer oval perimeter, because a non-circular hub will have high mechanical and manufacturing complexity. Due to this, depending on the propeller axis, the part of the propeller blades wetted by the flow will vary. This might lead to a small difference in the thrust generated by the propeller but it can be speculated that this contribution will be small enough to be ignored due to the fact that this effect will be limited to the most inboard parts of the blades which have low contribution to the thrust. It should, however, be noted that the current study is a preliminary analysis for the APPU project and for the chosen propeller model, a non-asymmetric hub will not lead to different conclusions. Nevertheless, the fuselage will have to be modified in further design iterations carried within the APPU project when higher fidelity propeller models will be chosen.

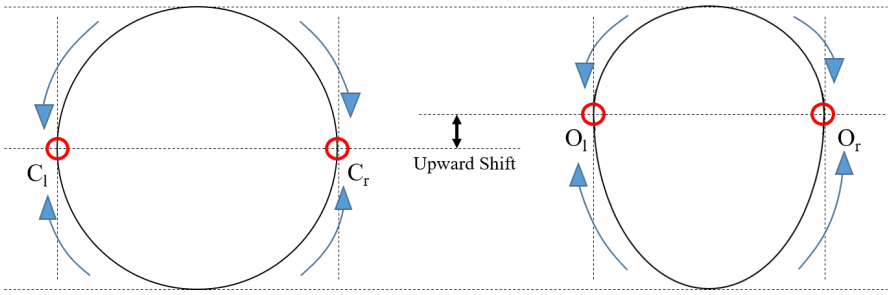

Figure 4.3: Depiction of the shift in the location of outer most curvature points where the circumferential velocity components are zero and only the axial velocity components remain. This possible implication of the asymmetry of the propeller hub could lead to variation in quantities like inflow angles.

4.2. EMPENNAGE DESIGN CONSIDERATIONS

Initially the empennage geometry, which for the current case consists only of the VTP, was created using OpenVSP, in a manner similar to the fuselage design. Although, the outcome was convincing, however it was found out that the geometry, although editable in CAD software, did not give the required amount of freedom. Since the VTP is the most crucial part for the current thesis and would require constant modification, it was decided to construct it using the software 'Catia V5'[59]. A similar geometry created in Catia would provide much more ease in the later steps of the project when the physical blowing slot will be implemented and its dimensions will be varied. This would give a higher level of control in terms of the VTP geometry and thus reduced the time for future iterations. It should also be noted that the airfoil used for the VTP model is NACA0010, similar to the one used by Jindal[16] in the 2D wake blowing analysis. Table 4.2 gives all the major A320 specifications based on which the VTP was modelled.

Parameter	Value	Unit
Surface area	21.50	m
Height/Span	6.26	m
Aspect ratio	1.82	-
Taper ratio	0.303	-
1/4 chord sweep	34	deg

Table 4.2: Empennage(only VTP) geometry specifications[19]

4.3. BLI PROPULSOR SIZING CONSIDERATIONS

The APPU propeller was decided to be modelled as an actuator disk. For this purpose, two major specifications were needed, namely, the propeller location behind the empennage and the blade length. A ball park value for these parameters was worked on using some preliminary tail strike and wake progression analysis. A brief study had been performed in-house on this topic, as shown in Figure 4.4. It was decided to proceed with the data obtained with slight modifications to fit the already chosen fuselage geometry. The hub dimension used in the tail strike calculation are still under discussion and therefore, it was decided to chose the blade length information, with the current hub, to yield the propeller diameter. The resultant blade height came out to be around 1m. Also, since the fuselage cross-section at the propeller location is not completely circular, the maximum height of 1.8m was chosen as the hub diameter, resulting in an actuator disk diameter of 3.8m. Table 4.3 shows the propeller specifications for the take-off condition used in the study. The fan boundary condition used to model the propeller requires a pressure jump as input. The calculation of this pressure jump is addressed in Appendix B and will be further discussed in chapter 7.

Parameter	Value	Unit
Blade Length	1	m
Effective Disk Loading	8.2	kN/m^2
Operating mach	0.23	-
Rotational Speed(n)	1500	rpm

Table 4.3: BLI propeller geometry specifications

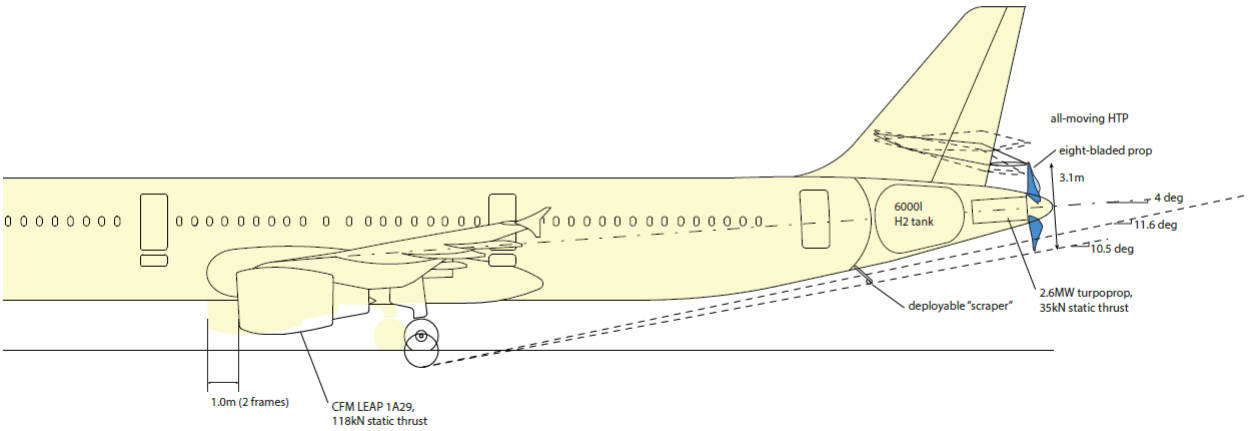

Figure 4.4: APPU design specifications and modifications as performed based on a preliminary calculation done inhouse in first design iteration(courtesy of Dr. R. de Vos)

5

COMPUTATIONAL SETUP AND PRE-SIMULATION ANALYSIS

The purpose of any computational work, specifically Computational Fluid Dynamics(CFD), is to provide an insight into the flow physics without actually carrying out the experiments which are not only expensive but also highly time consuming. For preliminary studies, such as the one presented here, it is better to get an idea of the flow behaviour using CFD tools before constructing a physical model to be tested in the wind tunnels, which is niether simple nor cheap. Computational methods are much less time and cost intensive and can resolve the basic flow physics with accuracy. However, real life physical phenomena are too complex to be modeled on virtual platforms, no matter how sophisticated they are. CFD simulation are constrained also by the various errors that can creep in due to mathematical assumptions, simplifications and solver choices. Nevertheless, for initial stage analysis, like the one presented in this study, the CFD methods work well. However, before diving into the analysis process, it is important to get an understanding of how these methods work. To start of, a typical modelling process will be described in section 5.1. This will include a description of the computational domain, governing equations, brief theory on near wall treatment useful during the near surface meshing procedure, operating flow conditions, chosen turbulence model, the choice of solver used for the simulations and finally, the boundary conditions. Following this, the meshing procedure will be laid down in section 5.2. A mesh convergence study based on a few preliminary results presented in section 5.3 will conclude this chapter.

5.1. COMPUTATIONAL MODELING: AN OVERVIEW

One of the most crucial steps of any computational model is the definition of the partial differential equations(PDEs) that are used to model the physical quantities of the flow. As can be seen in Figure 5.1, these PDEs, along with correct boundary conditions, are used to represent the physical system under consideration, in the best possible manner. However, the definition of these PDEs and boundary conditions bring along some assumptions and simplifications which contribute towards uncertainties and errors which need to be eliminated using experimental data.

The resultant equations are used to model a continuous system which can then be represented by the machinery in defined set of unknown values. It is this breaking of the continuous system into a set of nodes that is referred to as discretisation, in the computational world. Some of the most widely used methods by which this can be achieved are finite-difference, finite-volume etc. As mentioned before, each of these steps comes with associated errors. The errors that arise during the discreatization proceed are called discretization or truncation errors. The fundamental reason for these errors is hidden in the name itself, 'truncation'.

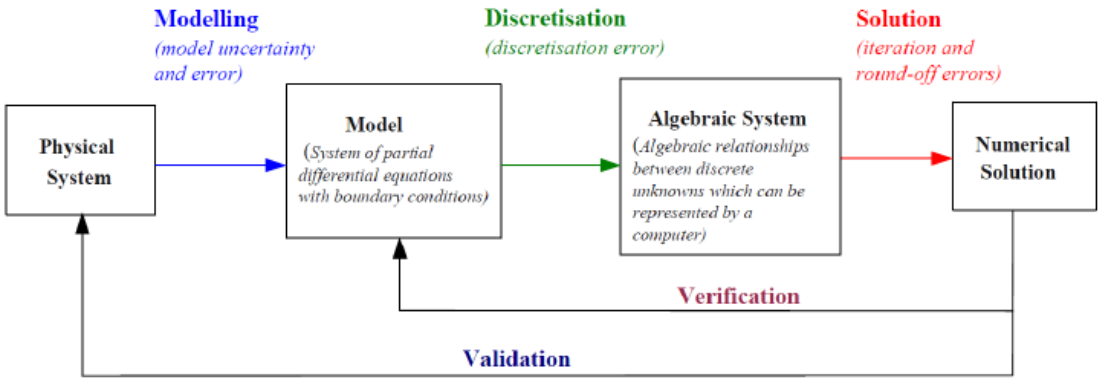

Figure 5.1: Basic computational modelling process employed in CFD[16]

To manage the complexity, time and resources required by this step, the higher order terms in the Taylor series, which is used to represent the continuous system, are truncated. This results in a discreet set of algebraic equations which the computers uses to iterate until a converged solution is obtained. For this iterative process, usually an initial guess estimate for the solution needs to be provided of the solution. The process then uses the obtained algebraic equations to correct this guess until the point the correction vector becomes small enough for the solution to be considered converged. Since, the correction vector can never reach an absolute zero, the process is usually stopped in between when the value is close enough to minimum. Some errors creep in due to this halt and are referred to as iteration errors. Also, the solution itself cannot be output with an infinite precision and needs to be rounded off at some point, thus leading to what are known as round-off errors. This final result can be verified using the initial solution of the assumed model equations and can then be validated with experimental data.

5.1.1. COMPUTATIONAL DOMAIN

Figure 5.2 shows the domain chosen for the simulations. Since only, half of the model needs to be simulated because it is symmetric about the xz-plane, the computational domain is also only restricted to the half geometry. Therefore, a hemispherical shape of the domain was chosen instead of a sphere. The preference of choosing the hemisphere as domain shape choice is because the flow would be simulated using a far field pressure condition. A rectangular or cuboidal domain is better suited for incompressible cases where a flow inlet and outlet needs to be specified or when there are slip walls like a road or conveyor belt, that needs to be simulated. Since the physical model is truncated with the outer domain boundaries, the far field pressure condition is used to define the flow at these boundaries. The flow inside this domain will be set up such that these far field conditions are always satisfied. More about the boundary conditions will be discussed in subsection 5.1.7. The far stream boundary is kept at 5 times the geometry length which in this case is taken as the fuselage length. This is done to prevent the occurrence of reverse flow due to back pressure. This corresponds to a distance of more than 35 times the maximum chord of the VTP. The boundary needs to be located far-enough downstream so that it does not influence the flow field upstream and allows the wake structure to fully develop. It should be noted that a larger distance between the model and the far-field boundary would be preferred. A larger distance is prudent for the cases when lifting surfaces like wing and horizontal stabilizers are included. However, in the current case, for the sake of computational cost and time, the domain has been confined to the mentioned limits. Nevertheless, it is assumed that the boundaries of the domain are extended sufficiently far away to neglect their influence on the results. Thus the velocity perturbations can be assumed to be negligible in the far field.

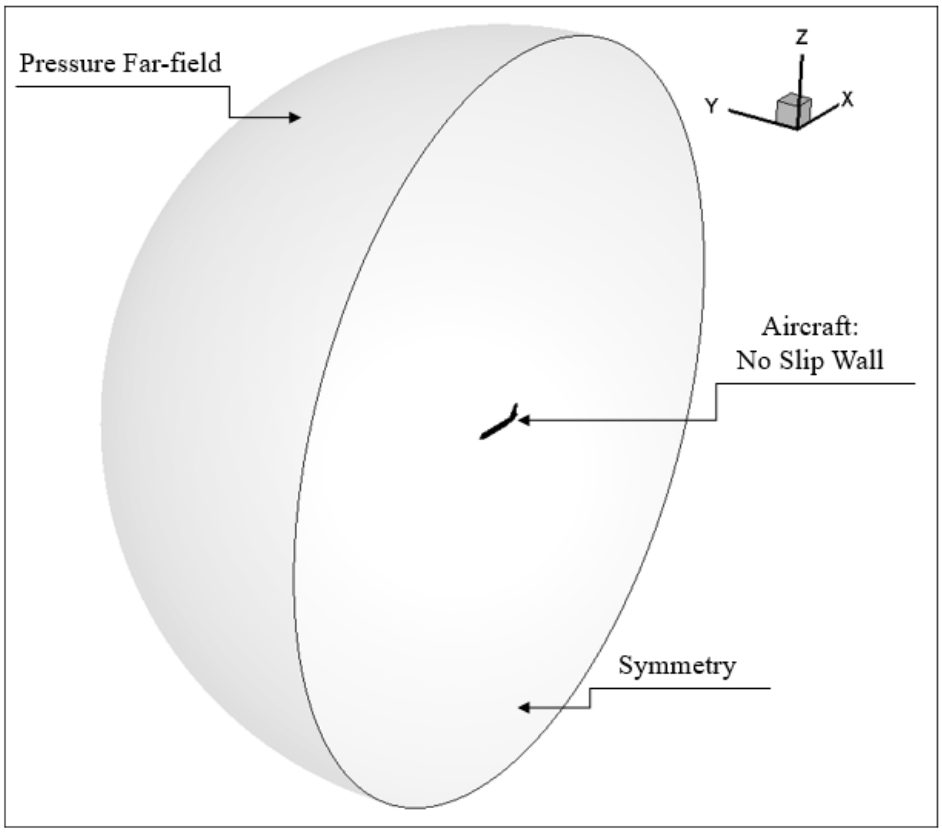

(a) 3D Hemispherical Domain with far-field and wall boundary conditions

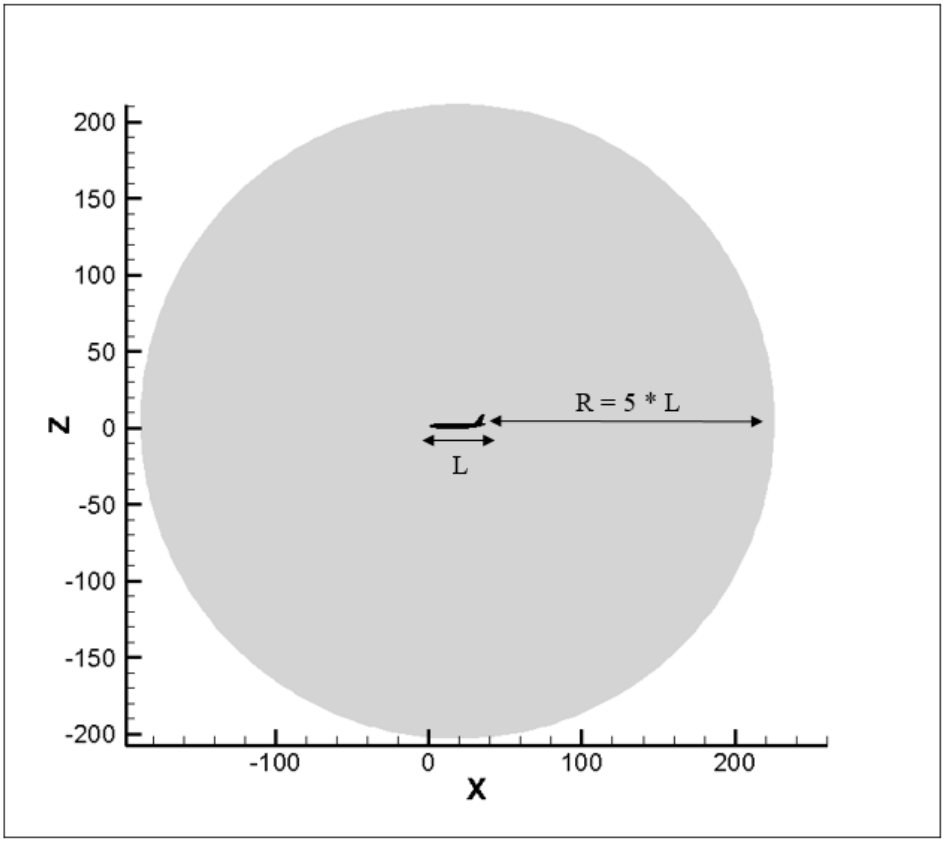

(b) Computations domain dimensions with respect to the geometry length

Figure 5.2: Computational domain and boundary conditions

5.1.2. GOVERNING EQUATIONS

As mention in the computational modelling description, PDEs are used to represent a physical model in mathematical terms. For fluid flows, the three principles of mass, momentum and energy conservation govern the flow and, their respective PDEs are required to model the flow. The problem at hand deals with a freestream Mach number of 0.23 which is low enough(M < 0.3) that the flow can be considered incompressible. Under this assumption the initial and boundary conditions can be used to define the solution well without the need of coupling them with the energy equation. However, the addition of the propeller increases the local flow Mach number beyond 0.32. Furthermore, the jet air injected at the blowing slots are of very high velocities ranging from 123m/s to 225m/s, depending on the case. Thus due to these factors, the assumption of incompressible flows is no longer accurate. Therefore, it is decided to move ahead with the compressible form of the PDEs where the density cannot be assumed to be constant and therefore cannot be taken out of the differentials. Now lets look at how the resultant PDEs look like for mass, momentum and energy[62–64].

CONTINUITY EQUATION:

Law of mass conservation says that *the increase of the total mass of the fluid in the CV is equal to the net mass flow into the CV + the formation rate of the fluid in the CV*[62, 65].
The mass conservation equation for a three dimensional, unsteady, compressible flow is commonly known as the continuity equation and is defined as follows:-

$$\frac{\partial \rho}{\partial t} + \nabla \cdot (\rho \mathbf{v}) = 0 \tag{5.1}$$

where,
ρ is the fluid density,
$\mathbf{v}$ is the velocity field

NAVIER-STOKES EQUATIONS:

The law of momentum conservation is the Newton's second law applied to Fluid Mechanics, which states that *the change of the total momentum in the CV + the exchange of momentum through the boundary of the CV is equal to the forces acting on the boundary + the body forces on the CV.*[62, 65]

The formulation for the equation for conservation of momentum is given in Equation 5.2.

$$\frac{\partial \rho \mathbf{v}}{\partial t} + \nabla \cdot (\rho \mathbf{v}\mathbf{v}) = -\nabla p + \nabla \tau + \mathbf{F} \tag{5.2}$$

where,
p is the pressure,
$\mathbf{F}$ are the body forces acting on the CV
τ is the viscous stress tensor, defined as

$$\tau = 2\mu \left(\nabla \mathbf{v} + \nabla \mathbf{v}^T \right) \tag{5.3}$$

where, μ is the molecular viscosity.

For the case of three dimensional flows, this equation can be expanded to a set of three separate equations pertaining to the conservation of momentum in the x, y and z directions. This set of equations is what is famously known as the Navier-Stokes equations, named after the french physicist Claude-Louis Navier and Anglo-Irish physicist and mathematician George Gabriel Stokes[63]. In the case of incompressible flows, these equations become simplified as the density moves out of the differentials, thus resulting in the equations that are commonly referred to as the 'Euler Equations'.

TOTAL ENERGY EQUATION:

The law of energy conservation is the first law of thermodynamics which states that *the energy increase in a system is equal to the heat transfer from the environment to the system - work done to the system.*[62, 65]

As mentioned earlier, this equation if of prime importance when dealing with viscid flows and cannot be decoupled from the mass and momentum equations. This added transport equation ensures a thermodynamic equilibrium in the system, meaning that the increase of internal energy of the fluid is equal to the difference of the energy extracted from or added to the fluid and the work done by the fluid.

$$\frac{\partial}{\partial t}\left[\rho\left(e+\frac{1}{2}u^2\right)\right]+\nabla\cdot\left[\rho\mathbf{v}\left(e+\frac{1}{2}u^2\right)\right]=\nabla\cdot(k\nabla T)+\nabla\cdot(-p\mathbf{v}+\tau\cdot\mathbf{v})+\mathbf{v}\cdot\mathbf{F}+Q \tag{5.4}$$

where,
e is the internal energy per unit mass,
k is the thermal conductivity,
T is the temperature,
Q is the internal heat energy of the system.

5.1.3. OPERATING CONDITIONS

Before diving in to the details of solver approach and making a choice on the solve and turbulent model selected for the current work, it would be helpful to know the operating conditions for which the current simulations will be performed. Table 5.1 gives an overview of the flow conditions which will be used. These are based on the take-off conditions for the A320. The flight speed is 79.83m/s corresponding to a take-off Mach number of 0.23. This leads to an operating Reynolds number of $2x10^8$ for the A320 fuselage of length 37.57m. It should be noted however that no angle of attack as been modelled so as to avoid too many physical phenomenon overlapping with each other. However, it is recommended to further continue this research in future in that crucial direction. The take-off conditions were chosen in order to simulate ground based condition, since one of the main aims of the APPU project is to limit the ground emissions to minimum. The standard ambient pressure and temperature were assumed along with an air density of $1.225 Kg/m^3$.

Parameter	Symbol	Value	Unit
Reynolds Number	Re	$2x10^8$	-
Free-stream velocity	U_∞	79.83	m/s
Atmospheric Pressure	P	101325	Pa
Density	ρ	1.225	kg/m^3
Temperature	T	298	K

Table 5.1: Operating conditions for the CFD simulations based on take-off ground conditions

5.1.4. SOLVER APPROACH AND CHOICE

The flow under consideration is of high Reynolds number and therefore, can be considered turbulent in nature. Turbulent flows can be analysed using three most used approaches: statistical, structural and deterministic. Statistical approach assumed that less is known about the details of turbulent flows from a practical standpoint and therefore, focuses on resolving the statistical behavior for solving and understanding the problem under consideration. The structural method on the hand, makes use of both experimental and numerical approaches to understand the underlying flow behavior. The importance of experimental aspect of the study lies behind the fact that velocities show correlations between different spatial and temporal positions. Lastly, the deterministic approach views turbulence as a chaotic solution to the Navier-Stokes equations which need to be resolved in pursuit of understanding the underlying physics and patterns.

Three deterministic methods are widely used to resolve flows for practical applications: Direct Numerical Simulation(DNS), Large-Eddy Simulations(LES) and Reynolds-Averaged Navier-Stokes(RANS) method. The DNS methods resolves all the time and length scales of the turbulent flow. In order to achieve this, a high temporal and spacial resolution is essential. This makes the DNS method highly expensive in terms of computational time and resources. For this reason, the use of DNS solvers is usually restricted to simple flows with low Reynolds numbers. In order to overcome this limitation and reduce the computational cost, the LES method can be used. Under this method the focus is kept on the larger scale eddies of the turbulent flow assuming that they are the most affected by the geometry and boundary condition. The effects of the smaller scales are taken to be more local and are unresolved. To distinguish which scales need to be resolved and which can be considered small enough not to be, a filtering system is used to separate the resolved and the unresolved scales. While many flow problems can be studied using LES, like flow transitions and separations, the approach is still in a fundamental research stage[66]. Furthermore, the computational cost, although lower than DNS, still remains a point of concern[67].

The most widely used method is the RANS methods by Reynolds[68]. This method is based on the observation that turbulent flows can be characterised by quantities represented in terms of their averages and fluctuations, where the time average part is of most physical interest. As a result, the NS equations are decomposed into mean and fluctuating parts, where the mean part is free of unknowns, leading to the averaged form of the NS equations. The effect of the fluctuations is then defined by additional models known as 'closure-models', named so because they are used to form a closed system of equations. This method yields comparatively good results for most practical applications at a much less computational cost.

For the current project, involving high Reynolds number flow with focus on the wake of the geometry, it was decided to choose RANS as the method of choice. This choice was made because RANS solutions work well for steady state problems and no large unsteady behaviour is expected in the problem at hand. Since the main interest lies with the mean velocity and pressure profiles in the wake region, the flow turbulence can be accounted for by modeling the fluctuations. As RANS is the chosen method of the current thesis, it is important to look a little deeper into its formulation.

REYNOLDS-AVERAGED NAVIER-STOKES(RANS) METHOD

The RANS model makes use of the decomposition of the instantaneous velocity flow field into the mean and the fluctuating parts. Thus the flow velocity can be represented as :

$$u = \overline{u} + u' \tag{5.5}$$

Using the incompressible form of RANS equations and applying the above definition for velocity to it, assuming no additional body forces, leads to the following formulation:

$$\rho\left[\frac{\partial \overline{u_i}}{\partial t} + \frac{\partial(\overline{u_i u_j})}{\partial x_j}\right] = \frac{\partial}{\partial x_j}\left[\mu\frac{\partial u_i}{\partial x_j} - \rho\overline{u_j' u_i'}\right] - \frac{\partial \overline{p}}{\partial x_j} \tag{5.6}$$

The appearance of additional shear stresses are due to the velocity fluctuations. These are commonly known as the Reynolds stresses. The closure models are used to define these non-linear stress terms. The chosen model for the current work has been described in subsection 5.1.5.

The velocity gradient term in Equation 5.8 can be divided in to symmetric and anti-symmetric parts which define the rate of strain deformations[69], as shown in Equation 5.7. The strain rate of deformation gives information on the shear stress and rate of rotation caused for a given vorticity in the flow, $\omega = \nabla x u = 2\Omega$.

$$\frac{\partial u_i}{\partial x_j} = S_{ij} + \Omega_{ij} = \frac{1}{2}\left[\frac{\partial u_i}{\partial x_j} + \frac{\partial u_j}{\partial x_i}\right] + \frac{1}{2}\left[\frac{\partial u_i}{\partial x_j} - \frac{\partial u_j}{\partial x_i}\right] \tag{5.7}$$

Substituting this in the RANS equation Equation 5.8:

$$\rho\left[\frac{\partial \overline{u_i}}{\partial t} + \frac{\partial(\overline{u_i u_j})}{\partial x_j}\right] = \frac{\partial}{\partial x_j}\left[2\mu\overline{S_{i,j}} - \rho\overline{u_j' u_i'}\right] - \frac{\partial \overline{p}}{\partial x_j} \tag{5.8}$$

5.1.5. TURBULENCE MODEL

As described in the definition of RANS equations, the turbulent properties of the flow are modeled by the fluctuations in the velocity flow-field. Additional turbulence models are required to describe the resultant non linear Reynolds Stresses which can be represented by τ_{ij}, described as follows:

$$\tau_{ij} = -\rho\overline{u_j' u_i'} \tag{5.9}$$

This leads to an addition of six stress terms which are unknown and require special models to be resolved. A lot of models have been developed over the years with strengths and limitations of their own. However, the most commonly used models are the Linear Eddy-Viscosity Models(LEVM) which are based on the Boussinesq hypothesis[70] which related the Reynolds stress term with the mean flow velocity gradients, as given in Equation 5.10. Majority of the turbulence models like Spalart Allmaras(SA) model, $k-\omega$ model and $k-\epsilon$ models, are based on the same hypothesis.

$$\tau_{ij} = \mu_t\left(\frac{\partial u_i}{\partial x_j} + \frac{\partial u_j}{\partial x_i}\right) = 2\mu_t S_{ij} - \frac{2}{3}\rho k\delta_{ij} \tag{5.10}$$

where, μ_t is the turbulence viscosity. Although, the turbulence viscosity is not a constant but a spatially varying quantity, it can be assumed to isotropic along the different directions. This means that the Reynolds stresses are assumed to be isotropic in all directions. This assumption used in LEVMs yields good results with reasonable accuracy at a considerably low computational cost. However, for more complicated flows involving swirls or strong flow separation etc., the isotropic assumption does not hold true. For such flows, the normal and secondary shear stresses are not well resolved using the LEVMs. However, such complex phenomena are not expected in the current work and therefore, the LEVMs approach works well. Since the main focus of the current research is on the wake of the empennage, the question is that which of the turbulence models available in Fluent is best able to capture this wake. A detailed analysis was performed by Jindal[16] to see the proficiency with which the different turbulence models are able to predict the wake. It was found out that the Spalart Allmaras method was the most efficient in predicting the wake. Therefore, the current research chooses the SA method as the preferred turbulence model and works under the assumption that the SA method predicts the wake well.

SPALART ALLMARAS

The Spalart-Allmaras model[71] is a one-equation model that solves a modeled transport equation for the kinematic eddy (turbulent) viscosity. The SA model was designed specifically for aerospace applications involving wall-bounded flows and has been shown to give good results for boundary layers subjected to adverse pressure gradients[72]. It uses the following transport equation to model the turbulence viscosity:

$$\frac{\partial}{\partial t}(\rho\tilde{v}) + \frac{\partial}{\partial x_i} = \frac{1}{\sigma_{\tilde{v}}}\left[\frac{\partial}{\partial x_i}\left((\mu+\rho\tilde{v})\frac{\partial\tilde{v}}{\partial x_i}\right) + C_{b2}\rho\left(\frac{\partial\tilde{v}}{\partial x_i}\right)^2\right] + C_{b1}\rho\tilde{S}\tilde{v} - C_{w1}\rho f_w\left(\frac{\tilde{v}}{d}\right)^2 \tag{5.11}$$

where, $\tilde{v}$ is the turbulence viscosity μ, apart from at the regions near the wall. The last and second to last terms of Equation 5.11 represent the turbulence destruction and production respectively. This specific definition has been presented by Bradshaw[73], however, many other formulation can be found in the literature. The model is limited in its capability to resolve free shear flows and turbulence decay. However, being one equation model, it is computationally less intensive and provides fairly accurate results for aerodynamic flows without very high complexity. For further detail into the workings of the SA model in Fluent, the reader is referred to open literature[72].

5.1.6. WALL MODELLING

Turbulent flows, like the one under consideration, are highly sensitive to the geometry wall. Not only is the flow velocity zero at the wall surfaces due to the no-slip condition, the viscous damping of the flow near the wall leads to a region of high gradients for pressure and momentum. To capture the flow physics in these regions with sufficient accuracy, special care needs to be taken while meshing. The purpose of this section is to assist in the same by providing the required theoretical insight.

The boundary layer near the wall consists of layers. The innermost layer, referred to as the 'viscous sub-layer' contains the flow which is almost laminar in nature. The transfer of momentum and mass are largely governed by the molecular viscosity in this region. The outer 'fully turbulent' layer, as the name suggests, is dominated by the presence of turbulence in the flow. Naturally, the layer in between these two, will be impacted by both the molecular viscosity as well as the turbulence, thus leading to a smooth transition between the innermost and the outermost layers.

To measure the turbulent length scales in the viscous sub layer, 'wall units' are used. Note that the mean of streamwise gradient of the flow is rather small. Thus, the inverse of the mean of wall vorticity, as given in Equation 5.12, can be used to define the time scale for this viscous sub-layer.

$$t_v = \left(\frac{\partial\overline{u}}{\partial y}\Big|_{y=0}\right)^{-1} \tag{5.12}$$

where u is the mean streamwise velocity and y is the coordinate measured normal to the wall.
The viscous length scale is usually described as $l_v = \sqrt{\nu t_v}$, for which the friction velocity can be defined as follows:

$$u_\tau = \sqrt{\frac{\tau_w}{\rho}} \tag{5.13}$$

This allows the earlier mentioned wall units to be used in defining the local velocities and lengths near the wall as:

$$u_+ = \frac{u}{u_\tau} \tag{5.14}$$

$$y_+ = \frac{y u_\tau}{\nu} \tag{5.15}$$

Figure 5.3 shows the different sub-layers of the boundary layer based on the distance from the wall, represented in terms of y^+ values. The viscous sub-layers is usually defined in the region with $y^+ < 5$. This is due to the fact that the viscous forces are the most dominant up to this point. Beyond this point however, the vortical effects, due to the turbulence, are just as important. This buffer layer is where most of the turbulence in the flow originates. Extensive research in the past has shown that the buffer layer usually extends to a y^+ of 60. Beyond this layer is the fully turbulent layer. From the Figure 5.3(a), a formulation for the mean velocity present in the viscous sub-layer can be seen as $u^+ = y^+$. This holds true only for the viscous sub-layer. For the intermediate layer, beyond $y^+ > 5$, the mean velocity is a function of the wall unit and can be given using the formulation in Equation 5.16.

$$\overline{u}^+ = \frac{1}{\kappa} ln y^+ + B \tag{5.16}$$

where, κ and B are the Karman constants whose values based on experimental data are 0.4 for κ and in the range from 5 - 5.5 for B

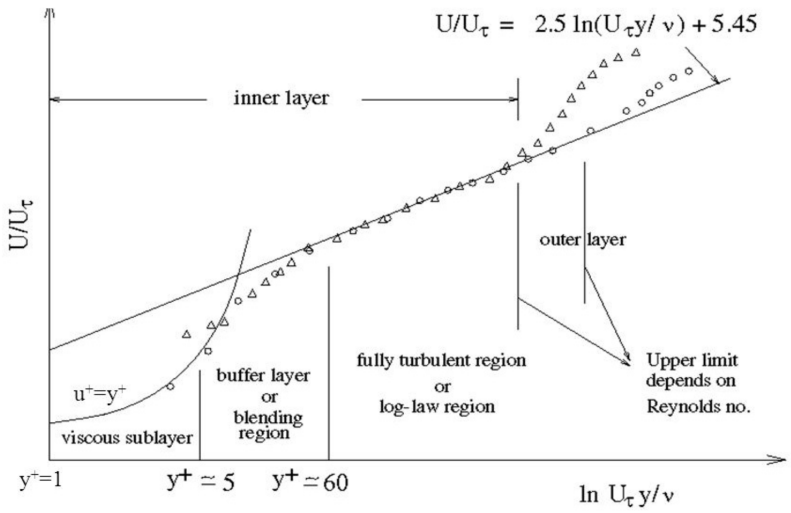

(a)

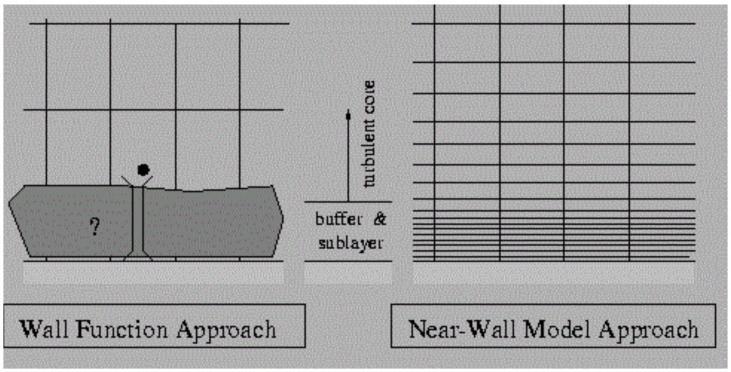

(b)

Figure 5.3: (a)Near wall region represented on a semi logarithmic with important divisions based on y^+ values [17], (b)Basic representation of the approach used in fluent to model the near wall region using inflation layers[16]

Now that the importance of wall units has been established, it is crucial that the region near the wall is meshed and computed with enough accuracy to capture the turbulent flow physics. Fluent offers two methods of achieving this feat. These are graphically presented in Figure 5.3(b). In the first approach on the left, referred to as the 'Wall Function Approach', the idea is that the inner layers of the boundary layer, which consists of the viscous sub-layer and the buffer layer, are not resolved with a highly fine mesh but are instead modeled using "Wall Functions". The wall functions are semi-empirical equations which are used to model the viscous effect of the inner viscous layer and the outer turbulent layer and close the gap between the two. This method is of particular attraction for high Reynolds number flows since the use of wall functions can reduce the computational time significantly due to the fact that the changing flow variables in the viscosity dominated region close to the wall($y^+ < 30$) are not resolved.

The second method, resolves these inner viscous layers. For this method, flow near the wall is subdivided into two parts, the viscosity dominated region and the fully turbulent region. A wall based Reynolds number is used to differentiate between the two. Consequently, the flow variables in each of these two regions are modelled using a different turbulence model. Proper capture of the viscous sub-layer required for this approach leads to a requirement of a highly refined mesh near the walls which puts a high strain on the computational resources and time.

The choice between the two models is subjective to the case being modelled and is also greatly influenced by the choice of turbulent model. Therefore, a method will be decided based on the turbulence model is chosen in subsection 5.1.5

5.1.7. BOUNDARY CONDITIONS

This section will describe the various boundary conditions applied over the computational domain boundary, some of which were shown in Figure 5.2. The first condition to consider is the far-field condition on the domain outer wall. A *pressure far-field* condition was applied to the domain outer boundary. This was chosen because it fairs better for compressible flow calculations where the density is given by the ideal gas law instead of being kept constant. This is also the reason why velocity inlet or pressure outlet conditions, which are specifically designed for incompressible flows, were not chosen[72]. Although the current operating condition for the flow is Mach 0.23 which is lower than 0.3, which is the usual threshold for incompressible flow, the research involves high velocity jet blowing inlet and also an addition of the propeller which will raise the local flow to compressible regime. Thus, a pressure far-field condition was a more logical choice. This was also mentioned in subsection 5.1.2 while describing the choice for compressible flow PDEs. The turbulence viscosity ratio, which can vary between 1 to 10 was kept to a default value of 10[16].

Also, since the geometry is symmetric about y-plane, only half of it is used for the simulation in order to reduce the computational time. Therefore, a *Symmetry boundary condition* was applied at the symmetry plane. Next, the fuselage and empennage walls were modelled using the *No-slip wall* condition making the velocity at the wall to be zero for viscous flows. Now, the remaining two important conditions, for the jet inlet and the propeller addition, need to be described. The blowing inlet was specified as a *Velocity Inlet boundary* for the blown configurations. It introduces the high speed jet inflow to the mean flow. Lastly, the BLI propeller was modeled in the fan-on configurations using the in-built *Fan Boundary Condition* of Fluent. The Fluent fan model is a lumped parameter model that is used to simulate the effect of a fan with known specifications on the overall flow field. With the fan model it is possible to specify an empirical fan curve that governs the relationship between pressure rise and velocity flow rate across the defined fan surface. However, for the current work, a constant pressure jump was supplied to model a close to actuator disk model. It is also possible to specify a swirl component to the flow by specifying radial and tangential components of the fan swirl velocity. However, to keep the flow complexity limited and prevent the interference of various complex physical phenomena, no swirl was imparted to the fan. It is not possible to model the fan blades using the fan model. It simply predicts the amount of flow through the fan. For a detailed explanation of the formulations involved in the model, the reader is again referred to Fluent user guide[72].

5.1.8. SOLVER SETTINGS

This section will describe all the remaining settings that were used in Fluent for the final simulations. The sensitivity of the results for the choice of the solution methods that will be mentioned in this section, has already been established in literature[16, 60, 69] and is therefore, not investigated as part of this thesis.

As described earlier, a steady RANS simulation is employed in this thesis to compute the mean velocity of the flow around the geometry. The numerical equations can be solved using two methods that are provided within Fluent. These are the Pressure-based and Density-based methods. A pressure based solver is used for the current work since the Mach numbers involved are low subsonic. Initially, the pressure-based approach was developed for low-speed incompressible flows. However, the method has been extended and reformulated to solve and operate for a wide range of flow conditions beyond its original intent. Therefore, it is the chosen solver since only parts of the flow, like the blowing jet and the propeller streamtube, will exhibit high speed compressible behaviour which can be handled by the Fluent pressure based solver. In both solvers, the velocity field is obtained from the momentum equations. In the density-based approach, the continuity equation is used to obtain the density field while the pressure field is determined from the equation of state. On the other hand, in the pressure-based approach, the pressure field is extracted by solving a pressure correction equation which is obtained by manipulating continuity and momentum equations[72]. An iterative process is required to reach the final converged solution since the continuity and momentum equations are coupled. A coupled algorithm for the pressure based solver is used for the current work. The iterative process for a coupled algorithm is faster than a segregated algorithm but at the cost of a higher memory requirement since solutions for both the equations need to be stored at the same time.

Now, to convert the transport equations to algebraic form, a control volume based discretization is employed in Fluent. The scalar flow variable values are described at the cell centre and then interpolated to get the values at the cell faces. The gradients of the scalar variables that are used to discretize the convection and diffusion terms, were calculated using the Least-Squared cell based method. A second order discretization scheme was used for pressure, modified turbulent viscosity and energy. The viscosity itself is modeled using the Sutherland's law[74]. The density and momentum equations were interpolated using a third order MUSCL scheme[72] to achieve a higher accuracy for the numerical solution. A hybrid solution initialization was done followed by the solution iterations. For a more detailed description into these methods and their formulations, the reader is referred to the Ansys Fluent theory guide[72].

Having established the methodology for the the current thesis and finalised the geometry specifications for the fuselage, empennage and the wake blowing system, the next step is to generate a mesh and perform a the mesh convergence study in order to chose a mesh capable of capturing the important physical phenomena of the flow, for the final simulations. Following section will describe the details of the mesh domain and lay down the meshing process. Finally a mesh will be chosen based on some preliminary results, to be used for the further simulations.

5.2. MESHING PROCEDURE

The selected geometry was prepared for the meshing procedure using the SpaceClaim tool[75] provided by Ansys. Here, the domain was constructed around the fuselage-empennage geometry. The hemispherical domain, created around the geometry can lead to a large number of cells if the refinement and cell size growth away from the aircraft surface is not properly defined. Care has been taken to avoid exponential increase in cell size due to absence of requirement away from the aircraft geometry. In order to minimize the computational load and to focus the meshing on the regions near the model, the main domain has been divided into smaller sub domains depending on the proximity to the geometry surface and desired regions of high refinement, as shown in Figure 5.4. This allows the cell size in the vicinity of the model and the wake to be refined further, while the surrounding flow is captured with less detail.

The larger hemispherical domain is divided into three parts. First, is the Innermost Domain, which is a rectangular domain with close proximity to the geometry surfaces. The edges of this domain are 2m from the closest surface on all sides. This region will have high refinement in order to accurately model the important flow physics in the fuselage-empennage structure vicinity like the fuselage-empennage junction flow and the development of wake of the empennage. An example of the refined mesh in the innermost region is shown in Figure 5.6. Second, are the set of 8 cuboidal blocks around the inner domain which will act as the transition zone from the fine inner mesh to the coarser outer mesh. These will not be as refined as the inner domain mesh but still have to be of small enough size to capture the potential flow effects and the effects of the propeller in fan-on configuration. Therefore, these blocks extend to at least 10 times the length scale of the mesh

elements specified in this region. It is assumed that this will provide a good transitional length from the inner to the final outer domain. It should be noted, that in general the growth rate between cells is kept to the default value of 1.2. Thus this automatically avoids any large jumps in the cell volumes while going from cell in one region to another. However, these transitional domain blocks will restrict the growth of the cells at the given value of cell size within the blocks, thus preventing the mesh elements from getting too large near the geometry. Finally, the rest of the remaining spherical domain will be coarsely meshed to conserve computational time and resources. Structures like vortices in the wake grow rapidly in size as they move downstream. Thus a coarser mesh is acceptable, as the gradients in the flow properties are relatively small in these areas.

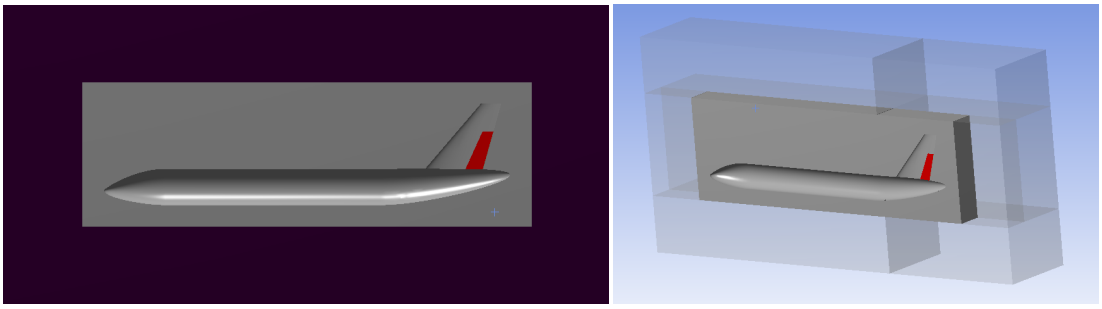

(a) (b)

Figure 5.4: Division of the computational domain into smaller sub-domains near the geometry for higher control over the meshing in different regions

One more domain, within the inner most domain, was set-up. This is known as the body of influence in the Ansys Mechanical terms[76]. The body of influence has been used in the current work to refine the region of most importance to the current study, which is the empennage wake region. Since, the focus will be kept on the wake filling capabilities of the wake blowing mechanism, it is important that the wake is captured with high accuracy. Therefore, a thin rectangular body, as shown in Figure 5.5, has been superimposed over the wake region of the model empennage which will restrict the element size in that region to an even finer value as compared to the already refined inner domain. The BOI is used instead of specifying a smaller domain size for the whole inner domain to conserve computational resources because with the reduction in element size, the corresponding increase in the mesh size, and therefore computation resources, is high.

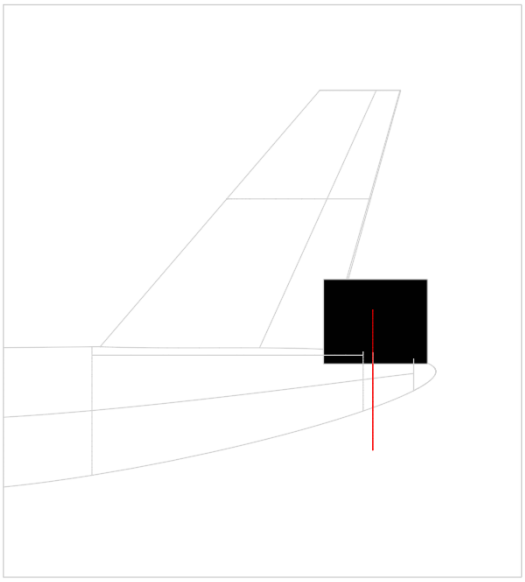

Figure 5.5: Depiction of the wake body of influence(BOI) used to locally refine the empennage wake flow to capture the wake properties with better accuracy

Figure 5.6 shows the surface mesh for the aft part of the geometry where the focus of the current work lies. Surfaces of the geometry were meshed structurally to aid in faster convergence of the solutions and yield more accurate results. The red line shows the location of the blowing slot. Care was taken to keep the surface cell size, upstream and downstream of the slot, to be same. The fuselage surface mesh was slowly increased in refinement towards the propeller location and the aft cone in order to capture the effect of the wake blowing mechanism and the propeller on the geometry surfaces with more accuracy. A good surface mesh also helps in achieving more accurate force coefficient values which will be later on shown to be one of the solution convergence criterion.

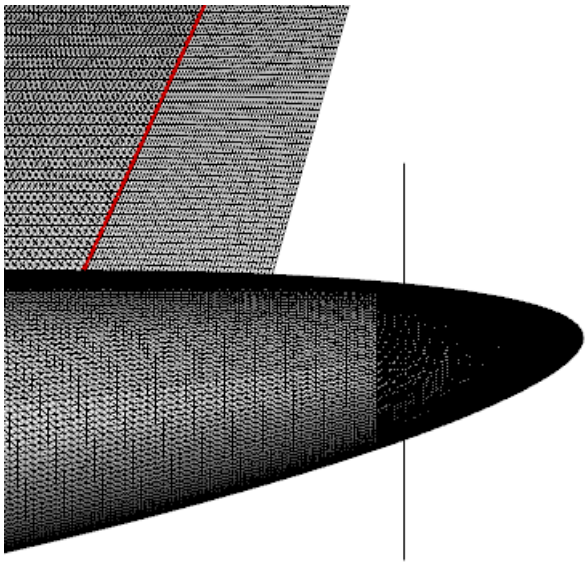

Figure 5.6: Close-up view of the structured surface mesh on the empennage surface upstream and downstream of the blowing slot(red line) and on the fuselage aft cone

The next point to be taken into consideration while meshing is the near wall mesh since it this region which will capture the wall boundary layers and govern the development of flow close to the model surfaces. The theory on near wall meshing and their role in facilitating the turbulence models to resolve the boundary layer has already been discussed in subsection 5.1.5 and 5.1.6. To achieve this with Ansys Mechanical software[76], the feature of prism layers were used. It is here that the wall units discussed in section subsection 5.1.6 will come into effect. The value of the desired wall units govern the first prism layer height. The choice for the ideal wall unit value is also dependant on the turbulence model itself. As discussed in section subsection 5.1.5, the Spallart Almaras method is chosen for this thesis. Although, a usually preferred value of $y^+ = 1$ is also suggested for the SA model[71], the robustness of Fluent provides flexibility to the user with the choice of y^+ value[72].

Originally, the SA model was developed for low-Reynolds number flows, requiring the viscosity-affected region of the boundary layer to be properly resolved. In the current version of Ansys Fluent, the SA model has been extended to a y^+ insensitive wall treatment model. This gives the software an added feature of modelling flows independent of the near-wall y^+ resolution. In order to achieve this, the inherent formulation for the wall treatement switches from a viscous sublayer formulation to a logarithmic based formulation depending on y^+ value. On grids with y^+ varying from 1 to 30, the model remains robust and provides consistent values for wall shear stress and heat transfer coefficients[72]. However, it should be kept in mind that although, the model is robust for these high values of y^+, in order to maintain its integrity, it should be ensured that the model boundary layer is still resolved with a resolution of 10-15 cells or more. For the current model, defining a value for y^+ was not so easy. Ideally, a constantly varying y^+ would be desired to capture the boundary layer

in the best way possible, however a uniform prism layer mesh has been applied to ensure smooth transition of prism layers at different locations and to reduce grid complexity.

Care needs to be taken while meshing the prism layers on and near the blowing slot. This is because the absolute height of the slot, even for the maximum slot height case, remains below 6.5mm. This leads to highly skewed prism layer elements at the blowing slot step since the mesh elements have to accommodate two 90%, edges at a distance of a few millimeters. Only the first few prism layers are generated with acceptable skewness levels. However, they are neither enough to capture the boundary layer or the blown jet nor are they orthogonal. Also, the velocity gradient of the flow near the slot region will be large due to the addition of the blown jet flow. Thus, the quality of the cells involved in this region needs to be high. To overcome this issue, it was decided to model the geometry as a clean empennage configuration(ie. without the slot), while modeling the slot cavity separately. This had two positive effects. Firstly, since the slot cavity in the VTP is now modelled as a separate body, it is possible to have a structured volume grid in this cavity because it is largely cuboidal in shape. This is desirable as it will enhance the accuracy with which the blowing slot jet flow will be captured and will also have a positive effect on the time taken for solution to converge. Secondly, this allows the prism layers to be modelled over the clean empennage surface, thus avoiding the sharp bends at the slot location. The important point to note here, is that the transition of the mesh from the slot cavity body to the prism layers needs to be smooth, orthogonal and without high volume jump. Thus, to adhere to these requirements, it was decided to choose an estimate for y^+ value such that the first layer height of the prism layers matches the last layer of the structured mesh of the slot cavity. A horizontal cross-section of the mesh at the empennage surface depicting this transition from the slot mesh to the prism layers is shown in Figure 5.7. Due to refinement constraints in the slot body in order to conserve computational time, this meant that the first layer height of the prism layers had to be $1.6e^{-4}m$. This corresponds to a y^+ value estimate of 25[77]. However, as established before, this high value of y^+ is permitted with the current version of Ansys Fluent. With this y^+ the boundary layer could be captured with around 25-30 prism layers for a prism height growth ratio of 1.18. Therefore, to be on a safe side 30 layers have been used in all the final meshes.

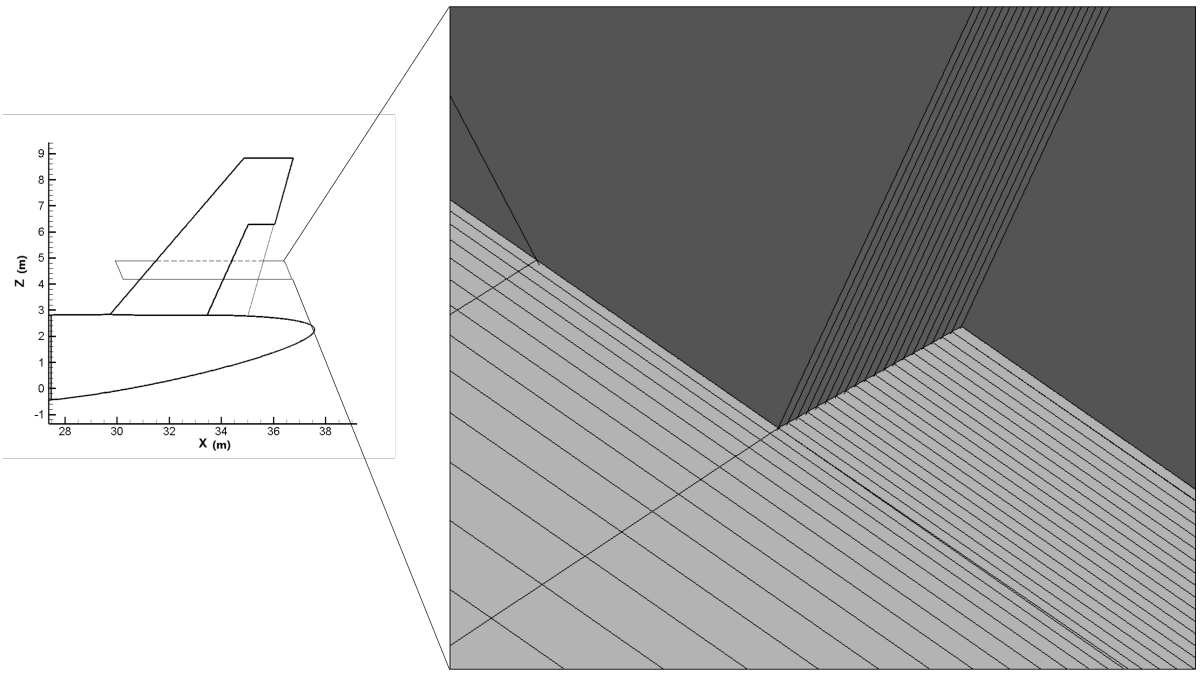

Figure 5.7: Smooth mesh transition from the blowing slot surface and cavity mesh to the outer volume mesh

5.3. GRID CONVERGENCE AND DEPENDENCY STUDY

Two points of concern that need to addressed in any CFD study are the convergence of the solutions for a given mesh and the dependency of the results on the mesh itself. While the former deals with making sure that the chosen grid is able to yield meaningful steady state solutions to the flow problem, the latter addresses

the influence of grid refinement over the converged values themselves. Therefore, the first objective should be to ensure that the selected mesh and solver settings are able to yield a converged solution, followed by a dependence study to arrive at a refined enough mesh that predicts these solutions with desired accuracy.

To study the mesh convergence, a common method is to analyse the residuals of the PDEs. A threshold value can be set for the residuals to govern when the residuals are low enough to consider the solution converged. However if the threshold is not low enough, it can result in premature acceptance of the solutions. This is due to the fact that in Ansys Fluent, these residuals are scaled and hence are highly sensitive to the relaxation factor. In the cases where a high relaxation factor is used, the residuals will drop quicker which can lead to a false impression of solution convergence. Therefore, it is better to analyse the coefficients of force instead. If the values of the selected force coefficients, whether lift or drag coefficient or both, stops changing, the solution can be assumed to have been converged. For the current case, both the lift and drag values were analysed. The convergence criterion for both of them are as follows:

- $\Delta C_D \leq 1E-5$
- $\Delta C_L \leq 1E-5$

For both the coefficients, the convergence condition was met around 2000 iterations. The corresponding values of the residuals, if still large and stabilising, means that the numerical errors have hindered further convergence of the results. While if they are very small and still reducing, then it can be assumed that the solution has converged and reached steady state. The value used to define the threshold for the residuals in current simulations was $R_i \leq 1E-7$. These criterion were met for most meshes under consideration, at around 7000 iterations or even earlier in case of highly refined meshes. Figure 5.7 shows the convergence for lift and drag coefficients for the three best candidates for the final mesh. The description of these meshes and the rationale behind choosing them is discussed in the following paragraphs along with the mesh dependency study.

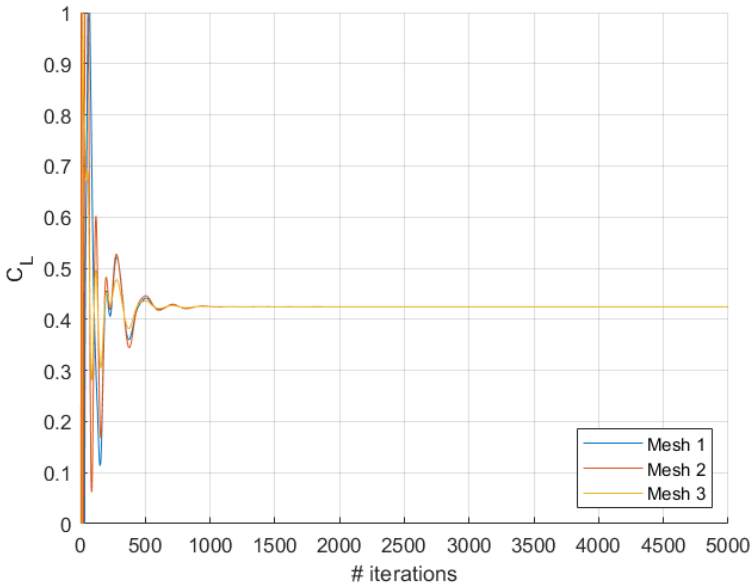

(a)

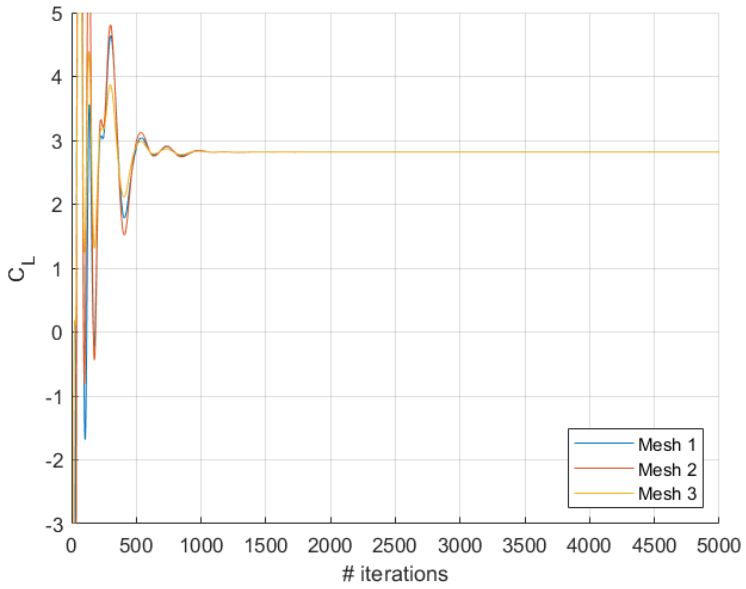

(b)

Figure 5.7: Solution convergence history for the (s)lift and (b)drag coefficients for the three best candidate meshes

Now that the procedure for determining the convergence of a mesh is established, a final mesh needs to be chosen for further simulations. This is where the importance of grid dependence study lies. Although, grid convergence is an indication for achieving viable solutions, the accuracy of the solutions is not defined. Even the really coarse grids lead to a converged solution but the values of the converged lift and drag coefficients were highly varied as compared to a finer mesh. This variation in the values started to reduce as the grid became refined enough to capture the relevant physics of the flow more accurately. However, to conserve computational time and resources, a trade off should be made between the accuracy of results and available computational resources.

A number of mesh refinements were made in order to improve the solution accuracy. To study the solution accuracy, three final meshes were shortlisted based on the level of refinement. It was found out that the solution was most sensitive to the inner domain refinements, the surface mesh refinement of the geometry and the element size in the wake BOI. Mesh 1 is the first refined mesh iteration where further refinement did not lead to significant changes to the force coefficient. This mesh consisted of 26 million cells due to high refinements in inner domain. It was decided to compare the converged solution of this mesh with two further iterations of meshes, Mesh 2 and 3. In Mesh 2 the BOI used to capture the wake was further refined from an element size of 0.01m to 0.005m. This increased the mesh size to 31 million cells. It should be noted that since the wake region is refined using the BOI to focus on the affected empennage wake in the final simulations, it is important to establish that the wake profiles themselves are not much affected by the grid refinement. Therefore, along with the force coefficients, a plot for the non dimensionalized wake velocity was plotted at the prospective propeller location at 75% of the chosen blade radius. This location was chosen since the empennage wake will potentially affect the highly loaded part of the propeller blade the most due to flow uniformity.The plot for the wake velocity profiles are shown in Figure 5.9.

The final Mesh 3, goes even further by using a refined BOI element size of 0.003 to analyse the affect on the empennage wake. However, this is not the only refinement addition in Mesh 3. The surface of the empennage has also been further refined to analyse the effect on the boundary layer over the wall downstream of the slot since this will affect how the wake develops, see Figure 5.8. The final size of this mesh came out to be 48 million cells, which is extremely high and needs high amount of computational resources. However, as seen in the Figure 5.7 and 5.9 and the corresponding values of force coefficient and minimum deficit velocity values in Table 5.2, the further refinement of the mesh had small to negligible effect. The values of the lift and drag coefficients only show a change in the fifth decimal places and can be thought of as constant for the

three meshes. Also, the minimum wake deficit velocity values only show a difference from Mesh 1 values by -0.4% and -0.08% for Mesh2 and 3 respectively. These differences are so small that the concern is shifted to the penalty in terms of computational time and resources that is required to achieve such precision. A plot showing the average time required per iteration for different mesh sizes is shown in Figure 5.10. It was found out that using the same amount of computational resources, the time taken for solution convergence for the three meshes were about 70 hours, 95 hours and 130 hours for meshes 1, 2 and 3, respectively. Therefore, it was decided to forgo such high level of precision and choose Mesh 1 as the final mesh for all the following simulations. Another point of consideration to be addressed while making this choice is that the current project will require constant changes to the blowing slot architecture and velocity inlet conditions which makes a lower size mesh even more preferable.

Mesh Type	**Lift Coefficient** [−]	**Drag Coefficient** [−]	**Min. Wake Deficit Velocity[m/s]**
Mesh 1 (26M)	-2.81674	0.42449	60.3431
Mesh 2 (31M)	-2.81677	0.42446	60.1046(-0.4%)
Mesh 3 (48M)	-2.81668	0.42450	60.2961(-0.08%)

Table 5.2: Lift coefficient, drag coefficient and minimum wake deficit velocity values for the final three mesh candidates under consideration

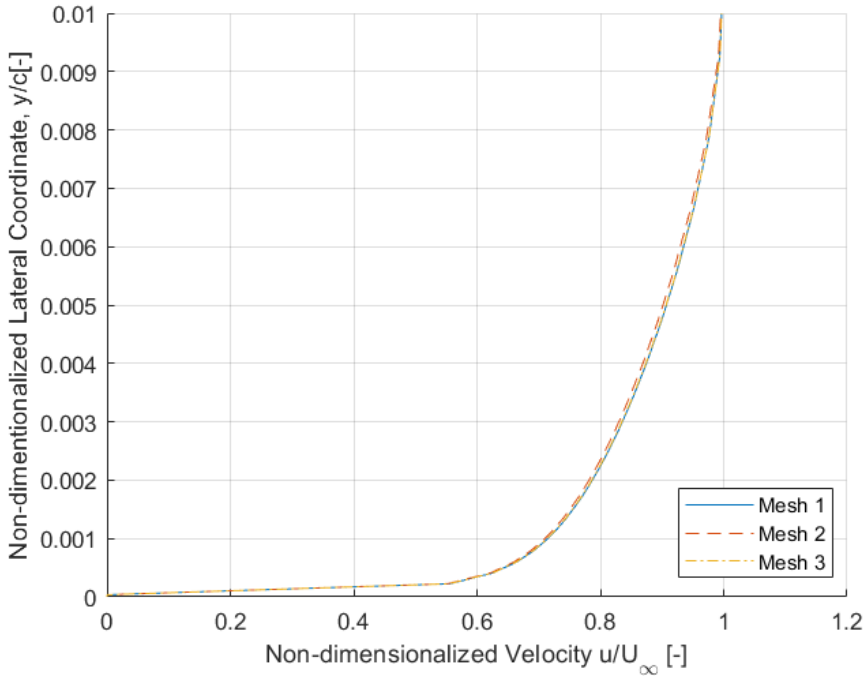

Figure 5.8: Sensitivity of the empennage boundary layer velocity profile, at a location of 0.8c from the leading edge at a spanwise location of 0.75R(0.75m) from the root, over the choice of mesh

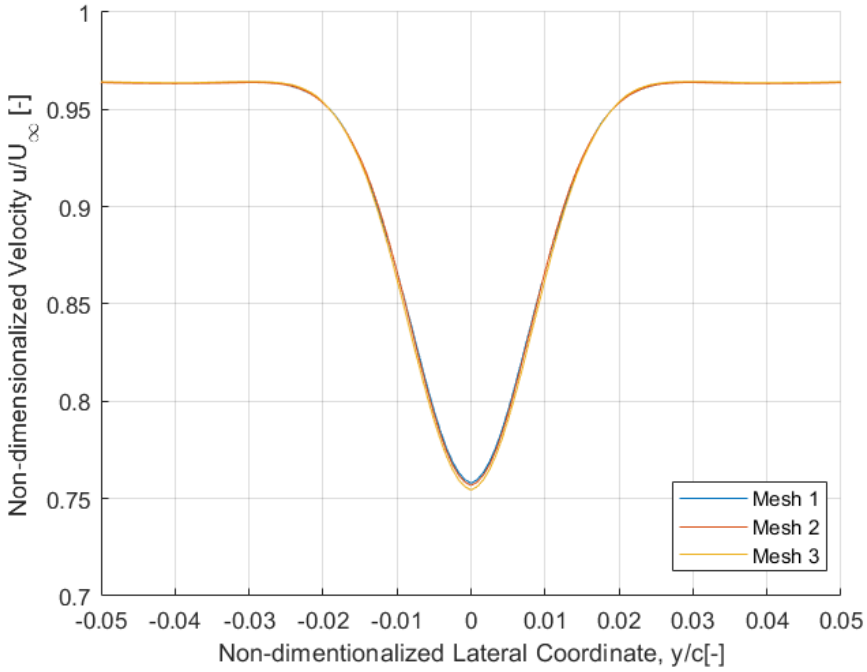

(a) Full wake profile

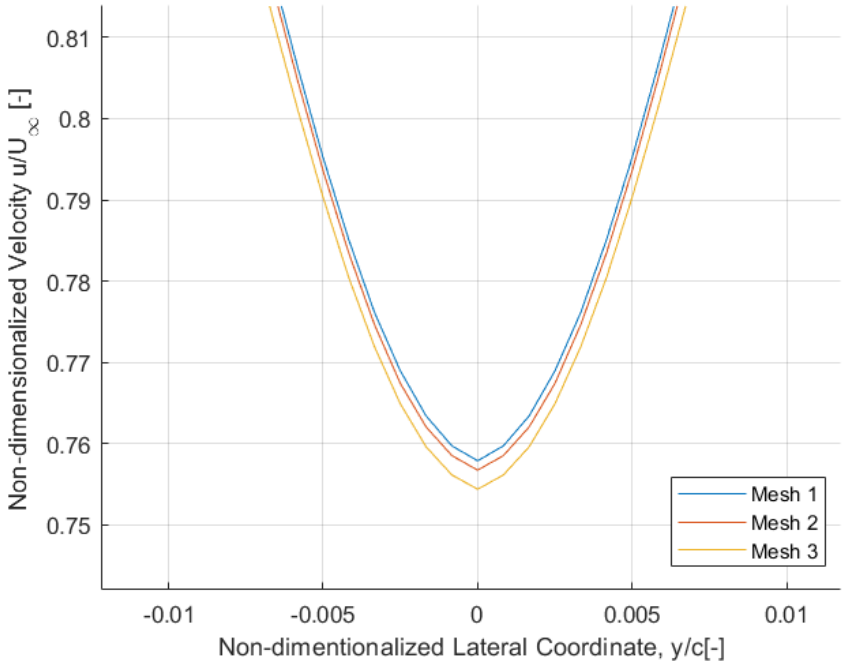

(b) Zoomed-in view of the central deficit velocity region

Figure 5.9: Wake velocity profiles for the three best mesh candidates to show the grid dependency of results and compare the differences in values between them

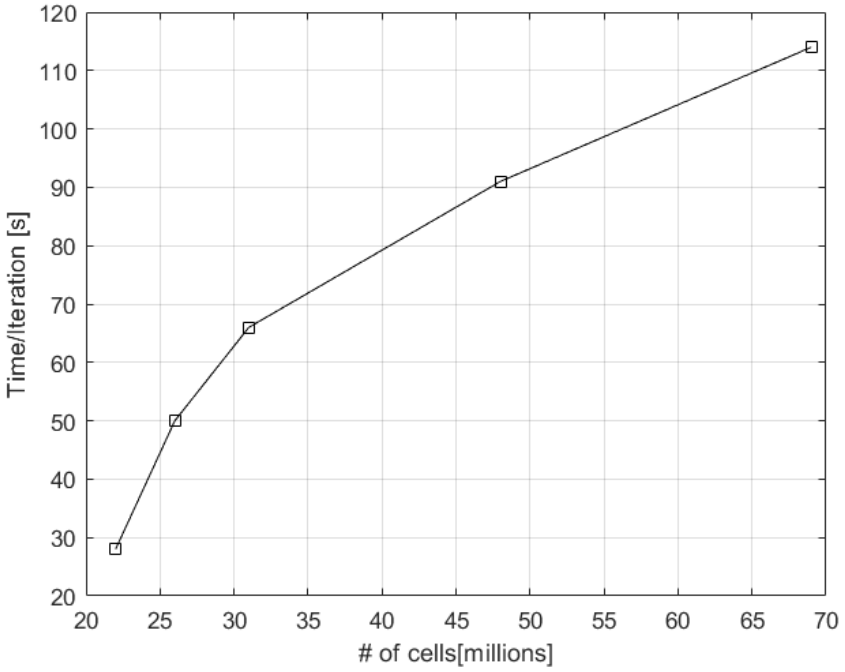

Figure 5.10: Average time per iteration for different mesh sizes

6

Blowing System Design And Fan-Off Configuration Analysis

In the previous chapter, the convergence of the of the mesh is quantified. After the selection of the mesh the next step is to proceed with the application of the spalart allmaras model, as discussed in the subsection 5.1.5, to the problem at hand. A systematic approach is employed to analyse the effect of the system design parameters on the 3D wake blowing mechanism. this will be done in two parts. First part will consist of the 3D wake blowing analysis in absence of the propeller. The relevance of this case is to understand the physics associated with the implementation of the wake blowing mechanism and how it fairs in a three dimensional setting as compared to the past studies done in 2D. This part of the analysis will be instrumental in delivering a flow profile which the propeller will see in idealing state. Since the idea behind the study is also to provide information which will help in designing of the BLI propeller, this section will form a crucial part of it. It will also give an estimate on the system settings which will be required for the blowing system when operated with the BLI propeller. This chapter will address the geometry specification, wake blowing system design and analysis parameters and the corresponding empennage wake analysis in section 6.1, section 6.2 and section 6.4 respectively.

6.1. Geometry Definition and Design Parameters

This section will dive into the details of the geometry specification related to the blowing system and explanations of the parameters used to design the blowing system. A more detailed explanation of the overall geometry was discussed in chapter 4.

6.1.1. Empennage and Blowing Slot Geometry Specifications

The airfoil chosen for the vertical tail is NACA 0010. The selection of the symmetric airfoil was based on the work by Jindal[16] where a 2D analysis was used to establish the dominance of chord-wise blowing over trailing edge blowing. The empennage has a sharp trailing edge with a root chord of 5.34m and a tip chord of 1.89m making the mean aerodynamic chord(MAC) 3.89m. For calculation of MAC is given in Appendix A. The maximum thickness is situated at 10% of chord, according to the NACA 4 digit airfoil definition. The values are reported in Table 6.1.

Parameter	Value	Unit
Root Chord	5.34	m
Tip Chord	1.89	m
Mean Aerodynamic Chord (MAC)	3.89	m
Maximum thickness (t_{max})	0.534	m
Sweep	34	deg

Table 6.1: Geometry specifications of the VTP with respect to the chosen airfoil, NACA 0010.

The empennage geometry, as shown in Figure 6.1, is designed to include the blowing slot in form of a step in both, the upper as well as lower vertical tail plane surfaces. The blowing slots will serve as the inlets for the high speed jet flow which adds momentum to the boundary layer of the existing flow in order to fill the empennage generated wake, discussed later in the results. The flow direction is taken as perpendicular to the blowing slot inlet surface, tangential to the downstream vertical stabiliser surface. The first parameter which was decided upon for the blowing slot design was the chord-wise location of the blowing slot. This location was fixed at the 70% chord line, meaning the slot is located at 70% of the local chord length from the leading edge, for any given cross section. For practical implementation, this location can be taken at the rudder line of the A320 vertical stabilizer, however for the case of current research it is fixed at 0.7c due to presence of rudder being out of scope. Rationale behind the choice is the fact that 0.7c as the chord-wise location for the slot was found to be most efficient according to 2D analysis of Jindal[16]. The VTP geometry is kept unchanged for locations upstream of the slot and the section downstream of the slot is translated towards the chord line(ie. in y-axis) by the magnitude of the chosen slot height. The slot does not extend throughout the span but is restricted to 55% of the stabiliser span. Although, this value is an overestimation by a factor of over 1.5 as compared the actual blowing slot influencing the propeller, which turns out to be about 34% of span, it is chosen in order to prevent any unknown flow effects creeping into the flow due to the blowing system and also to take into account the fact that the same geometry can be utilised for future work where a higher percentage of span-wise slot might be needed due to increase in propeller diameter. Another fact that needs to be taken into account while deciding the span length to be blown is that the direction of flow is not in the flow normal direction but perpendicular to the blowing line/surface, thus increasing the required blown span in order to fill the part of the empennage wake that would be encountered by the propeller. An analysis of the difference between the two flow directions is mentioned in subsection 6.4.5

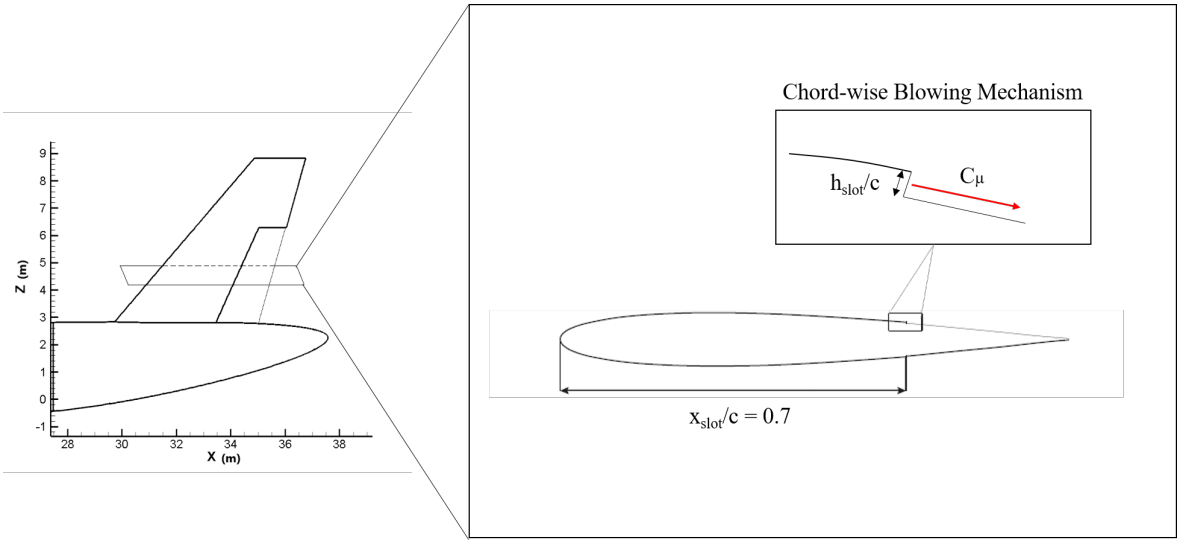

Figure 6.1: Wake Blowing Schematic showing the location of the wake blowing slot on the VTP and the direction in which the air will be blown over the downstream VTP surface

6.1.2. WAKE BLOWING SYSTEM DESIGN PARAMETER

This section addressed the parameters that will be modified in the blowing system design in order to reach a design which can best fill the wake of the empennage when the APPU propeller is not being operated. The design space of these parameters might change when looking at the fan-on cases and would be addressed in the corresponding section of the next chapter. section 6.4 shows the effect of the variation of these parameters on the empennage wake.

SLOT HEIGHT(h_{slot}/c)

As the slot chord-wise location is fixed, the next logical variable to look at for system design is the height of the slot, h_{slot}. This also determines the step by the magnitude of which the part of the VTP surface, downstream of the wake blowing slot, needs to be translated. To use it as a design parameter, the slot height will

be represented in non-dimensional terms as h_{slot}/c, where 'c' is the local chord of a given cross section. This means that, the absolute slot height varies along the span as the local chord varies, for a constant h_{slot}/c. An initial guess for the parameter is taken based on the 2D analysis[16], as 0.001. An iteration on either side of this value is take to understand the trend in which the height of the blowing slot will effect the wake of the empennage. The three values chosen for the current work are can be found in Table 6.2.

Slot Height	Value
$(h_{slot}/c)_1$	0.75x10^{-3}
$(h_{slot}/c)_2$	1x10^{-3}
$(h_{slot}/c)_3$	1.25x10^{-3}

Table 6.2: Range of h_{slot}/c tested for slot-design

BLOWING MOMENTUM COEFFICIENT(C_μ)

The definition of blowing momentum Coefficient, C_μ, has been adopted from work of Jindal[16] and is defined as follows:

$$C_\mu = 2\frac{h_{slot}}{c}\frac{v_{jet}^2}{U_\infty^2} \tag{6.1}$$

where, h_{slot}/c is the non-dimensional parameter slot height, v_{jet} is the inlet velocity of the air at the slot surface and U_∞ is the freestream velocity.
The range of values chosen for the coefficient is of the order 10^{-3}-10^{-2}, based on the order of values used in past works on pylon blowing[12, 16]. Corresponding jet velocity can then be calculated for the coefficient values for a given slot height. The freestream velocity is fixed at U_∞ = 79.83m/s for all cases. Table 6.3 gives the blowing momentum coefficient values investigated for the fan-off cases along with their corresponding jet velocities for the three slot heights.

Blowing momentum coefficients (C_μ)	Value
$C_{\mu 1}$	0.0060
$C_{\mu 2}$	0.0070
$C_{\mu 3}$	0.0080
$C_{\mu 4}$	0.0090
$C_{\mu 5}$	0.0095
$C_{\mu 6}$	0.0100
$C_{\mu 7}$	0.0110
$C_{\mu 8}$	0.0120

Table 6.3: Blowing momentum coefficients (C_μ) to be tested for slot-design optimization.

Since the blowing momentum coefficient is a non dimensional parameter taking into account both, the normalised jet velocity and normalised slot dimensions, the optimum value derived in the current work should be instrumental in filling the empennage wake even if the flight conditions are changed.

6.2. EMPENNAGE WAKE CHARACTERISTICS

It is important to specify how the wake would be defined. The purpose of wake filling is to fill the wake generated by empennage, which is encountered by the propeller, in an attempt to improve the uniformity of the inflow seen by the propeller. The main focus of this work is on the wake of the VTP. It can be assumed that for current case of viscous flow at zero angle of sideslip, the wake of the VTP will not exceed the maximum thickness of the airfoil cross section of the VTP. For the current design, involving NACA 0010 airfoil, this value is known to be at 10% of the chord at any given cross section. However if this is taken as the width of the wake, it would vary depending on the spanwise location of the cross-section. In order to eliminate this ambiguity, the mean aerodynamic chord of the VTP will be used to define the wake width and hence the wake edges. Therefore, the wake will be taken to start from non-dimensional lateral coordinate y/c_{mac} = -0.05 and end at

y/c_{mac} = 0.05. The wake start and end locations are shown schematically in Figure 6.2. This figure will also be used in a later section to explain other important wake parameters.

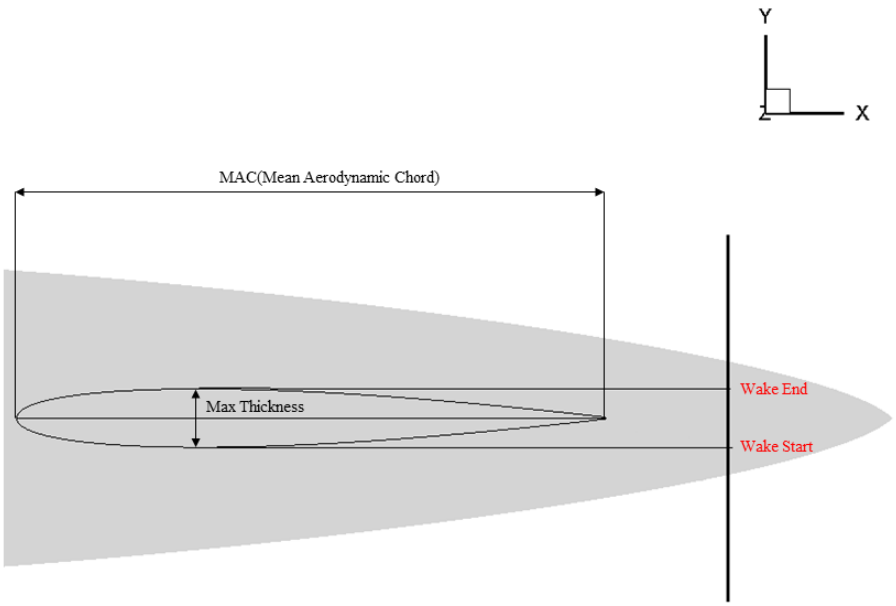

Figure 6.2: Description of the sign convention used to calculate the deviations of the extremas from the optimum

The observation plane for the wake profiles is taken at the prospective propeller location which is 1m distance behind the VT-fuselage junction. Due to the sweep of the VTP, the axial distance of the observation plane at different radial location will vary. Corresponding axial coordinate normalised with the local chord, will be specified as and when different radial location are investigated in the results.

It would also be helpful to address the various shapes that the wake profiles can take under different blown or unblown conditions. Figure 6.3 shows the 5 profiles that can be observed in different conditions. The Type A profile will be seen in unblown cases or cases where the blowing coefficient is considerably underestimated as compared to the optimum. Type B is usually seen in cases with blunt trailing edge or if there is a separation of flow ahead of the trailing edge. Since the current work deals with sharp trailing edge and the flow remains attached as the air is blown along the aft VT surface, wake of type B will not be dominant in the current results. Type C is usually observed when the blown velocity leads to an overshoot in the central lateral coordinate which means that the blowing coefficient is overestimated in this case. Type C also consists of two secondary minima which occurs due to either the slot thickness not being sufficient to energise the full thickness of the boundary layer or the distance downstream of the slot not being sufficient for proper mixing to accelerate the thick boundary layer. With the slot height been chosen in the same order of values as the displacement thickness(discussed in subsection 6.4.3) and the observation plane chosen at a sufficient distance behind the VTP, type C wake profile encountered in the present study is highly diffused. The minimas do not exist and the wake overshoot is small in magnitude such that the profile is close to the optimum profile where neither the deficit not the overshoot exist. Type D profile is primary observed where a blunt trailing edge highly influences the wake or the air is not blown along the VTP surface. Since the case under question involves sharp trailing edge and the air is blown along the VTP surface, this profile will again not be encountered. The last profile, type E referrers to the cases where a much higher than required values of blowing coefficient is employed. This is evident from the high central overshoot. There are no dominant secondary minimas present in any of the profiles observed in this work. Therefore, only type A and type E hold

significance. This means that the wake deficit velocity and shape can easily be defined by the central deficit itself and does not necessitate the inclusion of secondary deficits or overshoots. This brings the question that what is a good way to judge the quality of the wake in order to decide the most optimum profile. Following section will discuss this issue.

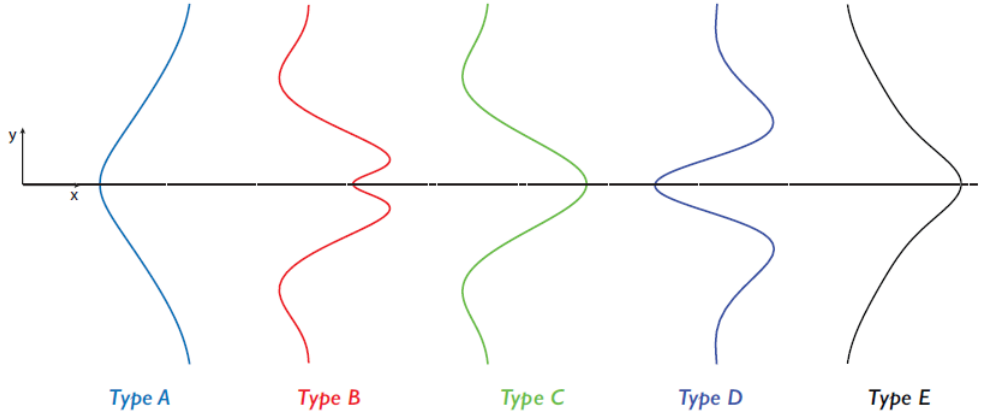

Figure 6.3: Different types of wake velocity profiles can can be seen at different axial location in blown or unblown cases[16]

WAKE QUALITY PARAMETERS

The definition of the wake width in order to define the part of the wake important to the study has been taken from y/c_{mac} = -0.05 to y/c_{mac} = 0.05. These locations will be referred to as the "Wake Start" and "Wake End" locations respectively, from this point on. The rationale based on the maximum thickness of the vertical tail airfoil, has already been discussed in detail in the previous section. This section will operate under the confines of this wake boundary and define some parameters like Wake Area Ratio(A_r) and Wake velocity deficit coefficient(δ) in order to derive a new quantity called the Wake Uniformity Coefficient or W criterion. As described earlier, focus will be kept primarily on Type A and Type E wake profiles shapes. However, the parameters described are applicable to any wake profile, known or not. The same definitions will also be employed for the fan-on configuration later when the actuator disk model will be included. Figure 6.4 gives a depiction of the relevant measurements and sign conventions that would be used while describing the wake quality parameters.

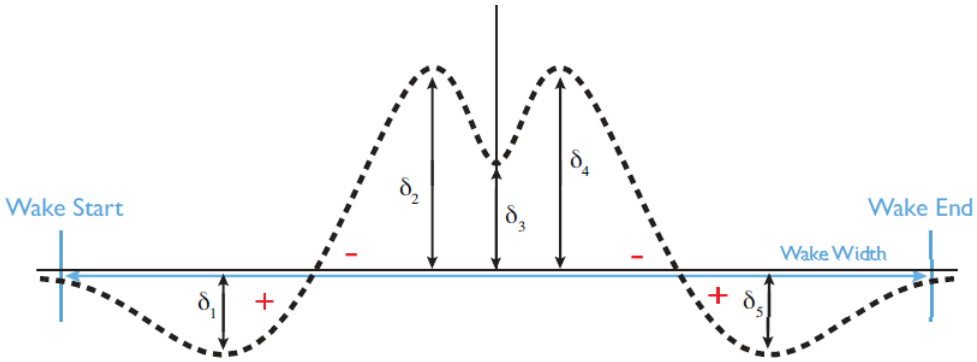

Figure 6.4: Description of the sign convention used to calculate the deviations of the extremas from the optimum

WAKE AREA RATIO (A_r)

Wake area ratio is the ratio of the area under the non-dimensionalized axial velocity curve of the wake(referred to as the "Wake Area") to the area under the same curve in absence of the wake. Figure 6.4 shows both the curves with the former depicted using the dotted black line and the latter using a solid thin black line. The area is taken between the wake start and wake end locations. The area used for normalising the wake area

can vary based on the application and focus area. For the present study, it is taken as the area under the same curve but in absence of the wake since achieving that is one of the aims of the study. Since the wake start and end locations are fixed so that they do not vary with local chord or axial location, the normalising area remains constant for the fan-off study. Just looking at the Wake area ratio to comment on the quality of the wake after wake filling can lead to misleading conclusions in cases where secondary minimas are achieved due to thick boundary layer or when central minima exists with secondary overshoots. In other words, such a situation can arise when both minimas and maximas are present in the wake profile. In order to address this ambiguity, wake velocity deviation coefficient parameter is introduced.

WAKE VELOCITY DEVIATION COEFFICIENT (δ)

The purpose of this parameter is to quantify the extremes that occur in the wake profile. Out of the 5 wake profiles in Figure 6.3, type B has the most number of extremas at 5. However, since this is not an exhaustive set of profiles that can occur in cases not investigated, it is better to take the maximum number of extremas in a wake profile to be addressed as 'n'. δ_i is defined as the deviation of each extrema from the optimum(see Figure 6.4). Then the wake velocity deviation coefficient can be defined as one minus the average sum of all δ_i's normalised with the free stream velocity U_∞, as shown in Equation 6.2. The reason behind subtracting the combined effect of the deviations from one is to draw a parallel between the various wake uniformity parameters. The reasoning is further explained in detail in the next parameter while defining the W criterion.

$$\delta = 1 - \frac{\sum_{i=1}^{n} \left(\frac{\delta_i}{U_\infty}\right)}{n} \tag{6.2}$$

The wake velocity deviation coefficient is a characteristic quantity in defining the quality of the wake. However, just like wake area ratio, the coefficient by itself can lead to false conclusions in case of presence of secondary minimas. Due to this reason, it would be better practice for future work to use methods such as standard deviation, mentioned as follows, to eliminate this issue.

$$\delta = 1 - \sqrt{\frac{\sum_{i=1}^{n} \left(\frac{\delta_i}{U_\infty}\right)^2}{n}} \tag{6.3}$$

However, due to the absence of major secondary minimas, the focus of the current work was kept to the central deviation for which the averaging method works just as well as the standard deviation. This brings the importance of the next parameter which combines these two and thus leads to a much more accurate representation of the wake quality, namely, Wake Uniformity Coefficient.

WAKE UNIFORMITY COEFFICIENT - W CRITERION

The aim of the employing wake blowing is to overcome the velocity deficit due to the presence of the vertical tail in order to provide uniform dynamic loading to the BLI propeller. Therefore, a parameter is defined to best represent the uniformity of the wake. This parameter is called the Wake Uniformity Coefficient(W) or can also be referred to as the W Criterion. Since wake area ratio and the wake velocity deviation coefficient are important indicator of wake uniformity but neither is exhaustive in itself, the W criterion will include the effect of both. Taking a normal product of the two will lead to a good indicator because as wake profile becomes closer to the optimum, both A_r and δ values tend to 1. Herein lies the reason behind subtracting the average deviation of all extremas from 1, in the definition of δ, so that it is consistent with the trend of A_r and does not lead to an ambiguity while defining the W criterion. The W criterion is best described using the formulation presented in Equation 6.4:

$$W = A_r.\delta \tag{6.4}$$

where A_r is the wake area ratio and δ is the wake velocity deviation coefficient. Since both A_r and δ are non-dimensional quantities, the W criterion is also non-dimensional with its value tending to 1 as the wake profile becomes more uniform and reaches optimum.

6.3. IDENTIFYING THE FOCUS AREA

Before the results of the wake blowing study are discussed, it would be helpful for the reader to understand the problem that will be tacked using plots for the base case without the implementation of the blowing system. This section will also help in identify the region of importance where the focus of the current study would be concentrated.

Three quantities will be called to aid in understanding the effect of the empennage wake on the propeller inflow plane. These are:

TOTAL PRESSURE COEFFICIENT, C_{P_T}

Total pressure coefficient is a quantity which can help identify the losses in the flow in terms of total pressure. It gives an indication of where the flow properties have reached free stream conditions in terms of total pressure, meaning that no more pressure losses exist in the flow. The total pressure coefficient is defined as follows:

$$C_{P_T} = \frac{P_T - P_{T_\infty}}{q_\infty} \tag{6.5}$$

where, P_T is the local total pressure, P_{T_∞} is the freestream total pressure and q_∞ is the free stream dynamic pressure.

According to the formulation for C_P, as given in Equation 6.5, a value of 0 refers to the free-stream total pressure while the negative values show the total pressure losses where -1 refers to a complete loss in total pressure as seen over the geometry walls in Figure 6.5. The empennage wake that would be encountered by the aft mounted BLI propeller has a deficit of almost 30%. This will be cause a sudden fluctuation in the flow properties experienced by the propeller inflow. Two of these flow quantities which will be important for the propeller blade design will be the dynamic pressure loading and the inflow angles that are experienced in the propeller inflow. These will be defined following this section. The contours for the total pressure coefficient, dynamic pressure coefficient and the inflow angles on the propeller plane can be seen in Figure 6.6

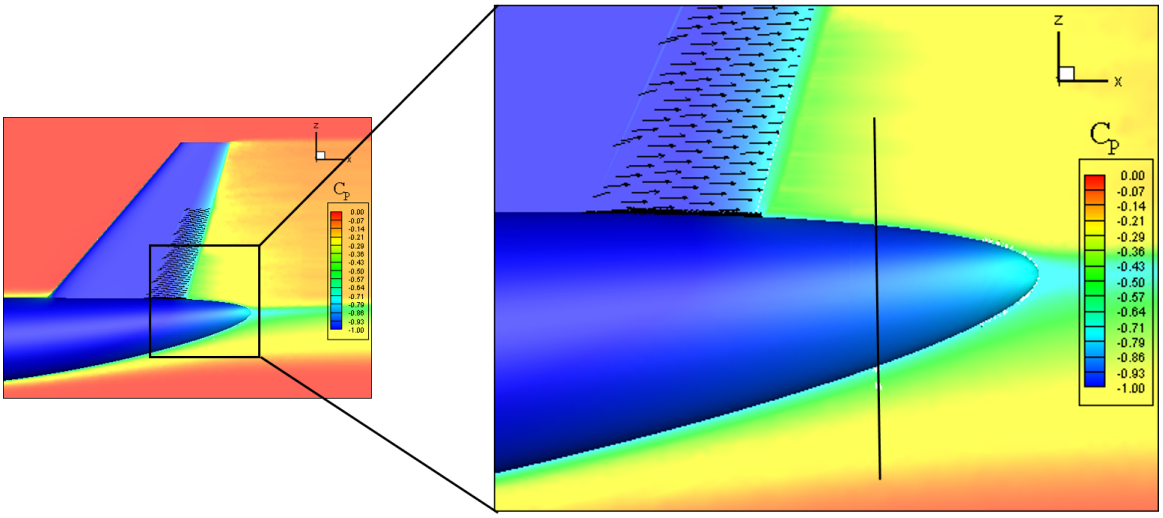

Figure 6.5: Total pressure contour plot along with velocity vectors over the VTP section downstream of the blowing slot to show the main focus region for the current study and empennage wake under observation

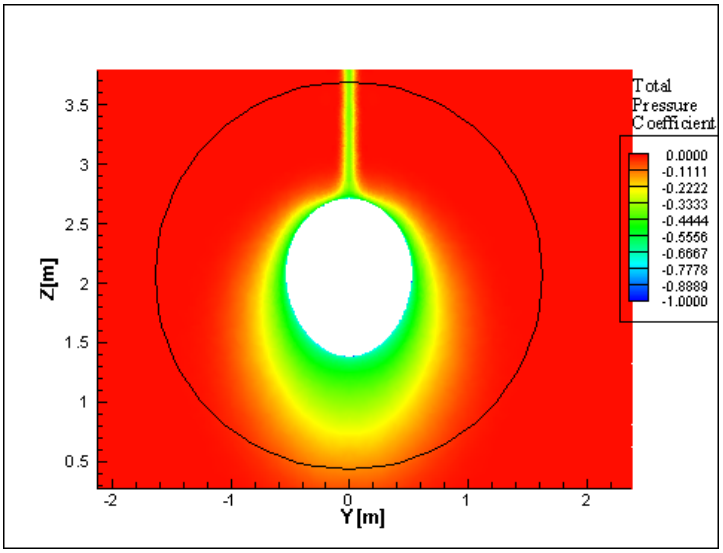

(a) Total Pressure Coefficient

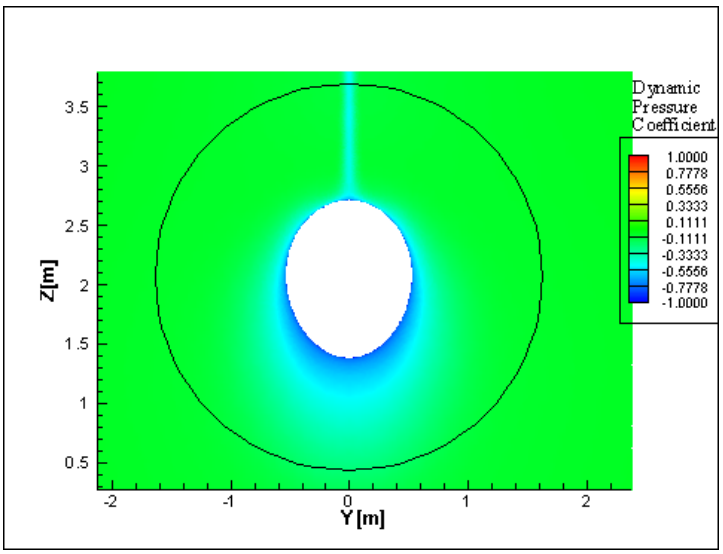

(b) Dynamic Pressure Coefficient

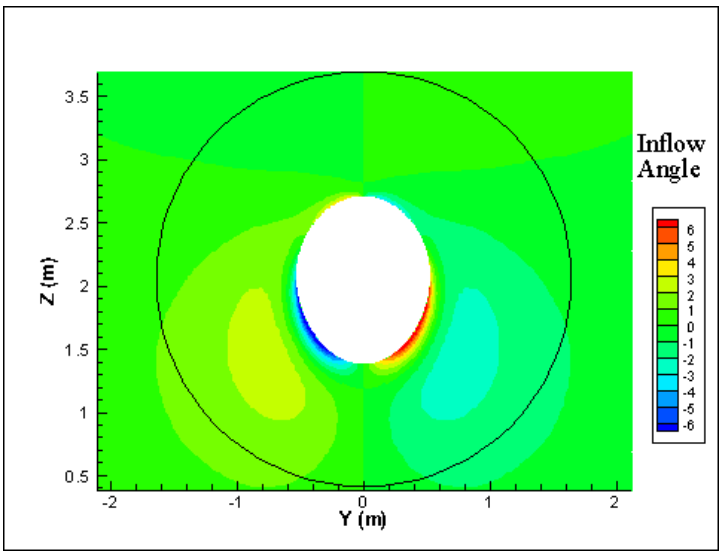

(c) Inflow Angles

Figure 6.6: Contours for relevant flow properties at the propeller inflow plane located 0.1m ahead of the chosen propeller location

DYNAMIC PRESSURE COEFFICIENT, C_q

The dynamic pressure coefficient is used to specify the dynamic pressure loading that the the propeller blades will experience as they revolve in the propeller plane. A more heavily loaded blade will generate more thrust while a disruption in the dynamic pressure loading, as seen in the empennage wake, will lead to performance penalties especially in form of higher tonal noise[12, 48]. The dynamic pressure coefficient can be defined as follows:

$$C_q = \frac{q - q_\infty}{q_\infty} \tag{6.6}$$

where, q is the local dynamic pressure and q_∞ is the free stream dynamic pressure.

The dynamic pressure deficit behind the empennage is evident from Figure 6.6. To understand the problem to be addressed better, a cyclic dynamic pressure loading plot for a blade radial location of 75% of the blade radius(R) is given in Figure 6.7. The conventional azimuthal location specification was adopted as specified in Figure 6.7(b), with the revolution starting at 0°. The blade section of 0.75R was chosen in order to pick a location which would be highly loaded and would have a major contribution to the thrust. The sharp drop in the dynamic pressure coefficient at 90° azimuth location, which is the location right behind the empennage, can be observed. It is this non-uniformity in the propeller inflow that would be attempted to eliminate within this research using the chord-wise wake blowing technique. Another dip can also be observed at a 270° azimuth location which corresponds to the lower fuselage section. However, this dip is much more gradual because the cause for this dip is the thicker lower fuselage boundary layer that is formed as a result of the fuselage upsweep. Since the thickness of the boundary layer decreases gradually, moving towards the upper fuselage, a gradual dip peaking at 270° is observed. However, addressing the later dip is not a part of this work.

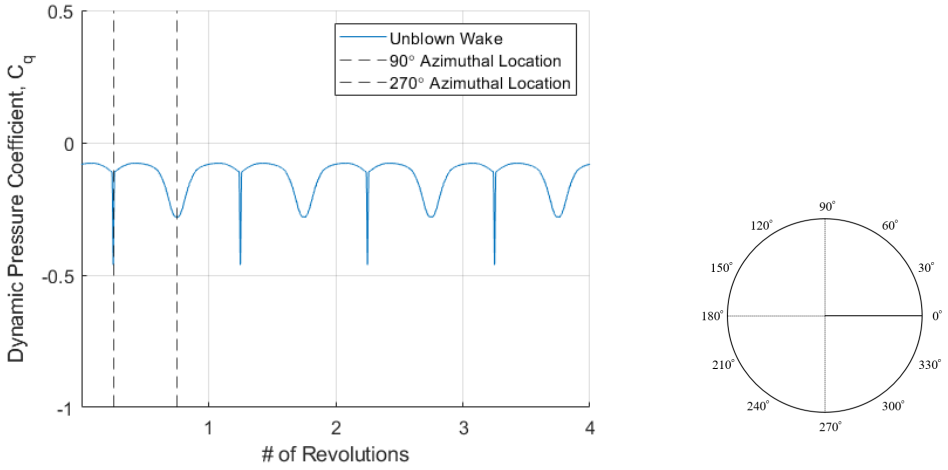

(a) (b)

Figure 6.7: (a)Dynamic pressure loading of the 0.75R section of the propeller disk for revolutions over time, (b)Polar convention for azimuthal location

PROPELLER INFLOW ANGLES, ϕ

Lastly, another important quantity to be taken into account while discussing propeller blade design and performance, is the propeller inflow angles. This angle can be defined as the inverse tangent of the ratio of the circumferential/tangential velocity of inflow(V_{circ}) to the axial velocity(V_{axial}), as mentioned in Equation 6.7.

$$\phi = tan^{-1}\left(\frac{V_{circ}}{V_{axial}}\right) \tag{6.7}$$

To understand the formulation of the inflow angles better, a schematic of the velocity components with respect to the propeller plane centre is given on the left in Figure 6.8 where the axial velocity is in a direction going into the plane. The inflow angle can then be described using velocity triangle as shown on the right in the figure. As seen in Figure 6.6, majority of the high inflow angles of ±6° are confined to the lower fuselage

side with the higher angles experienced near the hub. It would be prudent to investigate if the implementation of the wake blowing system will have any effect on the inflow angles. This effect would then need to be taken in account in the future while designing the propeller blade.

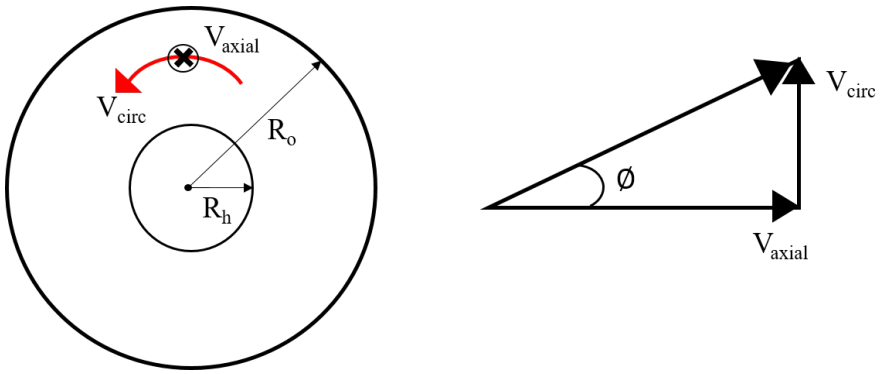

Figure 6.8: Pictorial representation of the circumferential and axial velocities(going into the plane) used to calculate the inflow angle, ϕ

By now, the reader should have an idea of the major focus region and flow properties that would be studied. However, it should be noted that a combined discussion on the effect of the wake blowing system on the above mentioned quantities will only be presented in the chapter 8 along with the fan-on configuration results. The purpose of this section was to show, with the help of some base case results, the problem that would be addressed in the current chapter for fan-off and the next chapter for fan-on configuration, using the technique of chord-wise wake blowing. For further graphical representation of the flow, some streamlines for the unblown case for the fan-off configuration can be found in Figure D.1. For contour plots of more flow properties like total pressure coefficient, velocity etc. the reader is referred to Appendix D, where plots are shown for unblown and blown cases for both the fan-off and fan-on configuration.

6.4. WAKE BLOWING SYSTEM ANALYSIS

This section will address the effect of the system design parameters discussed in subsection 6.1.2. Analysis will be made on their capability to mitigate the empennage wake, thus, leading to potential reduction in noise and performance penalties. The results of the design study will be presented. This chapter is focused on the cases where the effect of the propeller is not taken into account yet. Firstly, a basic analysis of the wake progression in absence of the blowing mechanism will be looked at to understand the target to be achieved. Then the effect of the physical implementation of the blowing slot on the wake deficit will be looked at followed by the effects of the variation in the design parameters. This will followed by an indication of the effect of the radial location on the wake. Lastly, it would be interesting to take a brief look at the effect of the blown jet velocity direction over the wake profiles specifically, corresponding to a few near-optimum blowing coefficients. The results involving the propeller installation effect will be discussed in the following chapter.

But before going to the actual results, it would be of interest to take a look at the physical locations where the data has been extracted in order to enable a more comprehensive understanding of the results. Figure 6.9 shows the locations of important observations points and planes and their spacing with respect to the geometry. The blowing slot can be seen located at 0.7c location. A prospective propeller plane is selected at a distance of 1m behind the empennage-fuselage junction. Profiles at two radial locations are chosen with respect to the chosen blade radius R: 0.1R and 0.75R, which correspond to 10% and 75% of the blade radius, respectively. The location 0.75R is of prime importance since it is usually a location of maximum loading while the 0.1R location is chosen in order to investigate the wake and flow patterns close to the hub. It is important to note that at these two radial locations, four axial points are selected going from behind the empennage to the prospective propeller plane. The locations are fixed in the axial direction at a distances of 0.25m, 0.5m, 0.75m, 1m behind the empennage trailing edge-fuselage junction, represented as $x_1, x_2, x_3 and x_4$ respectively. The x_4 location will be moved slightly upstream in the cases when actuator disk model will be implemented, and is discussed in the next chapter. These locations will be normalised with the local empennage chord at that x-plane and represented in non-dimensional terms. It is at these 8 locations that the wake analysis will be largely focused on. It is at these points that a rake in the lateral direction(y direction) is used to extract the

wake profiles in terms of axial velocity or total pressure.

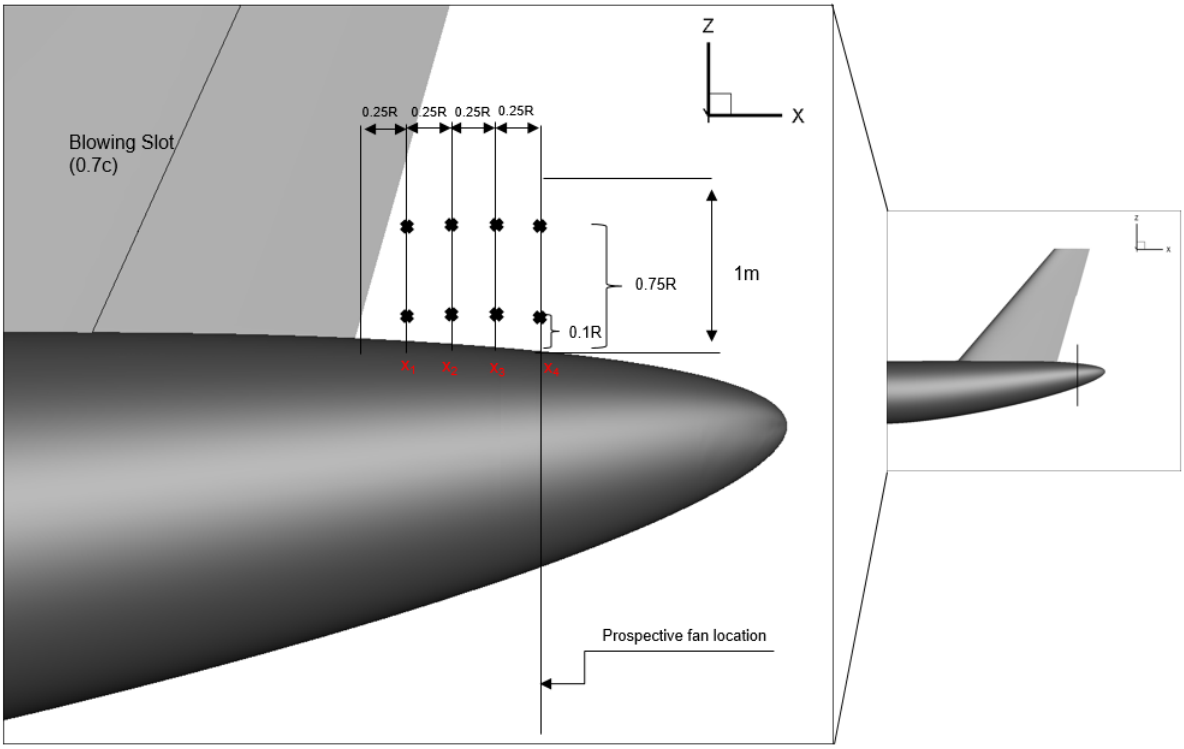

Figure 6.9: Data acquisition location with respect to the fuselage-empennage geometry and the prospective propeller plane for the fan-off cases. The 8 crosses, at 0.1R and 0.75R for 4 axial locations each($x_1, x_2, x_3, x_4 = 0.25m, 0.5m, 0.75m, 1m$), show the locations where the wake velocity profiles is investigated in the lateral direction going into the plane.

6.4.1. WAKE PROGRESSION

The purpose of this analysis is to understand the progression of the wake as it moves in the axial direction behind the empennage. Figure 6.10 shows the axial velocity normalized with the free stream velocity plotted against the lateral coordinate which has been normalised with the mean aerodynamic chord. The central deficit due to the loss in momentum of the flow can be observed in the profiles. It is evident from the figure that the wake velocity at the central deficit recovers more and more as the wake moves further downstream. This is due to the fact that as farther downstream as the flow is observed, the loss in the total pressure becomes lower until it reaches the free-stream total pressure, as can be seen in Figure 6.11 where, the total pressure normalised with the free-stream total pressure is presented along the lateral coordinate. However, it is interesting to see that an increase in the wake width is not observed as the wake progresses which would have been expected due to the diffusion of the wake due to flow viscosity[12].

The two figure also describe the difference in the profiles observed at two different radial location of 0.1R and 0.75R. The most prominent difference is that the deficit velocity value at x_1 axial location is much lower for 0.75R($u/U_\infty = 0.58$) location than 0.1R($u/U_\infty = 0.69$). This is due to the fact that the absolute distance between the empennage trailing edge and the x_1 axial location is much less at 0.75R due to the 34° sweep of the vertical tail. Similar observation can be made for the rest of the axial locations as well. Since the wake has less time to diffuse for 0.75R location, the deficit remains large as compared to 0.1R location where the wake has diffused more.

Another, important observation is that the effect of the fuselage boundary layer on the flow around it can be seen in the total pressure profiles. Due to the lower momentum fuselage boundary layer working along with the low momentum flow in the empennage wake, the overall total pressure loss is more for the 0.1R location at the same lateral coordinate, away from the wake centre. The total pressure profiles at 0.75R already reach the freestream value as compared to the still rising values for the 0.1R case. This is the manifestation of the lower shear force due to low momentum flow in a wider section of the wake at 0.1R, as can be seen in the wake

velocity profiles. Another contribution to the widening of the wake is the fact that the absolute maximum thickness of the VT airfoil cross section at 0.1R is larger due to a longer chord. The deficit in total pressure, due to the higher absolute thickness of the airfoil at 0.1R, contributes to the observation of a deficit till a larger lateral coordinate.

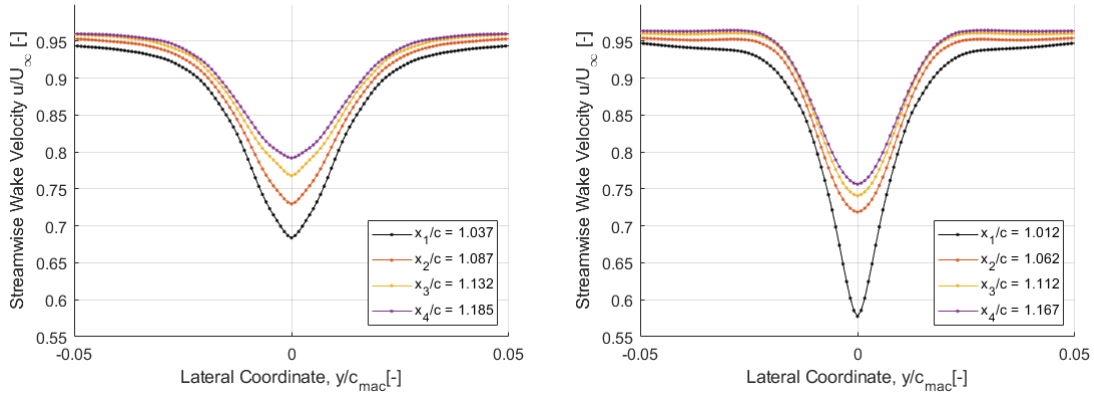

(a) 0.1R (b) 0.75R

Figure 6.10: Effect of the axial location on the normalized wake velocity profiles behind the empennage with a clean VTP without the presence of the wake blowing system

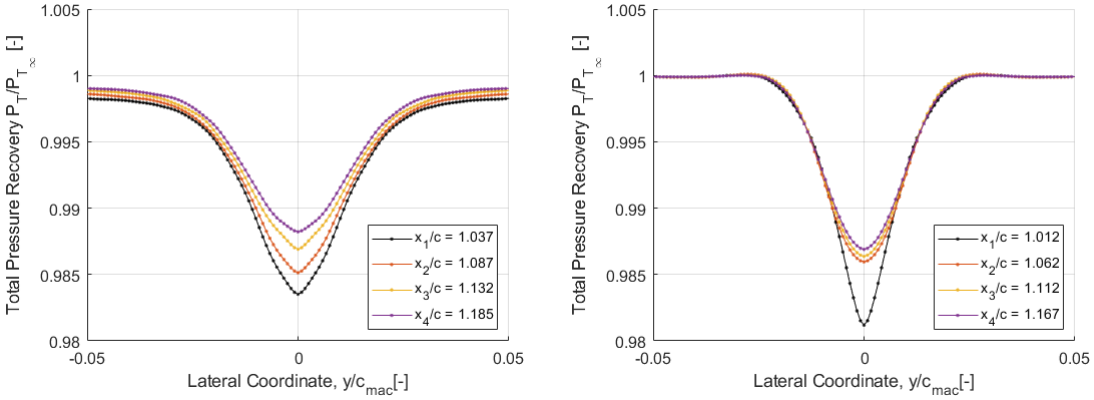

(a) 0.1R (b) 0.75R

Figure 6.11: Effect of the axial location on the total pressure behind the empennage with a clean VTP without the presence of the wake blowing system shown with the help of total pressure recovery(P_T/P_{T_∞}) profiles

6.4.2. IMPLEMENTATION OF SLOT FOR WAKE BLOWING

This section, although of not significance importance to the wake blowing system itself, is still of interest due to the fact that the physical addition of the slot in the VTP should influence the flow, no matter how small this influence is. Since this is not the prime focus of the study, a detailed analysis of the flow has not been performed but the relevant wake velocity profiles have been included to provide some information. Figure 6.12 shows the wake velocity profiles at x_4 location at a radial distance of 0.75R. One observation is that the maximum deficit in the velocity at the central lateral coordinate reduces with the addition of the slot. It can further be seen that this reduction increases as the height of the slot is increased. No definitive relation can be observed between the amount of reduction in the velocity deficit to the slot height. This raises questions on the fact that whether the trend that is observed with increasing the slot height is indeed due to it's effect on the flow or can be attributed to meshing or solver errors. Further investigation is required and it is recommended to perform a detailed mesh sensitivity study specifically focused on the wake, in order to comment on the positive effect of the physical slot in a fool proof manner. However, it cannot be denied that

a definitive deduction can be made that the slot will indeed have some amount of positive effect in reducing the wake deficit. This can largely be attributed to the enhanced mixing that takes place due to the presence of the slot. The boundary layer of the VTP surface ahead of the slot detaches from the surface at the slot location. This detached flow reattaches at a distance downstream to yield the new boundary layer downstream of the slot.

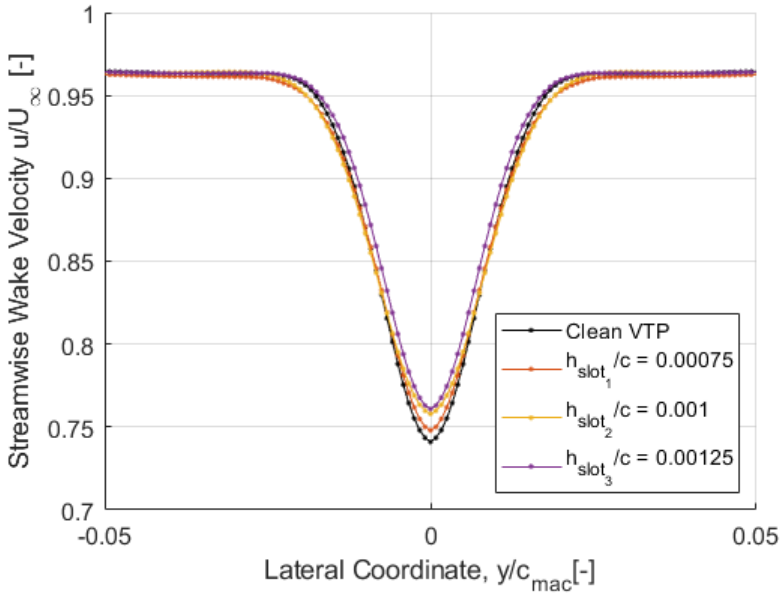

Figure 6.12: Effect of the wake blowing slot on the wake velocity deficit without the jet air injection

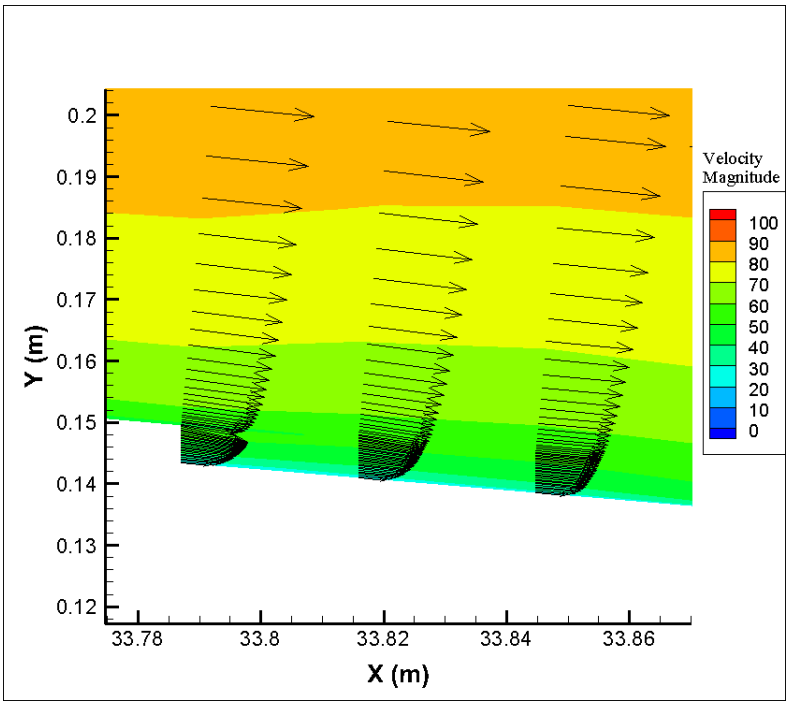

Figure 6.13: Effect of the wake blowing slot on the boundary layer along the VTP surface shown using velocity magnitude contours and velocity vectors

6.4.3. EFFECT OF BLOWING MOMENTUM COEFFICIENT, C_μ AND SLOT HEIGHT, $\frac{h_{slot}}{c}$

The variation of blowing momentum coefficient for the three slot height will be studied in order to achieve a near optimum blowing coefficient in each case. Since the primary aim of the study is to analyze the wake filling performance of the wake blowing system, the focus will remain on the wake velocity profiles which provide sufficient information for the quantification of the wake.

As mentioned in subsection 6.1.2, the first choice of the slot height which is taken to be $h_{slot}/c = 0.001$, was based on the optimized wake blowing configuration achieved by Jindal[16] for 2D chord-wise wake blowing. This value was also in line with the displacement thickness of the boundary layer for a NACA0010 airfoil calculated in xfoil[78] for the same flow conditions. This side analysis on xfoil provided a good validation for the initial choice of the slot height. The Figure 6.14 shows the wake velocity plots and also the plots for total pressure in terms of total pressure recovery, which is defined as the ratio of the local total pressure to the free-stream total pressure, for the range of blowing momentum coefficients being investigated. In an attempt to choose the values of the blowing momentum coefficients logically, the momentum loss in the boundary layer for a NACA0010 airfoil was investigated using xfoil. The momentum loss taken at the slot location of 0.7c yielded a blowing coefficient value which was much less than the coefficient required to overcome the loss in the wake. Part of this was because taking the loss at 0.7c location neglects the momentum loss that would occur downstream of that location. A considerable momentum overshoot is required to overcome the loss of the downstream empenaage surface. Nevertheless, with a combined look at the momentum loss and blowing coefficients used literature, it was decided that coefficients of the order of 10^{-3} were a good guess to start the analysis. The wake profiles have been taken at the 0.75R radial location for which the axial location is $x_4/c = 1.167$.

The primary observation has to be the proficiency of the chord-wise wake blowing system in filling the wake. It can be seen how the wake starts to fill more and more as the blowing coefficient increases. The addition of momentum to low momentum sublayer of the empennage boundary layer boundary layer helps in overcoming the total pressure loss due to the presence of empennage. Table 6.4 shows how the wake quality parameters vary with the blowing coefficient. Wake area under the normalized axial velocity curve increases as the wake velocity deficit is reducing. This brings the wake area ratio closer to it's optimal value of 1. Similarly, the wake velocity deviation coefficient δ, which takes into account the extremas that exist in the profile, also moves closer to unity. The trend for the two parameters is consistent with each other. As the central velocity deficit decreases, the area cover by the velocity profiles rises towards optimum. It is interesting to note that the initial slot height guess was proven to be very well chosen. This is concluded due to the absence of any secondary minimas in the velocity profiles, which would have occurred in case if not enough of the boundary layer height was energised by the added jet air. The absence of any secondary maximas or manimas also means that the distance of the observation location from the empennage is enough to enable proper mixing of the blown flow with the boundary layer. As mentioned while defining the wake quality parameter, the wake area ratio and velocity deviation coefficients cannot exhaustively define the wake quality separately. Thus, the W criterion is calculated which combines the effect of the two. Therefore, a value of W criterion closest to 1 would yield the most uniform wake velocity profile and will potentially be the desired inflow for the BLI propeller in APPU configuration.

Blowing Momentum Coefficient, C_μ	**Wake Area Ratio, A_r**	**Wake Velocity Deviation Coefficient, δ**	**W Criterion**	**% Difference from Optimum**
Unblown	0.956	0.783	0.749	-25.09
0.006	0.979	0.901	0.882	-11.82
0.007	0.985	0.933	0.919	-8.14
0.008	0.991	0.962	0.953	-4.67
0.009	0.997	0.988	0.985	-1.53
0.0095	1.000	0.999	0.999	-0.08
0.001	1.002	1.011	1.013	1.35

Table 6.4: Wake uniformity parameters for different blown and unblown configurations for a slot height of $h_{slot}/c = 0.001$

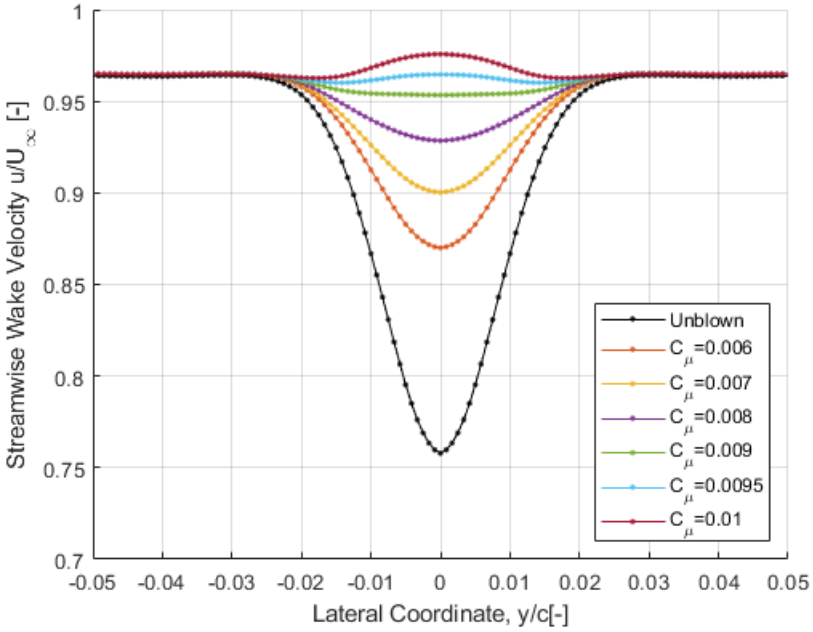

(a) Wake Velocity Profiles

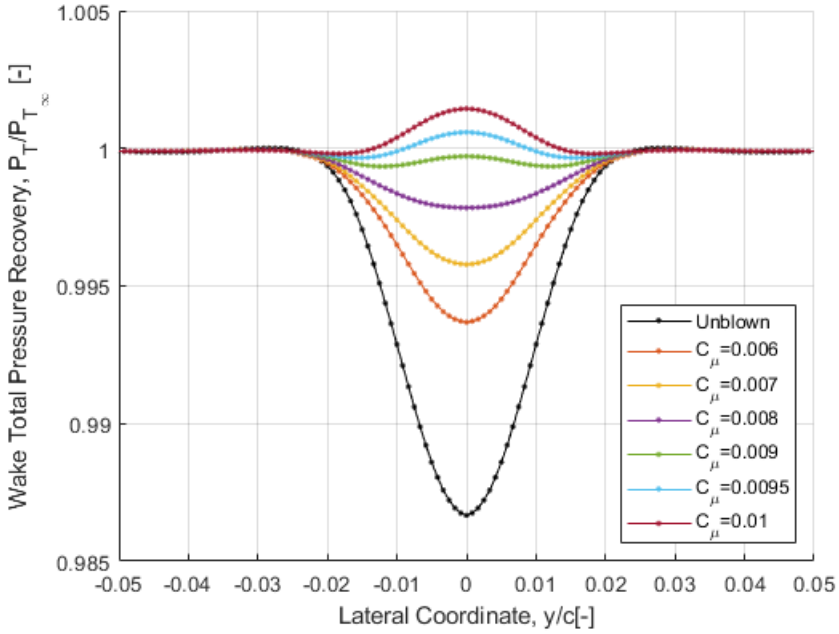

(b) Wake Total Pressure Recovery Profiles

Figure 6.14: Effect of varying blowing momentum coefficients on the wake velocity and total pressure for a slot height of $h_{slot}/c = 0.001$

For the current slot height, the optimum wake profile is observed in the case with blowing coefficient of 0.0095. The value of the W criterion for this case is only 0.08% lower than the optimum. For the blowing momentum coefficient values higher than 0.0095, the velocity overshoots past the desired value. This leads to a value of wake quality parameters of higher than 1. It should be mentioned here that the value of W criterion higher than 1, though not desirable, but can be favourable for current set of blowing coefficients in case the percentage difference from optimum is lower than other cases.

Figure 6.14 also shows the corresponding pressure recovery plots for the different blowing coefficient cases.

It should be kept in mind that although the profiles and their trend are highly similar to the velocity profiles, the absolute values of the quantity itself necessitated a more zoomed in inspection for the pressure recovery. Nonetheless, the inferences derived from the wake velocity profiles and quality parameters, remain the same. However, one additional inference which might be derived from the pressure recovery plots is that the total pressure at and around the central deficit region already starts to overshoot for the near optimum bowing coefficients for which the wake velocity is still slightly lower than the freestream value. This means that the total pressure becomes higher than the freestream pressure in the wake even when the axial velocity is lower than freestream. This can be attributed to two factors. Firstly, only the axial component of the velocity is used for the velocity profiles. The total velocity magnitude will be higher than this due to the contributions of the lateral and z components, no matter how small. Secondly, the velocity profiles give an indication of only the dynamic head of pressure. As the wake progresses, there would be some loss in the dynamic pressure due to energy dissipation due to the flow viscosity which would be seen an increase in the flow static quantities. This means there would also be some increase in the static pressure as the wake progresses. It can be the contribution of this additional static pressure which leads to the earlier overshoot in the total pressure recovery.

Now, since it has been established that the wake blowing mechanism is capable of filling the wake of the empennage in a more realistic 3D setting. It is important to move the analysis of the effect of the change in the slot height on the wake filling capability of the system. For this, it needs to be decided whether to chose the next slot height either larger or smaller. Looking from a requirements stand point, it would beneficial if the mass flow required for the wake filling can be kept as low as possible. Due to this reason, the next normalised slot height was chosen to be smaller than 0.001 by a factor of 0.00025. Thus, making $h_{slot}/c)_2 = 0.00075$. A detailed analysis of the required mass flow rates for different cases can be found in section 8.6. There is, however, one disadvantage of this choice. For a $h_{slot}/c = 0.00075$, the absolute height of the slot becomes lower than 5mm, which will present huge difficulty while manufacturing. Therefore, the third and the last slot height is chosen to be larger than 0.001 by the same factor of 0.00025. Thus making $h_{slot}/c)_3 = 0.00125$.

Figure 6.15 shows the wake velocity profiles for the slot height of 0.00075 and the corresponding wake quality parameters are mentioned in Table 6.5.

Blowing Momentum Coefficient, C_μ	**Wake Area Ratio, A**	**Wake Velocity Deviation Coefficient, δ**	**W Criterion**	**% Difference from Optimum**
Unblown	0.955	0.772	0.737	-26.31
0.007	0.988	0.943	0.931	-6.88
0.008	0.994	0.974	0.968	-3.21
0.009	0.999	1.004	1.003	0.32
0.0095	1.003	1.017	1.020	2.01
0.001	1.006	1.031	1.037	3.67

Table 6.5: Wake uniformity parameters for different blown and unblown configurations for a slot height of $h_{slot}/c = 0.00075$

It should be noted that the formulation of the blowing momentum coefficient given in the Equation 6.1 includes the effect of both, the slot height and the jet velocity normalized with the local chord and the freestream velocity respectively. This means that for the same blowing coefficient, as the height of the slot decreases, a higher inflow velocity jet will be added through the blowing slot. Thus, it was speculated that a lower optimum blowing coefficient will be required for this slot height. The theory was confirmed from the results and it can be seen that the W criterion is closest to the optimum value for the momentum coefficient of 0.009 which is lesser than what was achieved for slot height of 0.001. This is the perfect example of the case where a case with central velocity overshoot, although undesirable, is more favourable. The reason for this is that the aim of filling the wake is to reduce the unsteady loading on the propeller blades. The W criterion which represents the uniformity of the wake gives an indication on the fluctuation of the inflow velocity profiles from the optimum. Closer the W criterion is to 1, lower will be the fluctuations in dynamic loading and thus lower will be the noise and performance penalties. The contours for dynamic loading and other important physical quantities will be discussed in more detail in chapter 8, where a comparison is drawn between the fan-on and the fan-off configurations. The case with blowing coefficient 0.006 was excluded from the

study for $h_{slot}/c = 0.00075$ to conserve computational time and resources because it was concluded from results for $h_{slot}/c = 0.001$ that the a $C_\mu = 0.006$ was a highly underestimated value as compared to the optimum and therefore, highly unlikely to be a candidate for optimum coefficient even for the lower slot height.

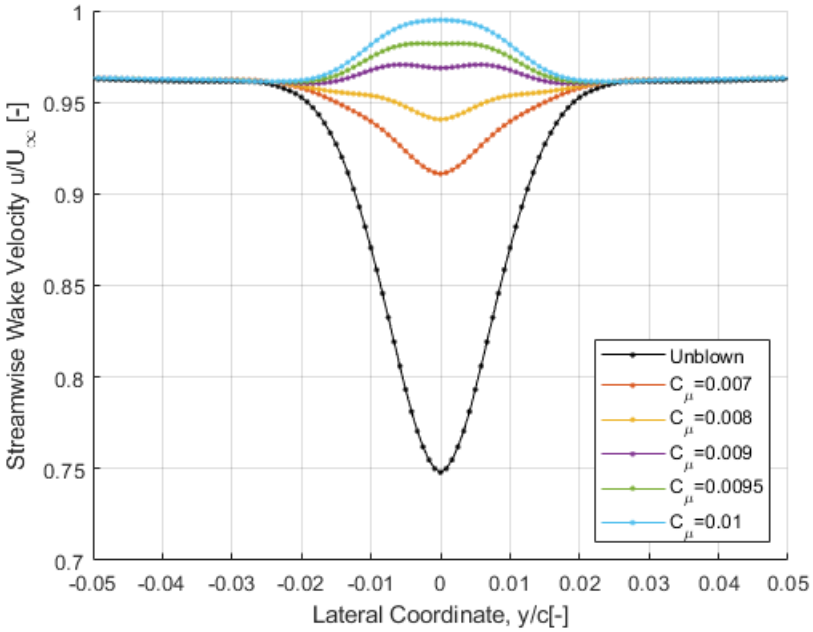

Figure 6.15: Effect of varying blowing momentum coefficients on the wake velocity profiles for a slot height of $h_{slot}/c = 0.00075$

As mentioned before, the next and the last slot height to be investigated was $h_{slot}/c)_3 = 0.00125$. The explanation of the relation between the blowing momentum coefficient, slot height and the corresponding required jet velocity, works here just as well. Since the slot height as increased now, therefore a smaller jet velocity will be injected in the boundary layer for the same momentum coefficient. This means that the optimum coefficient will increase which can be seen in Figure 6.16 and the corresponding W criterion values can be seen in the Table 6.6. It should be noted here that since a higher optimum blowing momentum coefficient was expected, the coefficients lower than 0.009(optimum coefficient for $h_{slot}/c = 0.00075$) were not simulated in a calculated attempt to conserve computational time and resources. Furthermore, a very close to optimum value was achieved for W criterion in the case of $C_\mu = 0.01$. Since the current study is not aimed at fine tuning the wake blowing system to obtain the most efficient coefficient, the design space for blowing momentum coefficients was not expanded to higher values. One additional observation that can be made from the wake velocity profile for the case with $C_\mu = 0.01$ is that it fills the regions away from the central deficit with the best uniformity. It can be again commented that the higher slot height is able to energise a larger proportion of the boundary layer, thus leading to a more uniform wake profile without the need of raising the blowing coefficient to a higher value, which for the case of $h_{slot}/c = 0.00075$, undesirably lead to an overshoot in the central velocity. To make further deductions, it would be interesting to see the profiles and the uniformity parameters of the optimized cases for the three slot heights together.

Blowing Momentum Coefficient, C_μ	**Wake Area Ratio, A**	**Wake Velocity Deviation Coefficient, δ**	**W Criterion**	**% Difference from Optimum**
Unblown	0.961	0.786	0.756	-24.44
0.009	0.994	0.966	0.960	-3.96
0.0095	0.997	0.980	0.977	-2.29
0.001	1.000	0.994	0.994	-0.64

Table 6.6: Wake uniformity parameters for different blown and unblown configurations for a slot height of $h_{slot}/c = 0.00125$

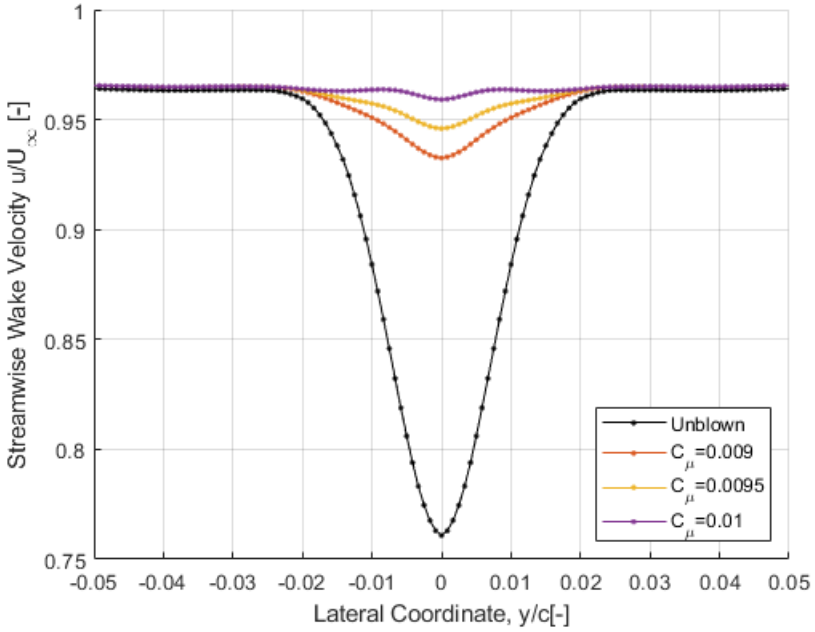

Figure 6.16: Effect of varying blowing momentum coefficients on the wake velocity and total pressure for a slot height of $h_{slot}/c = 0.00125$

Figure 6.17 shows the wake velocity profiles for the most optimised blowing momentum coefficient for each of the three slot heights. The corresponding W criterion for the three cases and the respective difference from the ideal value of 1, is presented in Table 6.7. The overshoot for $h_{slot}/c = 0.00075$ is more prominently visible here. Out of the three cases, $h_{slot}/c = 0.001$ with $C_\mu = 0.0095$ is closest to the most optimum case with an only 0.08% difference from the most optimum W criterion value as compared to the 0.32% and 0.64% difference for cases with $h_{slot}/c = 0.00075$ and $h_{slot}/c = 0.00125$ respectively. However, any of these three cases can be employed since they differ from the optimum by less than 1%. Therefore, better governing parameters would then be system limitations for example in terms of mass flow rate available for the system. This is further is addressed together with the fan-on cases in section 8.6.

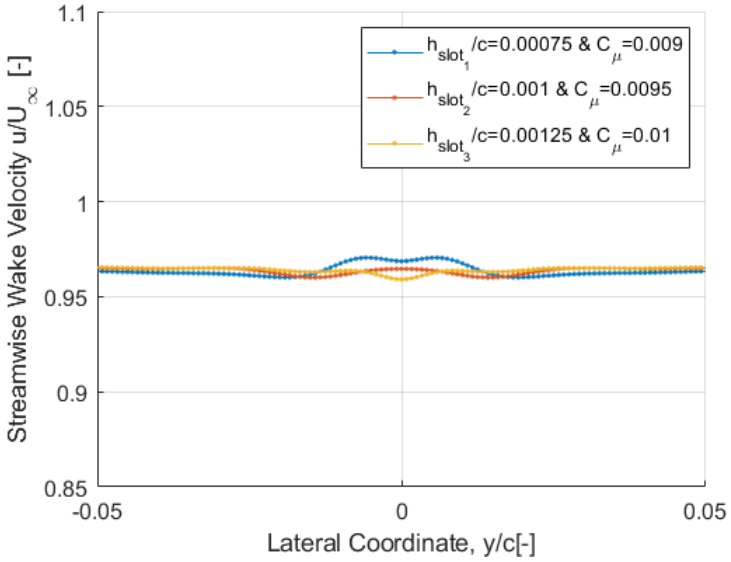

Figure 6.17: Comparison between the most optimum wake velocity profiles based on the values of W criterion for each of the 3 slot heights: $h_{slot}/c = 0.00075, 0.001, 0.00125$

Blowing Parameters [Case]	W Criterion	% Difference from Optimum
$(h_{slot}/c)_1 = 0.75\mathbf{x}10^{-3}$, $C_\mu = 0.009$	1.003	0.32
$(h_{slot}/c)_2 = 1\mathbf{x}10^{-3}$, $C_\mu = 0.0095$	0.999	-0.08
$(h_{slot}/c)_3 = 1.25\mathbf{x}10^{-3}$, $C_\mu = 0.01$	0.994	-0.64

Table 6.7: W criterion values and its deviation from the optimum the most uniform wake velocity profiles achieved for each of the 3 slot heights: $h_{slot}/c = 0.00075, 0.001, 0.00125$

Additional quantities to further understand the implication of the wake blowing mechanism on the overall flow and aerodynamics are addressed in chapter 8 along with their respective fan-on counterparts to better emphasise on the comparison. Quantities such as drag coefficient and mass flow rate, which will play a part in the final design of the system in future, will be addressed. Crucial quantities like dynamic loading and inflow angles, which will govern the future design of the APPU fan, will also be touched upon.

6.4.4. ANALYSIS FOR DIFFERENT RADIAL LOCATION

This section will address the variation in the wake velocity profiles as they progress behind the empennage to the prospective propeller plane location while looking at the difference between the 0.1R and 0.75R radial location. This is specifically important in order to comprehend the effect of the wake blowing system in a three dimensional and more realistic setting.

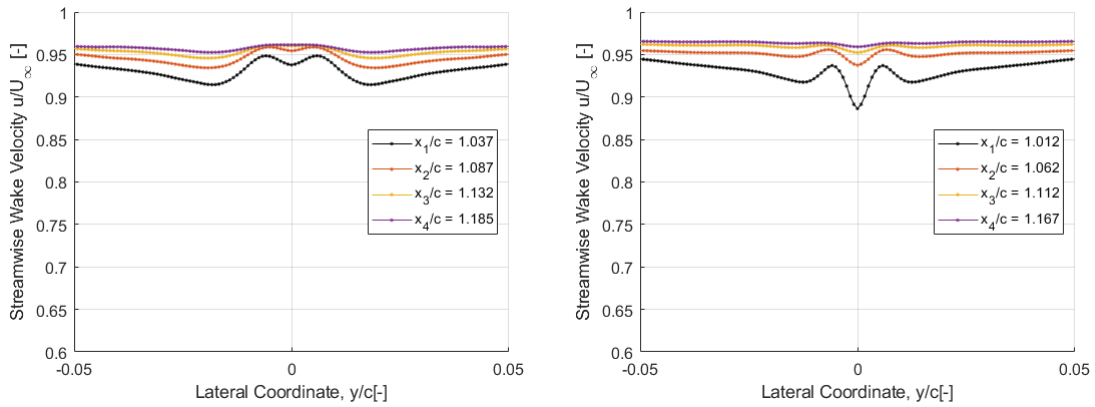

(a) 0.1R (b) 0.75R

Figure 6.18: Effect of the radial location with respect to the chosen propeller blade radius on the uniformity and progression of the 'blown' wake velocity plots for the four axial locations, X_1, X_2, X_3, X_4

Figure 6.18 shows the wake profiles for two radial locations 0.1R and 0.75R. For each location four axial location, specified in the beginning of section 6.4, were investigated to understand the progress of the wake behind the empennage. Since the behaviour of the progression was same for all three slot height cases, only the final case of $h_{slot}/c = 0.00125$ is discussed here. The profile at $x_4/c = 1.167$ for 0.75R was discussed in the previous section. It is interesting that for the same radial location, but closer to the emennage at axial location, x_1, the profiles shows 2 secondary maximas and two secondary minimas. This closely resembles the Type B profile that was discussed in section 6.2. This is attributed to the fact the location is in such close proximity to the empennage that the blown wake has not yet mixed with the empennage boundary layer and the wake deficit effectively. The outer secondary minimas are due to the residual low energy flow because of the thick empennage boundary layer. The two maximas can easily be attributed to the added momentum due to jet air blown into the empennage boundary layer to energize it. However, the viscous sublayer starts to grow again due to the interaction of jet flow with the VTP surface downstream of the slot. Therefore, when the flow leaves the empennage trailing edge, there is still a central deficit present in the wake. However, more axial distance is required for the blown flow to mix with the deficit flow and result in a more uniform profile. This increased uniformity can be seen as the wake progresses from x_1 to x_2 to x_3 and finally to x_4.

Now, the trend and the observations along with their corresponding explanations remain the same for the profiles taken at radial location of 0.1R. However, it should be noted that the profile at x_1 for 0.1R looks much more established in terms of flow mixing. In other works, there already seems to be a higher degree of mixing between the blown flow and the deficits. This is due to the fact that although the profiles are taken at the same axial location for both 0.1R and 0.75R, the corresponding absolute distance of these four locations from the empennage trailing edge are very different. This is due to the 34° sweep of the vertical tail plane, as explained early in section 6.4. This difference can also be seen in the axial coordinates represented after normalizing with the local chord. The x/c values for 0.1R are much greater than for those at 0.75R.

6.4.5. EFFECT OF JET VELOCITY DIRECTION

This small segment is included to explain the effect of the chosen jet velocity direction on the wake filling. This was a preliminary study conducted to support the choice that the jet velocity will be blown perpendicular to the blowing slot surface instead of along the flow normal direction. The profiles in Figure 6.19 are for the case of $h_{slot}/c = 0.001$ and for near optimum blowing coefficient, $C_\mu = [0.009, 0.0095, 0.01]$, since these are the coefficients of interest. For the cases where the jet air is blown is flow normal direction, the central velocity deficit is filled at a lower blowing coefficient but at the cost of much more prominent presence of the secondary deficit in the profiles caused due to the thick boundary layer of the empennage. This advantage and disadvantage of blowing in flow normal direction over slot perpendicular direct can be explained by the basic phenomenon of presence of shear in viscous flows. When the air is blown perpendicular to the slot surface, this jet is at an angle with the general flow around the geometry which is in the axial direction. This leads to a cross flow between the jet flow and the potential flow around the aircraft. Due to the air viscosity, the jet flow tries to align itself in the direction of the general flow. This induces extra mixing between the blown jet flow and the empennage boundary layer thus leading to a near absence of secondary minimas. However since, the jet is at an angle to the normal flow, the component of velocity in axial direction is smaller, and thus, the mere magnitude of the axial velocity deficit that is overcome, is slightly lower than what is recovered with the flow normal jet for the same blowing coefficient.

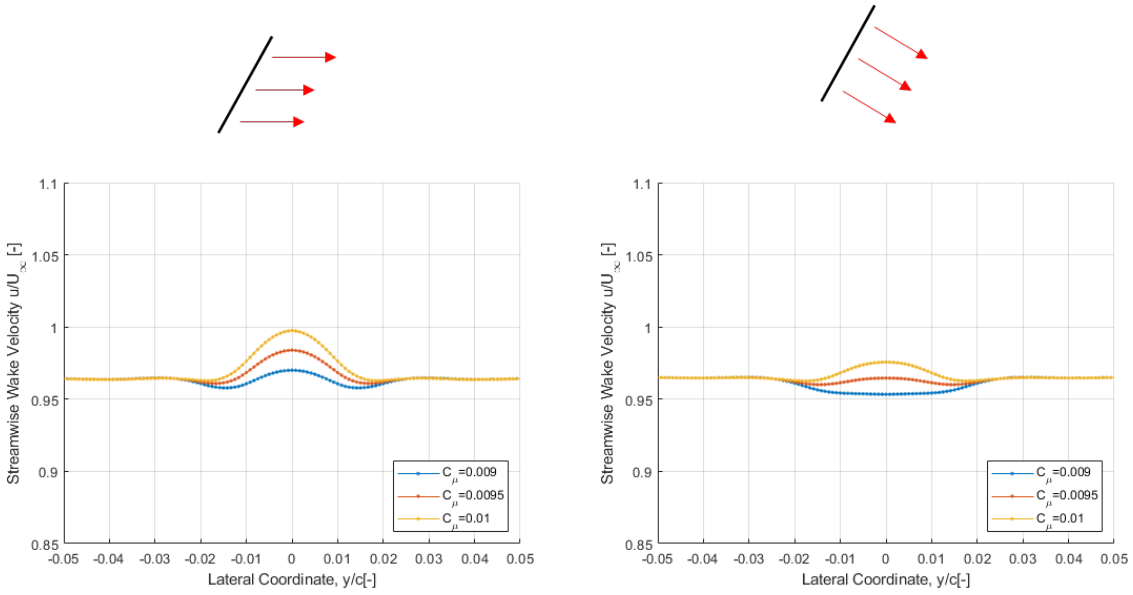

(a) Blowing in flow normal direction

(b) Blown in direction perpendicular to slot surface

Figure 6.19: Effect of the direction of the jet air blown through the wake blowing slot on the near optimum wake velocity profiles for the case with $h_{slot}/c = 0.001$

Therefore the only penalty is that a slightly larger blowing coefficient was required for slot perpendicular direction. However, the penalty in terms of added mass flow required, which increased from 0.98Kg/s for the flow normal direction to 1.07Kg/s for slot perpendicular direction, was only 0.09Kg/s which is small compared to mass flow rate requirement of the whole system. Since one of the objectives of this study is to comment on the proficiency of the wake blowing mechanism in filling the empennage wake and achieving a higher degree

of uniform flow, it was decided to go proceed with the jet velocity that fared better in that aspect. Thus the decision was made to proceed with the blowing the air in the direction perpendicular to the slot.

7

BLOWING SYSTEM ANALYSIS: FAN-ON CONFIGURATION

This chapter consists of the second part of the 3D wake blowing analysis which includes the application of the actuator disk model in order to simulate the BLI propeller. The relevance of this case is to understand the implication of the addition of the aft propeller on the wake blowing mechanism in terms it capability to fill the empennage wake. The chapter will begin with a brief description of the Fan design parameters used in the current study. This will be followed by a wake analysis study in section 7.2, similar to that of the fan-off configuration. Certain physical quantities which will be of interest to study, with respect to the inflow field experienced by the propeller, will be discussed in chapter 8, all the while drawing a comparison with the fan-off configuration.

7.1. FAN DESIGN PARAMETERS

The basic definition of the BLI propeller being used to simulate the APPU propeller configuration was discussed in section 4.3 along with its specifications. Since, the fluent boundary condition used to simulate the propeller is called the Fan Boundary Condition, for the sake of consistency the BLI propeller will be mainly referred to as the fan from now on. This section will primarily concern itself with the fan design parameters which were chosen for the current study. A sensitivity analysis of these parameters is beyond the scope of this thesis and therefore, fixed values for fan design parameters are taken (see section 4.3). As for the wake blowing parameters, slot height and blowing momentum coefficient will again be varied for the analysis. For their description, the reader is referred to subsection 6.1.2.

As seen in subsection 5.1.7, the fan boundary condition feature of fluent requires one major parameter, which is the pressure jump across the fan disk. Therefore, this will form one of the design parameters for this study. A calculation for this pressure jump is mentioned in Appendix B, which yields a value of 8.2kPa. Now, the other two variables important for the APPU configuration are the distance from the empennage and the fan diameter. The distance from the empennage, although important for the blade design and the APPU system in general, is not exactly a fan specification. Thus, the logical second choice for the Fan design parameter is the 'Fan Diameter', which is in this case the actuator disk diameter. The two fan design parameters are mentioned in Table 7.1. As mentioned in section 4.3, this is taken to be 3.8m. Based on the APPU design and fan requirements, the value of fan diameter can be changed. It can be accordingly modified in the current model to generate new data if such a time comes. But for this study it is kept constant. It should be noted that the fan diameter is not a non-dimensional quantity. Therefore, a better choice for design parameter would have been the advance ratio but since the physical design of the fan and its blades is not yet know, the fan diameter forms an appropriate selection.

Parameter	Value	Units
Fan Pressure Jump	8.2	kPa
Fan Diameter	3.8	m

Table 7.1: Fan Design Parameters

7.2. BLOWING SYSTEM ANALYSIS FOR FAN-ON CONDITION

This section will address the effect of the wake blowing system design parameters in the case when the effect of the fan is now taken into account. Analysis will be made on their capability to mitigate the empennage wake, thus, leading to potential reduction in noise and performance penalties. The results of the design study will be presented in Figure 7.2. A comparison will be drawn with the results of the wake blowing system design study for fan-off cases.

Although, the subsequent sections will discuss the results for the effect of the wake blowing system on the wake velocity profiles in the fan-on configurations, the focus region where the study would emphasize, remains the same as mentioned in section 6.3. The cyclic dynamic pressure loading of the 0.75R blade section around the propeller plane will also remain similar with the exception that the value of the coefficients themselves will increase due to the higher local flow velocity within the propeller streamtube. The results presented in this section will show what specifications of the wake blowing system would be required in order to fill the empennage wake. It will focus more specifically on the wake velocity profiles and the effect of the wake blowing system parameters on those profiles. However, for further representations of the flow streamlines and flow properties, apart from the ones that will be discussed in chapter 8, the reader is referred to Appendix D, where plots are shown comparing unblown and blown cases for both the fan-off and fan-on configuration. Just like the fan-off cases, it would be beneficial for the reader to understand the results laid out in the following sections if a brief about the data acquisition locations is provided at this stage(see Figure 7.1).

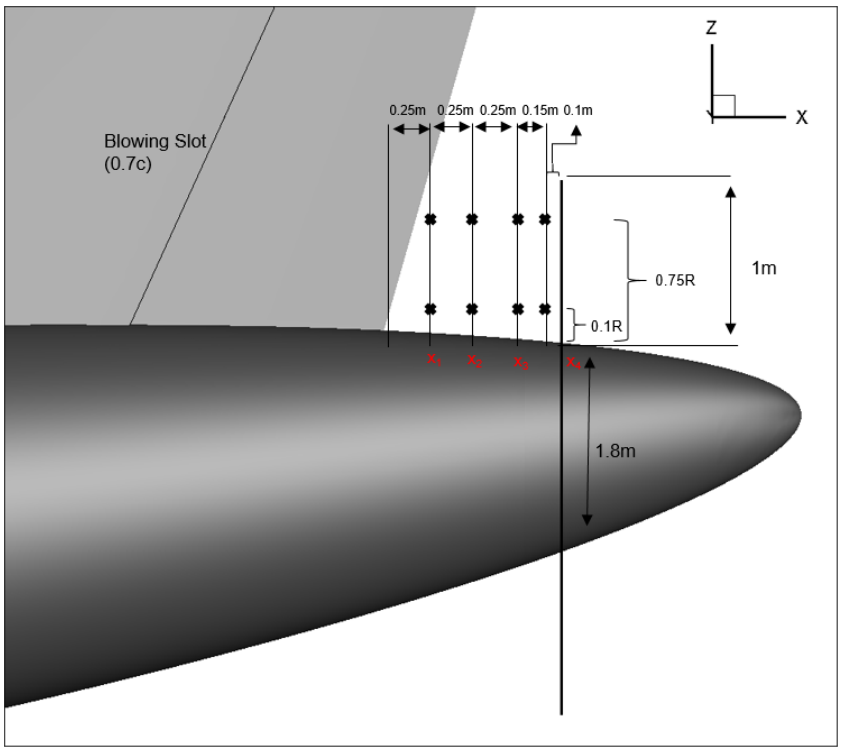

Figure 7.1: Data acquisition location with respect to the fuselage-empennage geometry and the prospective propeller plane for the fan-on cases. The 8 crosses, at 0.1R and 0.75R for 4 axial locations each($x_1, x_2, x_3, x_4 = 0.25m, 0.5m, 0.75m, 0.9m$), show the locations where the wake velocity profiles is investigated in the lateral direction going into the plane.

Most of the data acquisition points and the terminology remains the same, with one slight change. Since

the x_4 axial location, which was the prospective APPU fan location, is now finally used to model the fan as an actuator disc, this location is no longer feasible for data acquisition due to the fact that it now contains a singularity due to the presence of an infinitely thin fan model. Therefore, the x_4 location has been moved slightly upstream, specifically, by a distance of 10cm. The reasoning behind this choice was that this location was neither too far from the actuator disk plane to cause major difference in the observed flow properties and profiles, and nor too close that these properties start showing uncharacteristic behavior due to the presence of the singularity. Two locations closer to the actuator disk plane(5cm and 2.5cm) were also studied briefly before ending on the current choice. Though, neither of these locations showed major problematic behaviour but the chosen axial location fared better. The observation plane for the results and contours showed in chapter 8 was also taken at the new x_4 location for both the fan-on and fan-off results.

EFFECT OF BLOWING MOMENTUM COEFFICIENT, C_μ AND SLOT HEIGHT, $\frac{h_{slot}}{c}$

This section will dive into the wake blowing system analysis with the presence of the actuator disc. To begin the analysis, it is prudent that the results from the fan-off configuration be kept in mind in order to understand how the wake design parameters have changed and what it means for the wake uniformity parameters. Just like in the case for fan-off, the first slot height to be studied was $h_{slot}/c = 0.001$. The Figure 7.2 shows the performance of the wake blowing system in terms of its capability to fill the empennage wake for the fan-on configuration while showing again the fan-off case for comparison. The first thing to note is that the presence of the actuator disk speeds up the flow in its streamtube. Since the wake axial velocities have been plotted against the lateral coordinate, this manifests in terms of an overall upwards shift of the plots. The value of the normalised axial velocity now extends beyond 1 by almost 25% due to the fact that the velocities are still being normalized with respect to the freestream velocity which is much less than the local flow velocities induced by the fan in its streamtube.

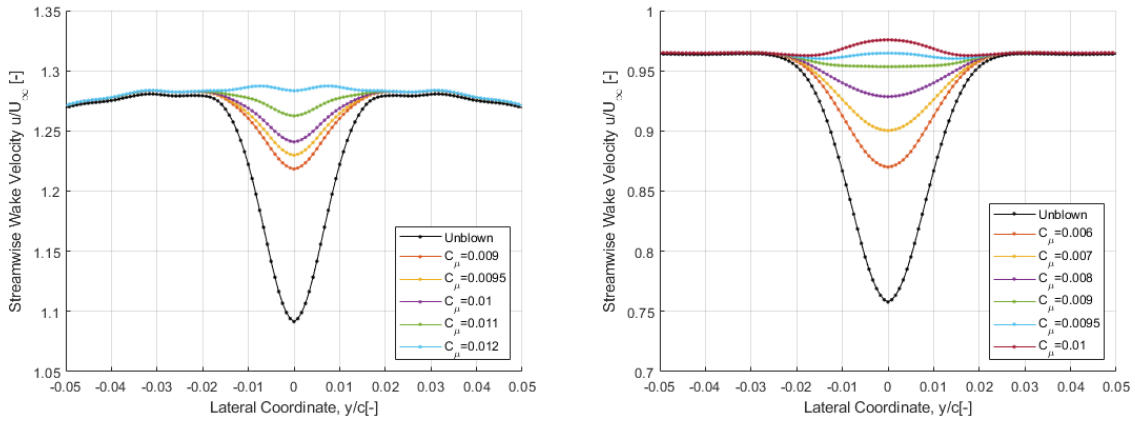

(a) Fan On (b) Fan Off

Figure 7.2: Effect of varying blowing momentum coefficients on the wake velocity profiles for $h_{slot}/c = 0.001$ in the Fan-on case, in contrast with profiles from the Fan-off case

Second observation, also due to the addition of the actuator disc, is that the wake velocity values at lateral coordinate corresponding to wake edge are lower than the no-deficit velocities in the wake just outside the central deficit.In other words, the velocity curve bends downwards towards the wake edges. This means that the axial velocity of the flow starts to decrease, which is not because of the empennage wake. The reasoning behind this is in the fact that the fan is modeled as an infinitely thin disk and the properties specified on the disk manifest in terms of a sudden jump across this disc. The flow upstream and downstream of this disk change due to the presence of this pressure jump. Thus leading to the formation of what can be called as the propeller streamtube. To simplify the problem for better understanding, consider fan plane as a suction device. The static pressure ahead of the disk becomes low which is complemented by a corresponding rise in dynamic pressure, keeping the total pressure conserved. This rise in dynamic pressure, manifests as a high increase in the flow velocity. In an invicid flow, this would mean a uniformly high velocity flow within

the whole cross section at any point in the upstream part of the propeller streamtube. However, since the current case models the flow viscosity, this means that a shear layer will be created between the flow inside and outside of the streamtube, preventing a sudden jump in pressure. Since there is no pressure difference there should be no velocity jump across this shear layer either. This shear layer therefore, tries to speed up the flow outside the streamtube while trying to slow down the flow speed inside the streamtube in order to prevent a sudden jump in velocity, thus preventing a region of flow discontinuity at the streamtube edge. It is due to this reason that the flow starts to slow down, going away from the centre, which can be seen with the increasing lateral coordinate.

Now, let's look at the effect of increasing blowing coefficient for this case. Before exploring the results, it is important to note that for the fan-on study, two extra iteration of blowing momentum coefficient were added beyond 0.01, ie. 0.011 and 0.012. This was done in response to the fact that the wake blowing system proved less effective with the presence of the fan. It can be seen from the wake velocity plots and W criterion values that a higher blowing coefficient is required to achieve an optimum velocity profile. Where the optimum coefficient for the fan-off configuration was found out to be 0.0095, with a deviation in W criterion from the optimum of only 0.08%, in the fan-on configuration for the same coefficient the deficit still remains prominent with the W criterion value still remaining 5.24% short of the optimum. One possible reasoning for this behaviour is that the presence of a higher velocity local flow. This means that more momentum need to be imparted to the boundary layer in order for the same amount of mixing. This is evident from the variation in W criterion value for each 0.001 magnitude increase in the blowing coefficient. It can be see from Table 7.2 that the W criterion improves by about 2% for an increase in blowing coefficient of 0.001, whereas going back to the fan-off configuration(see Table 6.4), it can be seen that for the same coefficient change, the W criterion value improved by 3%-3.5%.

Blowing Momentum Coefficient, C_μ	**Wake Area Ratio, A**	**Wake Velocity Deviation Coefficient, δ**	**W Criterion**	**% Difference from Optimum**
Unblown	0.972	0.847	0.824	-17.63
0.009	0.989	0.948	0.937	-6.27
0.0095	0.991	0.957	0.948	-5.24
0.001	0.992	0.965	0.958	-4.22
0.0011	0.995	0.982	0.978	-2.23
0.0012	0.998	0.999	0.997	-0.29

Table 7.2: Wake uniformity parameters for different blown and unblown configurations for $h_{slot}/c = 0.001$ in the Fan-On case

Thus it can be concluded that the increase in the jet velocity by same magnitude induces much less mixing in case of the fan-on flow, thus necessitating a higher blowing coefficient. This will have a penalty on the mass flow rate required to achieve a more uniform inflow profile for the propeller(further discussed in section 8.6). Last but not the least, looking at the W criterion values for the unblown cases for both fan-on and off configurations, it can be seen that the initial deficit that has to be overcome is much smaller in case of fan-on at 17.63% as compared to the considerably higher 25.09% in case of fan-off. This is somewhat expected due to the fact that a higher speed flow, induces a higher shear in the boundary layer leading to a smaller boundary layer displacement height. This would result in a wake where the velocity deficit is lower. However, a part of the reason for the lower deviation in unblown W criterion value, as well as, lower W criterion value variation for a constant blowing coefficient jump, can be attributed to the fact that the magnitude of the normalising area for wake area ratio and the normalising zero wake deficit u/U_∞ has increased. Therefore, a same absolute change in the wake area and velocity deficit deviation will be registered as a smaller increase in A_r and δ, and therefore also, W criterion. Therefore, it would be interesting to see the same plots in future attempts at this topic but with the fan-on axial velocities normalised with the local velocities instead of the free stream velocities. However, since this would also require a corresponding modification in the blowing momentum coefficient definition, from freestream velocity to local flow velocity, the wake blowing analysis will lead to the same final conclusion for achieving the optimum.

Figure 7.3 shows the corresponding wake velocity profiles for the remaining two slot heights for the fan-on configuration. Their respective wake uniformity parameters are mentioned in Table 7.3 and 7.4. The trend

is similar as the fan-off configuration but with higher blowing momentum coefficients as already described with $h_{slot}/c = 0.001$ results. An observation that can be made for all three slot height is that the slope of the curve near the central deficit region is higher for the near optimum blowing coefficient cases than as compared with the fan-off results. This can again be attributed to the higher shear force in the boundary layer and wake regions due to a higher local velocity. Also, for the $h_{slot}/c = 0.00125$ it can be seen that a coefficient of 0.012 is still not sufficient for the remove the velocity deficit. However the deficit and the non-uniformity has been reduced to a point where the W criterion value is only 2% lower than the optimum. Although, an addition of just one more iteration will potentially lead to the optimum for $h_{slot}/c = 0.00125$, this much resolution is not desired at such initial phases.

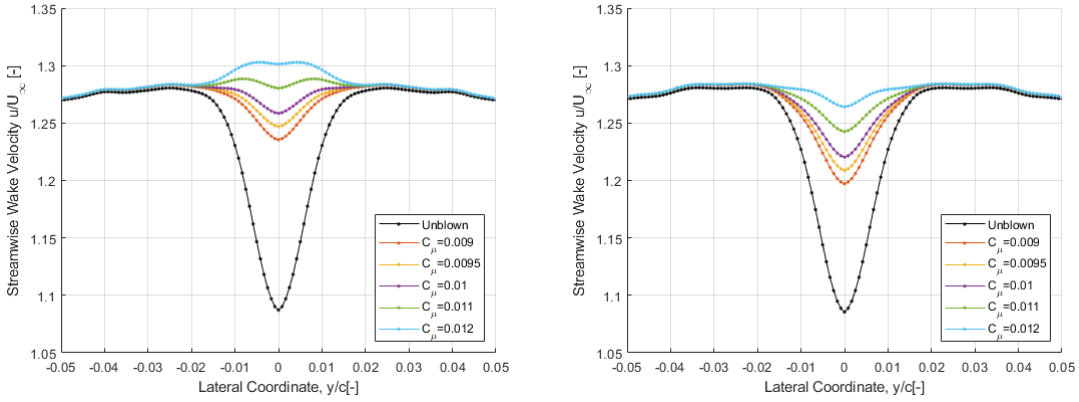

(a) $h_{slot}/c = 0.00075$ (b) $h_{slot}/c = 0.00125$

Figure 7.3: Effect of varying blowing momentum coefficients on the wake velocity profiles for $h_{slot}/c = 0.00075$ and 0.00125, in the Fan-on case

Blowing Momentum Coefficient, C_μ	Wake Area Ratio, A	Wake Velocity Deviation Coefficient, δ	W Criterion	% Difference from Optimum
Unblown	0.973	0.842	0.819	-18.06
0.009	0.992	0.960	0.953	-4.74
0.0095	0.994	0.969	0.963	-3.68
0.001	0.995	0.978	0.974	-2.63
0.0011	0.998	0.996	0.994	-0.60
0.0012	1.001	1.012	1.014	1.37

Table 7.3: Wake uniformity parameters for different blown and unblown configurations for $h_{slot}/c = 0.00075$ in the Fan-On case

Blowing Momentum Coefficient, C_μ	Wake Area Ratio, A	Wake Velocity Deviation Coefficient, δ	W Criterion	% Difference from Optimum
Unblown	0.973	0.842	0.819	-18.07
0.009	0.988	0.930	0.919	-8.13
0.0095	0.989	0.940	0.929	-7.07
0.001	0.991	0.949	0.940	-6.03
0.0011	0.993	0.966	0.960	-4.00
0.0012	0.996	0.983	0.980	-2.02

Table 7.4: Wake uniformity parameters for different blown and unblown configurations for $h_{slot}/c = 0.00125$ in the Fan-On case

Figure 7.4 shows the optimised wake velocity profiles for all three slot heights. As mentioned before, the case with slot height $h_{slot}/c = 0.00125$, although already close to the W criteria of 1, can be further optimised for a

more uniform profile. This would again establish the fact that the blowing momentum coefficients required for the different slot height increases as the slot height increase. This linear relation, although of importance, is also evident from the formulation of the wake blowing coefficient which itself depends linearly on the non-dimensionalized slot height. However, it would be of interest to see how the W-criterion values depend on the variation in the slot height and the blowing coefficients. Figure 7.5 shows the dependency of the W criterion the blowing momentum coefficients and on the slot heights.

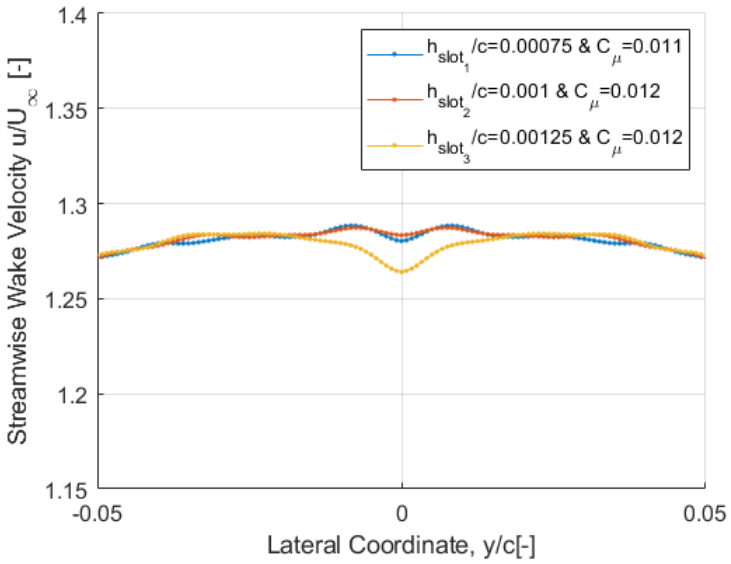

Figure 7.4: Comparison between the most optimum wake velocity profiles based on the values of W criterion for each of the 3 slot heights: $h_{slot}/c = 0.00075, 0.001, 0.00125$

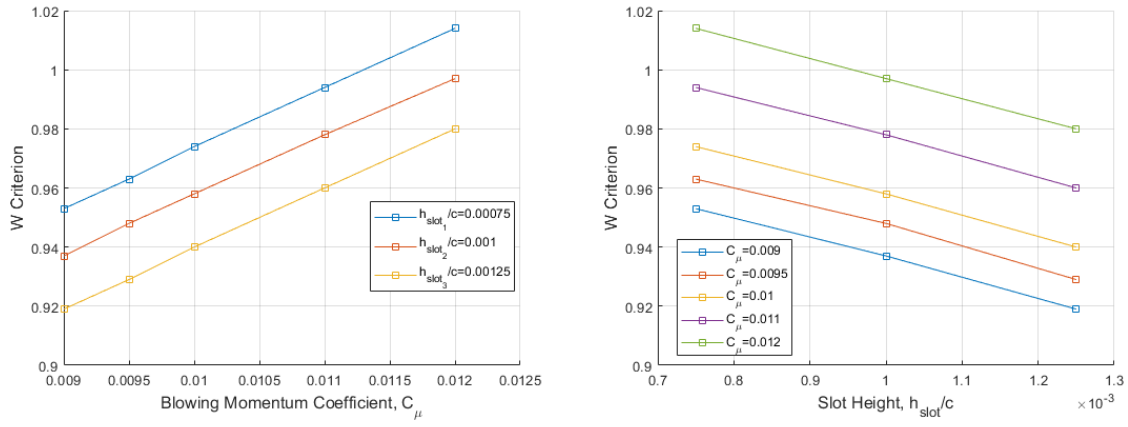

(a) (b)

Figure 7.5: Dependency of the W criterion the blowing momentum coefficients and on the slot heights

A linear relationship of the W criterion is observed with both, the blowing momentum coefficients and the slot heights. This is somewhat unexpected, but has a simple explanation which can be depicted using the formulation Equation 7.1.

$$W \propto A, \delta \propto \delta_3 \propto C_\mu \propto h_{slot}/c \tag{7.1}$$

where δ_3 is the normalized velocity at central deficit, as shown in Figure 6.4.

The dependence of W criterion being linear is due to the fact there have not been any considerable secondary maximas or minimas in the blown wake velocity profiles. Therefore, the values of the wake uniformity parameter, A(Wake Area Ratio) and δ (Wake Velocity Deviation Coefficient), which depend on a combination of all the deficits and maximas, can be assumed to be directly dependant on the normalized velocity at only the central minima/deficit. Now, the dependence of this central deficit has been clear from the wake velocity profiles to be linearly decreasing with increasing blowing coefficient values. This, not only leads to a linear dependence of 'δ' on the blowing momentum coefficient but also, a near linear effect on 'A'. And, the formulation of C_μ clearly shows a linear relation between C_μ and h_{slot}/c. Thus, leading to the linear relation of the W criterion with C_μ and h_{slot}/c. However, if there would have been secondary maximas and minimas, they would have possibly effected either A or δ or both, in a non linear way, leading to a non-linear dependency of W on the blowing system design parameter. It should be noted that this dependency is subjective to the blowing slot location on the empennage surface and the distance between the empennage and the observation location, which for the current case is in front of the propeller at 0.75R. It was already observed from the wake progression study at different radial locations that the profiles varied between 0.1R and 0.75R cases because of the difference in the absolute maximum airfoil thickness and the distance of the observation point from the empennage(see subsection 6.4.4). It should also be noted, that these implications are based on the results received for a specified mesh for a specified solver. It can be expected that if solvers or software, which are more proficient in resolving the boundary layer and wake flow, are used then the wake profiles will be more resolved which might lead to a better capture of secondary extremas which might have been missed in the current study.

Lastly, availability of data for three slot heights at five different blowing coefficients each, leads to the opportunity of performing a basic data extrapolation study. In Figure 7.6, the data for the W criterion for different permutations of slot heights and blowing coefficients was plotted using a contour plot. The line for the optimum W criterion value of 1 can seen on the top left corner of the plot. Extrapolating this line, could provide information on the optimum C_μ required for a chosen h_{slot}/c or vice-verse. Please note that, the extrapolated values would work best for the current setup of the wake blowing system and might require some adjustments to fit any modifications to the system design.

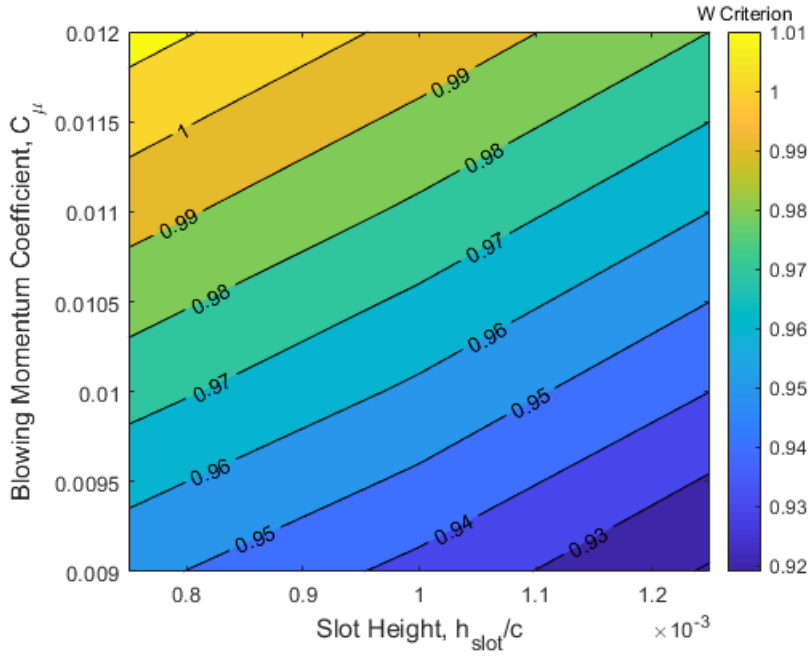

Figure 7.6: Contour of the W criterion data based on 3 slot heights and 5 blowing momentum coefficients

8

Discussion of Results

Since an extensive CFD analysis has been performed during the course of this thesis, it will be helpful to supplement the empennage wake blowing results with some visually aiding contours for better understanding of the interaction of the wake blowing system with the BLI fan inflow and also, to some extent, the section of the upper fuselage between the two. This section will begin with a discussion on the total pressure coefficient. It will also be of interest to look at the inflow angles as well as the dynamic pressure loading that the prospective fan blades will experience in the fan rotational plane. These will provide information which can potentially derive the design for the APPU fan blades. This will be followed by an analysis of the vorticity that will potentially be encountered by the fan. While taking about the wake blowing mechanism and the aft BLI propulsor, it is important not to forget about their impact on the aircraft as a whole. For this purpose a drag study will be presented followed by the mass flow rate analysis showing the air mass flow rates that would be required at the blowing slot inlet if the wake blowing system is to be installed. For these comparisons, only the cases with the most optimum wake filling characteristics will used for both the blown fan-off and the blown fan-on case. Again, the reader is referred to Appendix D, where surface contour plots are shown comparing unblown and blown cases for both the fan-off and fan-on configuration, for other flow properties like velocity(see Figure D.3) etc.

8.1. Total Pressure Coefficient

To get a better understanding of the flow at the fan intake, the distribution of total pressure was studied for the fan-on and fan-off configurations for both the unblown case and the most optimum blown case. The distribution is presented in terms of the total pressure coefficient, C_{P_T} which was defined in section 6.3 and the contours were plotted at the propeller inflow plane location of 0.1m ahead of the propeller itself. These contours are shown in Figure 8.1.

The primary observation is the deficit in total pressure in the fuselage boundary layer and the empennage wake. Considering the basic definition of boundary layer thickness in terms of total pressure reaching the freestream value, it is interesting to observe the difference in the boundary layer thickness between the lower and the upper fuselage. This is due to the upsweep of the aft fuselage and is a well established effect[61]. However, the absolute magnitude of this boundary layer is of importance to the APPU project since one of the highlights of the project is the use of the BLI propulsor. The boundary layer increases from a few centimeters on the aft upper fuselage surface to about 0.8m on the lower fuselage surface. For boundary layer velocity profile plots, the reader is referred to Figure D.4-D.7. The upper, smaller thickness of the boundary layer can be attributed to the fact that the fuselage surface is more flat with minimal curvatures leading to a lower loss in pressure in the near wall flow as compared to the upsweep on the lower side of the fuselage. The speeds of the flow around the lower fuselage are influenced by a much smaller pressure gradient leading to a lower shear force and thus a much larger boundary layer. The boundary layer thickness is effected greatly by the local flow velocity which is governed by the pressure gradient in the near wall region. It is precisely this effect which can be seen in the contours for the total pressure coefficient in case of the fan-on configuration. The presence of the fan, speeds up the local velocities in its streamtube. This leads to an increased amount of shear force within the viscous sublayers, and thus, a smaller overall thickness of the boundary layer.

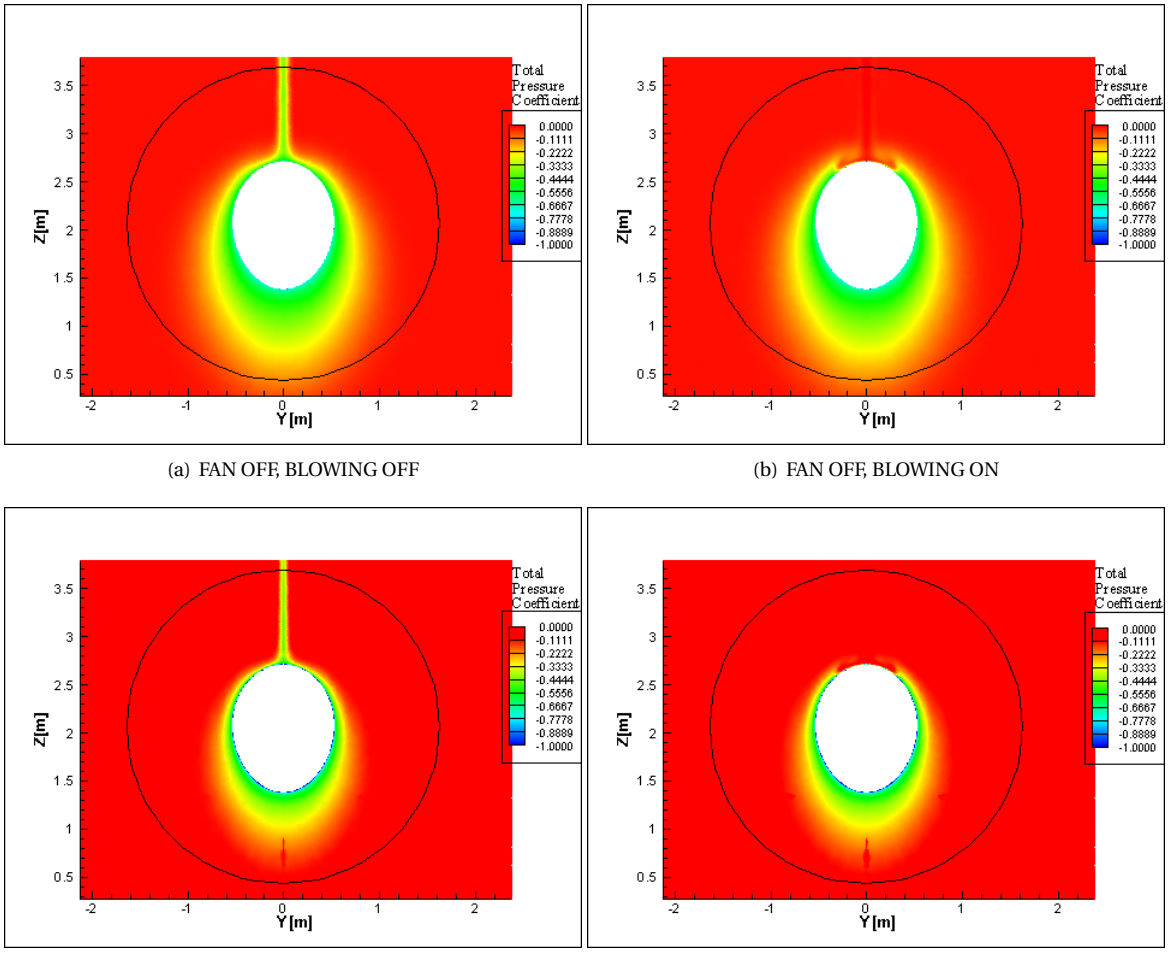

(a) FAN OFF, BLOWING OFF

(b) FAN OFF, BLOWING ON

(c) FAN ON, BLOWING OFF

(d) FAN ON, BLOWING ON

Figure 8.1: Contours for total pressure coefficient for the unblown and the most optimum blown case for both, the Fan-On and Fan-Off configurations, taken on an observation plane located 0.1m ahead of the actuator disk for $h_{slot}/c = 0.001$

Next, the effect of the blowing momentum coefficient over the recovery of the total pressure that is lost due to empennage wake, is dominant in the contours. The contours validate the finding provided in section 6.4 regarding the capability of the blowing system in achieving a near 100% recovery of total pressure in the wake. However, it is interesting to see that there seems to be some complementary recovery in pressure over the upper fuselage as well. This is due to the fact that the current blowing system extends to the empennage-fuselage junction. Also, the jet air is blown through the slot in a perpendicular direction which makes it directed towards the fuselage. These two factors together lead to a component of this jet flow interacting with the upper fuselage boundary layer and energising it to result in the observed recovery in total pressure. It should be noted, that the difference in the thickness of the deficit pressure region on the upper side of the fuselage in the fan-off and fan-on configurations, leads to a slight difference in their blown cases. Since there is a thicker region of lower pressure on the upper side of the fuselage in fan-off configuration, it can be seen that a part of this region away from the fuselage surface, still remains deficit in terms of total pressure. This is due to the fact that the resultant effect of the interaction of the jet with the fuselage surface is more pronounced close to the surface. More axial distance is need for the jet flow to induce mixing to the deficit regions away from the surface. This effect is not seen in case of fan-on configuration since the higher local flow reduces the deficit region enough, such that the chosen axial distance is enough for the jet flow to energise the region completely.

However, this is not the main purpose of employing the wake blowing. The idea behind the mechanism is to provide a more uniform inflow for the BLI fan, thus assisting in its acoustic performance. Two major factors

which derive the performance and design of a fan and its blades are the dynamic pressure loading of the fan disk and the corresponding inflow angles that would be experienced by the blades. These will be discussed in the subsequent sections.

8.2. DYNAMIC PRESSURE LOADING

The dynamic pressure loading of a fan is a factor which governs the design of fan blades. A highly loaded blade is preferred for a high thrust requirement but the benefit is offset by the difficulty in the design process. With the discussion of this section, it can be hoped that some additional relevant information will be provided to aid in the blade design process of the fan for APPU configuration. These along with the inflow angles, govern the flow profile around the fan blades. In an ideal case, the fan will see a uniform distribution of the dynamic pressure in its rotational plane. However, this is rarely the case. For the fuselage-empennage combination under consideration, two factors contribute towards making this this distribution non-uniform. These are the deficit in dynamic pressure due to the aft fuselage upsweep and the deficit due to the wake of the empennage. It is the focus of the current thesis to try and mitigate the contribution that the empennage brings to this non-uniformity. To that end, Figure 8.2 shows the dynamic pressure loading that is expected over the fan rotational plane in fan-on and fan-off configurations.

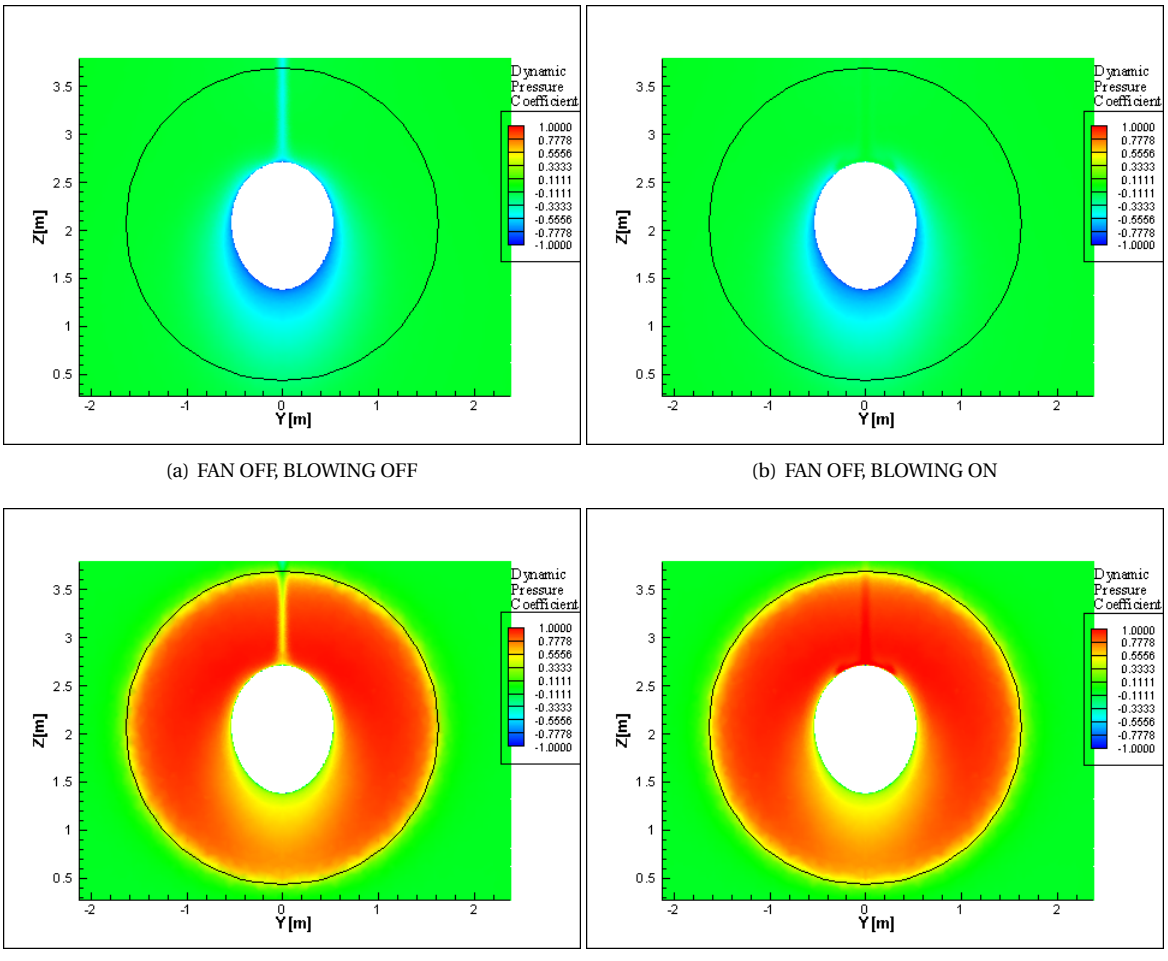

(a) FAN OFF, BLOWING OFF

(b) FAN OFF, BLOWING ON

(c) FAN ON, BLOWING OFF

(d) FAN ON, BLOWING ON

Figure 8.2: Contours for dynamic pressure coefficient for the unblown and the most optimum blown case for both, the Fan-On and Fan-Off configurations, taken on an observation plane located 0.1m ahead of the actuator disk for $h_{slot}/c = 0.001$

These contours are another validation of the wake filling ability of the blowing system to mitigate the dynamic pressure deficit which can be seen in the unblown cases at twelve o'clock location ie. at an azimuth of 90° (see Figure 8.4). To better visualise the wake filling effect on the dynamic loading, the contours for difference in

the dynamic pressure coefficient for the blown and unblown cases for the fan-on configuration are given in Figure 8.3 in the plot on the right. The figure on the left shows the sole effect that the addition of the fan has on the dynamic pressure coefficient in the fan plane. Two improvements can be suggested based on the blown fan-on contour. Firstly, the wake blowing system works too well for region near the fuselage surface. This is somewhat undesirable since it adds to the non-uniformity in loading that the inboard blade will experience when going behind the empennage. This can be removed by either employing differential blowing where the coefficient changes in spanwise direction according to requirement or starting the blowing slot at a location slightly away from the fuselage junction. However, these efforts might not be very fruitful since the inboard part of the fan blades contribute less to the thrust and the performance of the fan. Secondly, since a uniform wake blowing momentum coefficient is chosen for the slot surface, this fills the wake well towards the fan tip too. This will again be seen as a non-uniformity by the fan bade and might even lead to supersonic tip Mach numbers and a contribution to the tonal noise part of noise emission. However, this can easily be resolved by carefully restraining the blow span of the VTP.

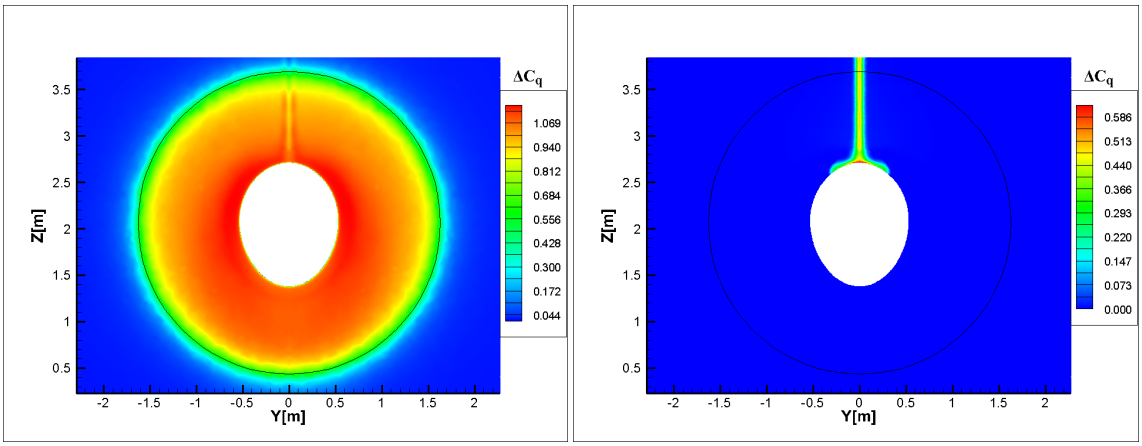

(a) Effect of Fan: (Unblown Fan-On)-(Unblown Fan-Off) (b) Effect of Wake Blowing: (Blown Fan-On)-(Unblown Fan-On)

Figure 8.3: Change in dynamic pressure loading due to the addition of the fan and due to implementation of the wake blowing system, represented in terms of difference in dynamic pressure coefficient for $h_{slot}/c = 0.001$

The above mentioned observations have been quantified in the Figure 8.4. The figure shows the dynamic pressure coefficient values at different azimuthal locations for the blown and unblown cases for fan-off and fan-on configurations for $h_{slot}/c = 0.001$. The corresponding individual effects of the fan and wake blowing are also shown using ΔC_q values(blue and red lines, respectively), along with the values for their combined effect(yellow line). It is important to note from the C_q plots that, where the fan helps in reducing the non-uniformity in loading at 270° azimuth location, it has the opposite effect on the 90° location. The C_q at 90° location for the unblown fan-off case is -0.468 and goes up to -0.087 which leads to a uniform C_q loading. This is a jump of 0.38 points. On the contrary, in the fan-on configuration, this jump is of about 0.5 as the C_q goes from 0.368 in unblown case to 0.861 in blown case. This can be attributed to a steeper velocity gradient in the wake which was previously discussed as being due to the higher shear forces induced by the steeper pressure gradient in fan-on configuration. The same can be seen in the slightly unfavourable contribution of the blue line in ΔC_q plot at 90° location.

Another point to note is that the blown cases that yielded a uniform wake velocity profiles, now show a slight overshoot behind the empennage at the 90° azimuth location. The wake velocity profiles that were analysed until now were taken in the horizontal lateral direction behind the empennage at the propeller inflow plane location. However, it is evident that a better indication of propeller loading would be a polar profile for a specific blade cross-section like 0.75R varying from a few degrees below to few degrees above 90° location. Also, please note that the spiky behaviour of the plots for fan-on configuration can be speculated to be due to the mesh. However, since the region near the empennage wake is more refined, the drop in dynamic pressure coefficient can be assumed to be accurate.

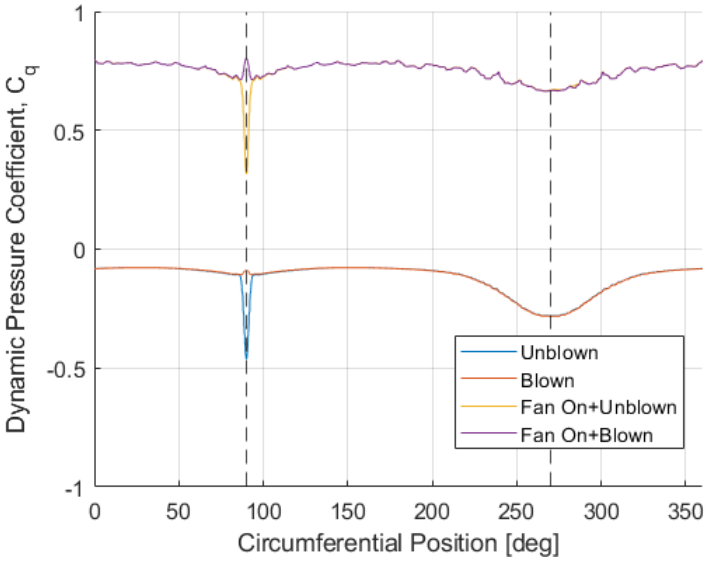

(a)

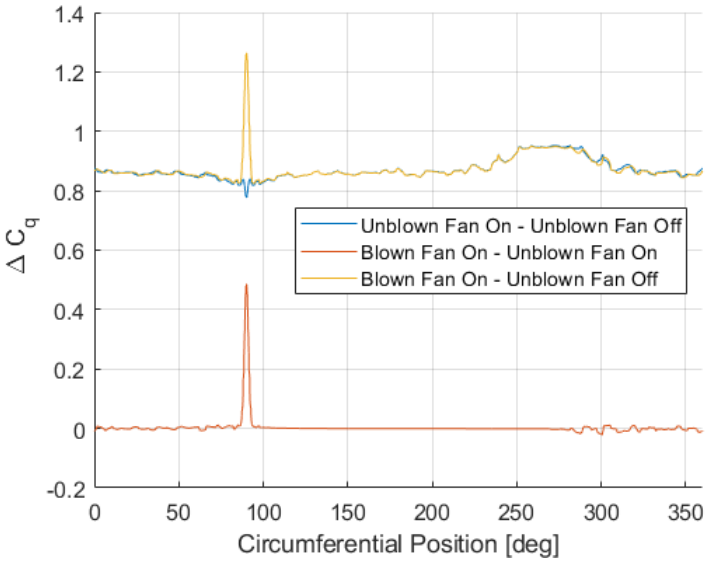

(b)

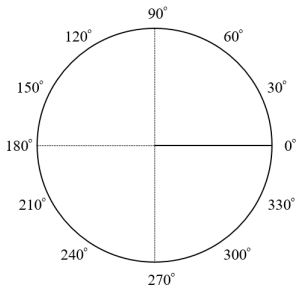

(c)

Figure 8.4: Effect of addition of wake blowing system with $h_{slot}/c = 0.001$ for Fan-On and Fan-Off cases on the (a) dynamic pressure loading for the optimum blowing cases around the azimuthal locations(c) for a blade height of 0.75R and (b) respective changes caused due to addition of fan(blue) and addition of wake blowing system (red) and the combined change to the base case due to the combination of the two(yellow)

The main reason for the overshoot is the fact that the absolute distance from the empennage changes as the propeller moves in a circle. This is due to the change in the horizontal projection of 0.75R section position over the vertical axis. The effect of the radial location on the wake filling was discussed in subsection 6.4.4 where it was seen that at locations closer to the root, the absolute wake width increases due to a thicker airfoil, thus leading to a higher probability of secondary deficits. It can be speculated that it is these deficits that still remain and can be seen in the polar plot at locations away from 90° azimuth. Thus leading to a relative overshoot in the dynamic pressure loading. It can also be speculated that a spanwise differential filling of wake might lead to a more seemingly uniform loading for the fan.

8.3. INFLOW ANGLES

The inflow angles are the circumferential angles seen by the fan blade at different azimuthal locations in the rotation plane and are shown for the blown and unblown cases for the two configurations under study in Figure 8.5. It is important that these values do not get high enough to cause stalled flow over the blades or supersonic flow speeds which might lead to shocks because these can have a large adverse effect on the thrust produced by the propeller. The overall effect of the wake blowing system on the inflow angles is somewhat negative and specifically focused in the hub region near the upper fuselage surface. As can be seen in both the fan-on and fan-off configurations, blowing the wake of the empennage leads to much higher inflow angles near the blade hub on the upper fuselage surface. The magnitude of these valued can even reach up to $9-10°$ very close to the hub in case of blown fan-off.

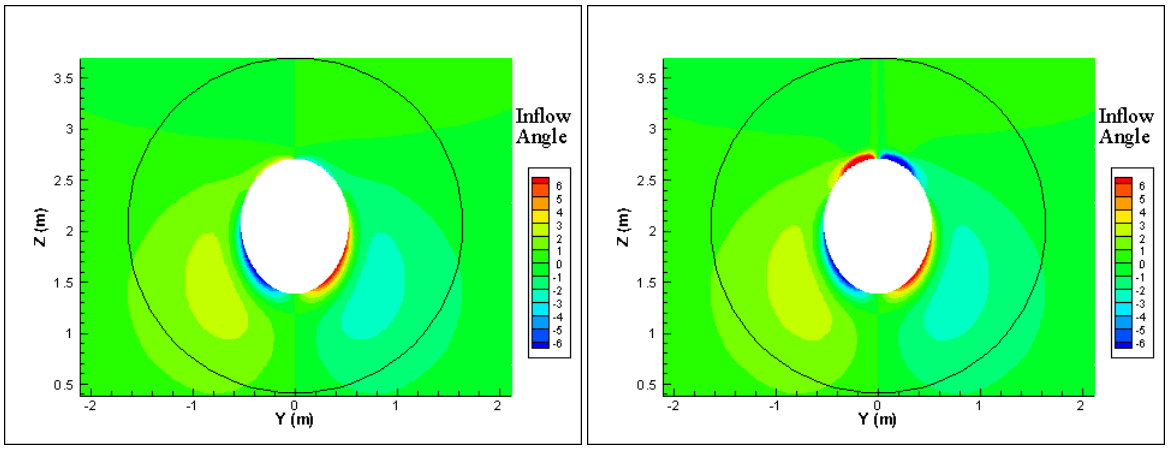

(a) FAN OFF, BLOWING OFF

(b) FAN OFF, BLOWING ON

(c) FAN ON, BLOWING OFF

(d) FAN ON, BLOWING ON

Figure 8.5: Contours for the inflow angles that the fan blades will experience for the unblown and the most optimum blown case for both, the Fan-On and Fan-Off configurations, taken on an observation plane located 0.1m ahead of the actuator disk for $h_{slot}/c = 0.001$

However, the addition of the fan, which is essentially a suction disk, causes a flow straightening effect which

aligns the flow more towards the axial direction. This effect along with a higher axial flow velocity leads to a higher dominance of the axial velocity component over the circumferential velocity component. Thus, restricting the inflow angle values to near $\pm 6^\circ$ for the blown case. The presence of the fan also causes a considerable favourable effect on the inflow angles at the lower fuselage, which can get high near the hub due to the fuselage upsweep. The lower fuselage inflow angles, which were earlier over the values of $\pm 5^\circ$, are now restricted to only $\pm 2^\circ - \pm 3^\circ$. However, the negative impact of the wake blowing on the upper fuselage might not be of much concern since it is too close to the hub to derive any major blade design parameters. It would be more fruitful to base the designs on the angles reached on the lower lateral side of the fuselage away from the surface, since those will be experienced by the highly loaded part of the blades. Nevertheless, the effect of the wake blowing should not be ignored since it does induce a gradient of over 12° in a very short rotational span, going from over $-6^\circ to + 6^\circ$ across the empennage wake.

8.4. VORTICITY

The main focus of this research is to achieve a good degree of uniform fan inflow using the wake blowing technique. However, along with this, the physical properties of the flow like vorticity are also of interest. A brief vorticity study is included to see how the x, y and z components of the vorticity are influenced by the addition of the fan and the blowing system, shown in Figure 8.6. One of the more observable impacts of the blowing system can be seen in the plots of x component of the vorticity where it induces rotation to the flow about the axial direction. Since the jet is blown along the vertical tail aft surface, the direction of jet is opposite on the two sides of the VTP. This induces a counter-rotational influence on the flow behind the empennage on the two sides. This effect cancels out a similar effect that is induced by the fuselage upsweep. It should be noted that there is another small region of high vorticity in the unblown fan-on case towards the actuator disk tip, behind the empennage. This effects starts to develop slightly inboard and intensifies towards the tip. This could be due to the fact that at a higher radial coordinate in the fan plane, the distance of the plane from the VTP reduces. This, along with the higher local flow velocity in the fan streamtube with the flow directed towards the fan plane, induce a higher rotation to the flows leaving the trailing edge of the VTP on either side which can be seen as the rise in the x-component of vorticity. A similar effect also happens at the lower fuselage where the effect of fuselage upsweep, on the vorticity, is intensified. It is suggested that further implication of this component should be investigated before arriving at a final blade design for the APPU fan.

The effect of the blowing system on the y-component of vorticity is much more straight forward. The unblown cases show the effect of the fuselage aft cone curvature on the downward and upward rotation of the flow at the upper and lower fuselage locations respectively. The effect on the lower fuselage is much more pronounced and spread over a wider region due to the upsweep of the aft fuselage. A similar effect is also seen in the z-component of vorticity where due to the fuselage upsweep, the flatter lateral side of the cross-section and the converging shape of the aft fuselage cone, a curl in induced in the flow, rotating it towards the fuselage surface. The addition of the blowing system, which adds a high velocity jet, with the main component of jet velocity in the axial direction, is to reduce the contribution of the y-component of vorticity on the upper fuselage. This is due to the role that the high speed flow plays in driving the flow more axially and preventing it from curling.

The addition of the fan causes a converging effect on the flow in and around the streamtube. Since this work deals with viscous flows, this leads to development of shear between the various flow layer, leading to an induced gradient of the axial and z-component of velocities with respect to z and x direction respectively. This can be seen as a negatively induced vorticity on the upper circumference of the disk and a positive vorticity on the lower circumference. A similar effect of the fan can be seen in the z-component of vorticity as well, with the interaction between x and y velocity components being more pronounced on the lateral sides. But, the behaviour of the z-component of vorticity is much more complex. Apart from the already mentioned effect due to the fuselage upsweep, the flatter lateral side and converging aft fuselage cone, there is a similar role played by the VTP. The concave contour of the VTP airfoil, converging to end at the trailing edge, induce a rotational component to the flow x and y velocity components. Their gradients with respect to y and x directions respectively, lead to the dominant vorticity effect seen in the empennage wake. Here again, the blowing system plays a positive role in reducing this empennage induced vorticity. As there is no longer a pressure deficit behind the empennage, the tendency of the flow to curve inwards towards the central lateral coordinate no longer exists. Moreover, as it was seen that the optimum blowing coefficient, in terms of

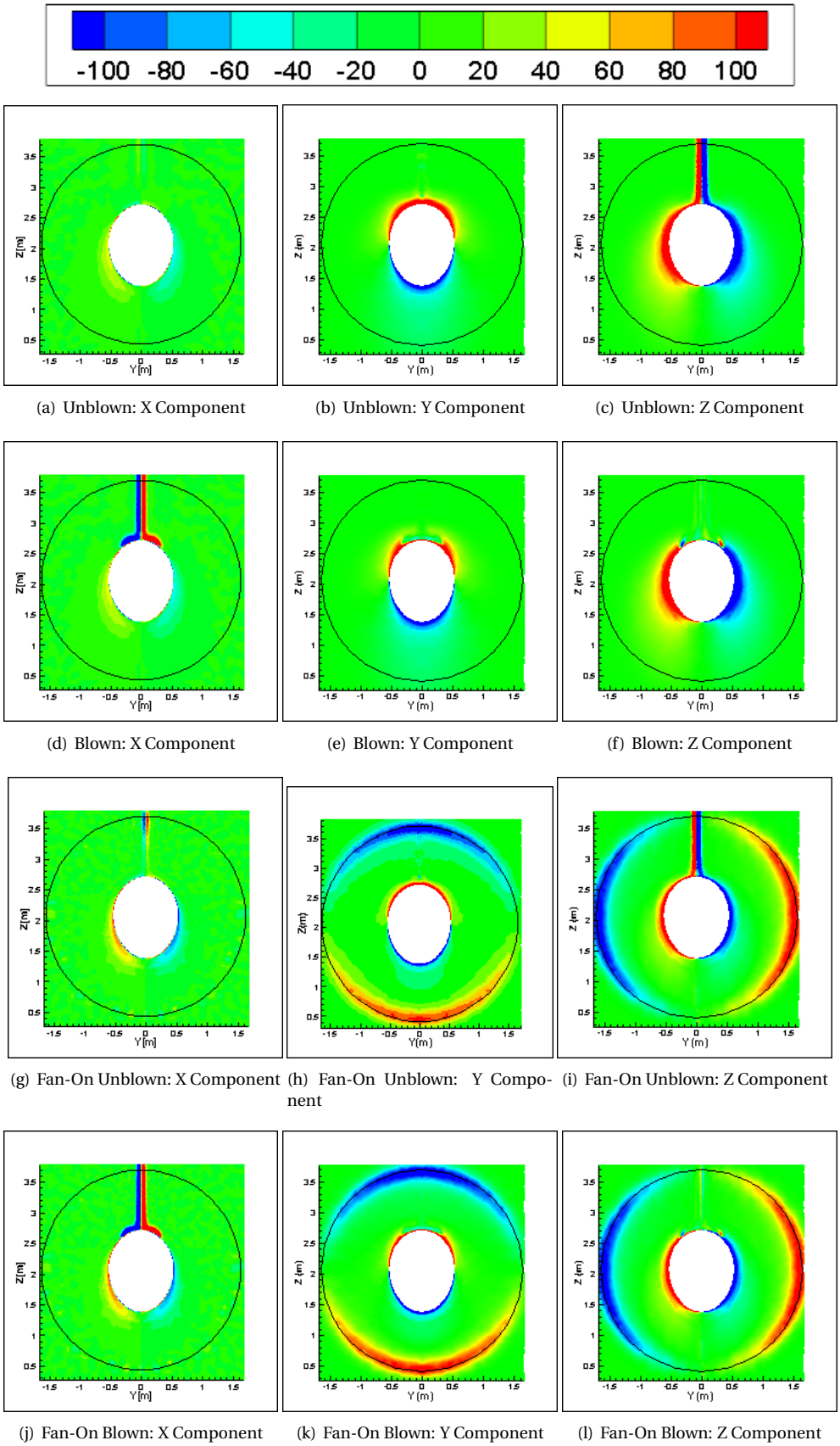

(a) Unblown: X Component (b) Unblown: Y Component (c) Unblown: Z Component

(d) Blown: X Component (e) Blown: Y Component (f) Blown: Z Component

(g) Fan-On Unblown: X Component (h) Fan-On Unblown: Y Component (i) Fan-On Unblown: Z Component

(j) Fan-On Blown: X Component (k) Fan-On Blown: Y Component (l) Fan-On Blown: Z Component

Figure 8.6: Contours for the x,y and z components of vorticity that the fan blades will experience for the unblown and the most optimum blown case for both, the Fan-On and Fan-Off configurations, taken on an observation plane located 0.1m ahead of the actuator disk for $h_{slot}/c = 0.001$

uniform velocity profile(or in other words, uniform dynamic loading), means a slight overshoot in terms of total pressure, some very minute effects of this can be faintly seen in the empennage wake in terms of reversal in vorticity direction. What is more visible is the interaction effect of the blown wake with the fuselage. This interaction leads to diverging effect induced in the flow as the flow moves from the VTP to the fuselage and tend to diverge away from the fuselage surface. This effect mixed with the opposite effect of the flow curling inwards due to converging nature of aft fuselage cone, leads to the region of high vorticity gradient where the direction of the z-component of the vorticity is flipped in a very short span.

8.5. EFFECT ON DRAG

At this point, the reader will have gained insight into the effects of the wake blowing system over the local flow behind and around the empennage, including its effect on the propeller inflow plane. However, it is just as important to look at the sole and combined implications of installation of the wake blowing system and the APPU propeller on the drag of the model. For this analysis, again the best blown case was chosen which was for $h_{slot}/c = 0.001$ with $C_\mu = 0.0095$ in fan-off configuration and $C_\mu = 0.012$ in fan-on configuration.

A preliminary drag study was performed for the aircraft geometry in question with the total drag values for the blown and unblown cases for the two configuration laid out in Table 8.1 in terms of drag counts. The pressure and viscous drags were calculated for the geometry such that the total drag, sum of the two, not including any other contribution. The table shows that the additional contribution of the wake blowing system to the total drag in any of the configurations is much less than the contribution of the installation of the fan. The contribution of the wake blowing system to the pressure drag of the system is negligible due to the fact that its influence on the flow around the whole geometry is minimal. Thus, leading to only some pressure changes in regions behind the empennage, as seen in the static pressure contours over the geometry surfaces in Figure 8.7. However, its major effect, although small, lies in the increase in viscous drag. This effect is also focused near the aft VTP region. The rise in viscous drag is due to the fact that the high speed jet flow from the slot leads to much larger shear forces on the VTP surface down stream of the slot, which leads to a rise in the skin friction coefficient resulting in the rise in viscous drag. This can be seen in the skin friction coefficient contours in the Figure 8.8. On the other hand, the fan largely impact the local flow and its pressure properties, resulting in a much larger shift in the pressure drag and thus the total drag.

Case	**Drag Counts** ($1DC = 0.0001C_D$)
Unblown	66.60
Blown	70.14 (5.3%)
Fan On + Unblown	99.20 (48.9%)
Fan On + Blown	102.20 (+53.9%)

Table 8.1: Drag coefficient represented in terms of drag counts for the whole aircraft body for the unblown and optimum blown cases for the fan-on and fan-off configurations for $h_{slot}/c = 0.001$

Since the target aircraft for the APPU concept is the Airbus A320, it would be informative to compare these values with the A320 drag coefficient values. Although, no official data on A320 drag coefficients was available, Sun[79] predicted the zero lift drag(C_{D_0}) contributions of common aircraft models. For A320, the C_{D_0} for take-off was found out to be 0.078(ie. 780 drag counts). This was validated with a python code(Appendix E) where empirical formulations from Torenbeek[80] and Raymer[81] were used to calculate the drag and lift coefficient contributions of the different aircraft component to the whole aircraft lift and drag. The code generated a value of 673 drag counts for the zero lift drag. This value is underestimated as compared to the former. This can be due to the interference drag not being taken into account and also due to the use of estimate figures for the aircraft dimensions. However, it still gives a value in the correct ball park. Therefore, using the code, a drag coefficient value can be calculated based on only the involvement of the fuselage and the vertical tail, as is the case for this research. This value of the zero lift drag for fuselage-VT combination came out to be around 107 drag counts. This value is in line with the estimates based on the drag break down for aircraft components for A320 aircraft given by Kornilov[82]. Although, this is not an ideal choice for comparison because the current version of the code is based on generic assumptions on root and tip chord thickness and also models the fuselage as cylindrical, but this gives an indicative idea into whether the changes seen due to the blowing system and fan are considerable or not.

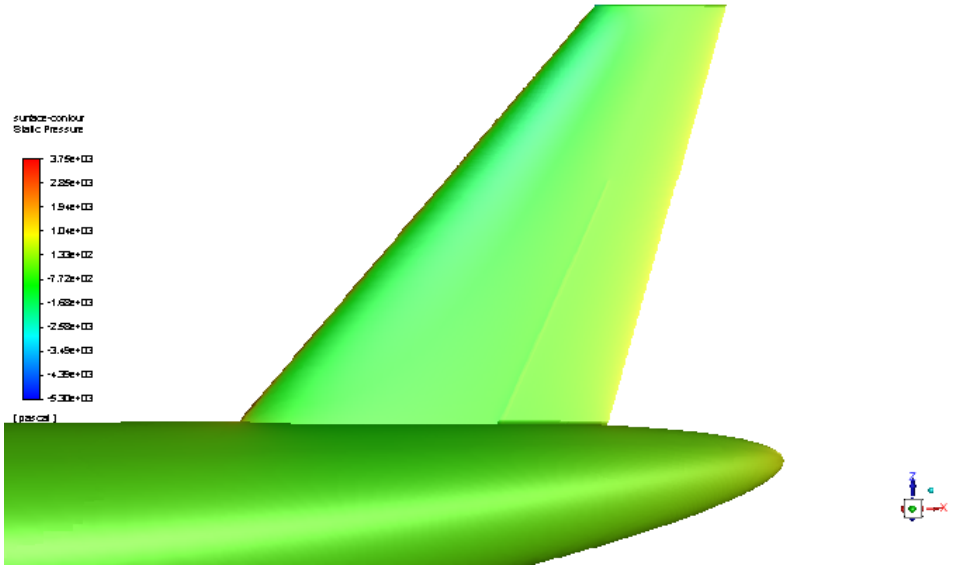

(a) Unblown Fan-off

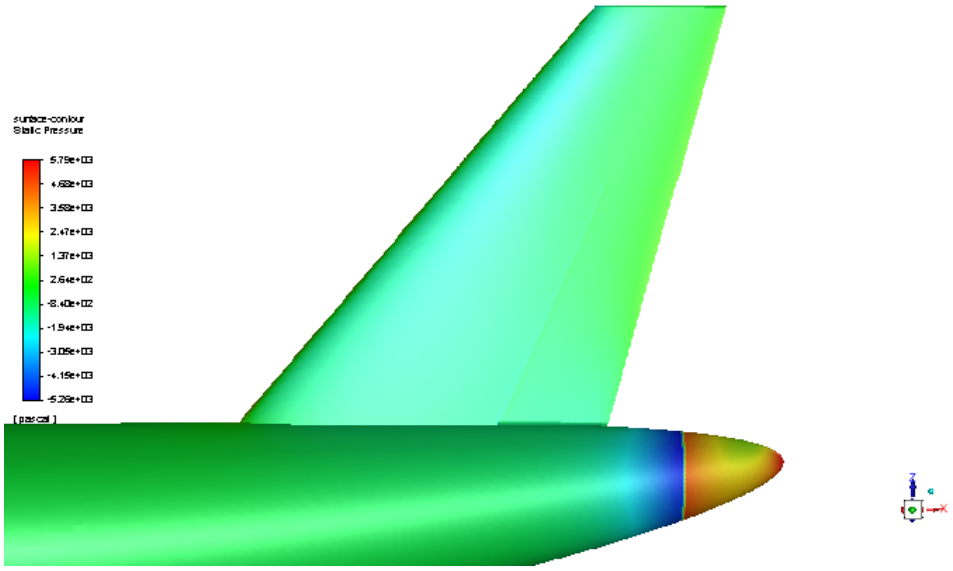

(b) Unblown Fan-on

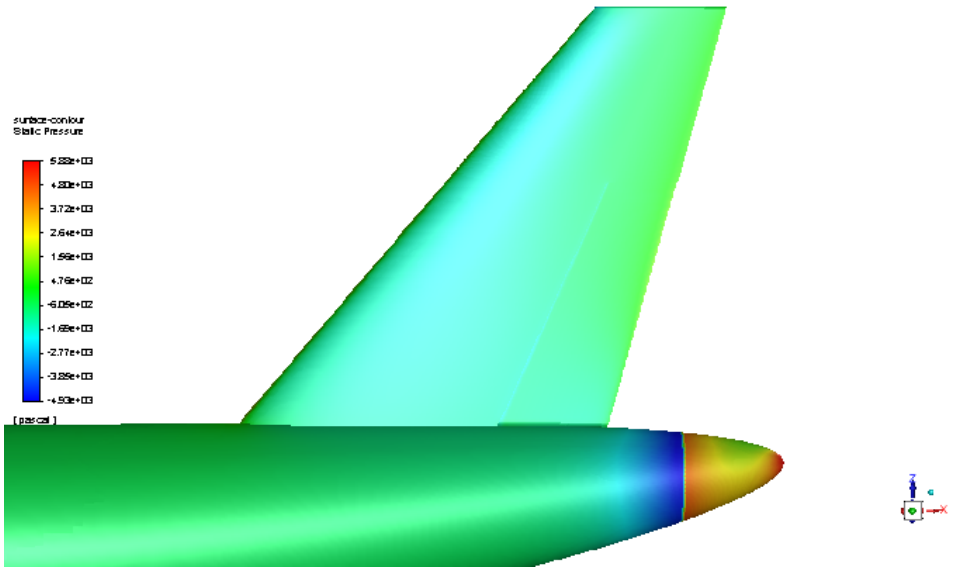

(c) Blown Fan-on

Figure 8.7: Effect of the fan and the wake blowing system on the local surface static pressure

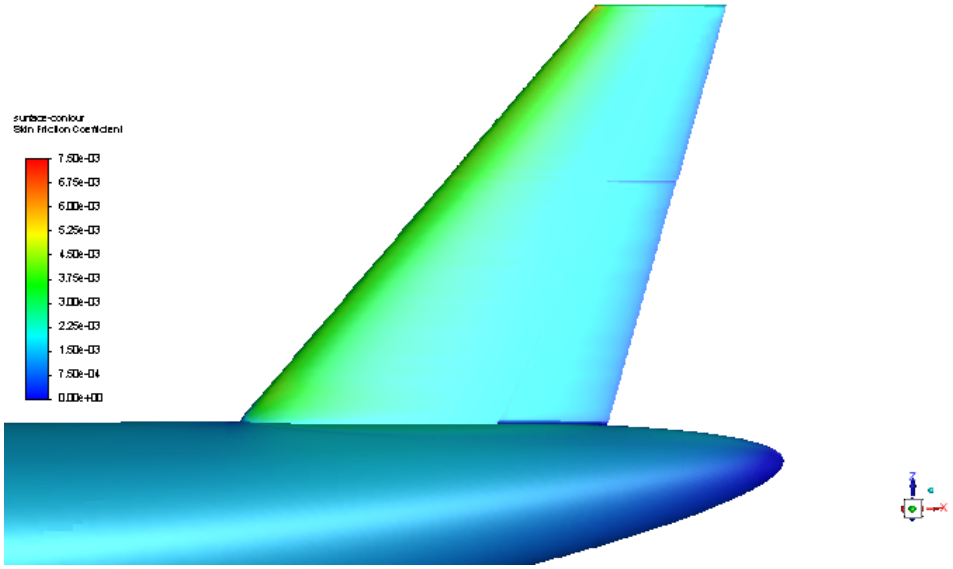

(a) Unblown Fan-off

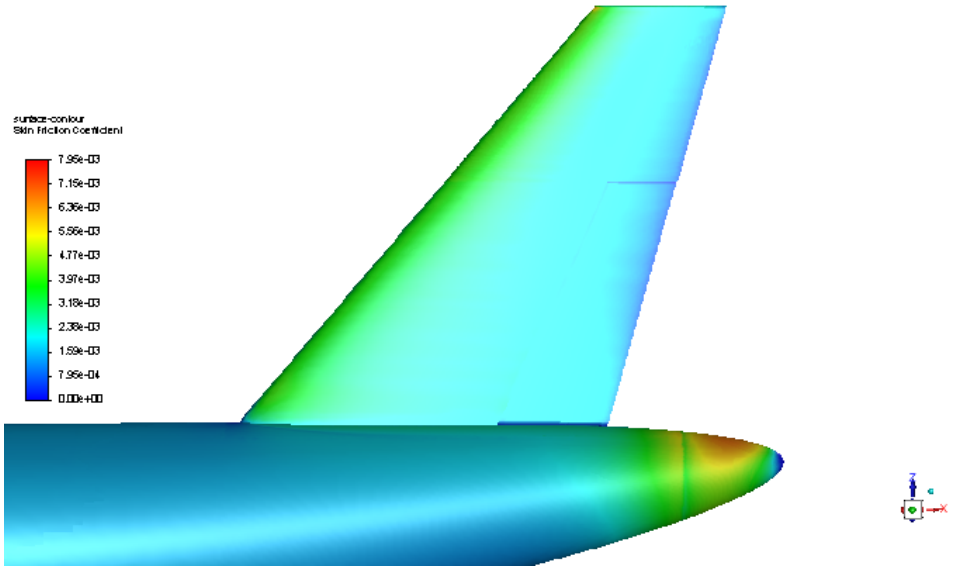

(b) Unblown Fan-on

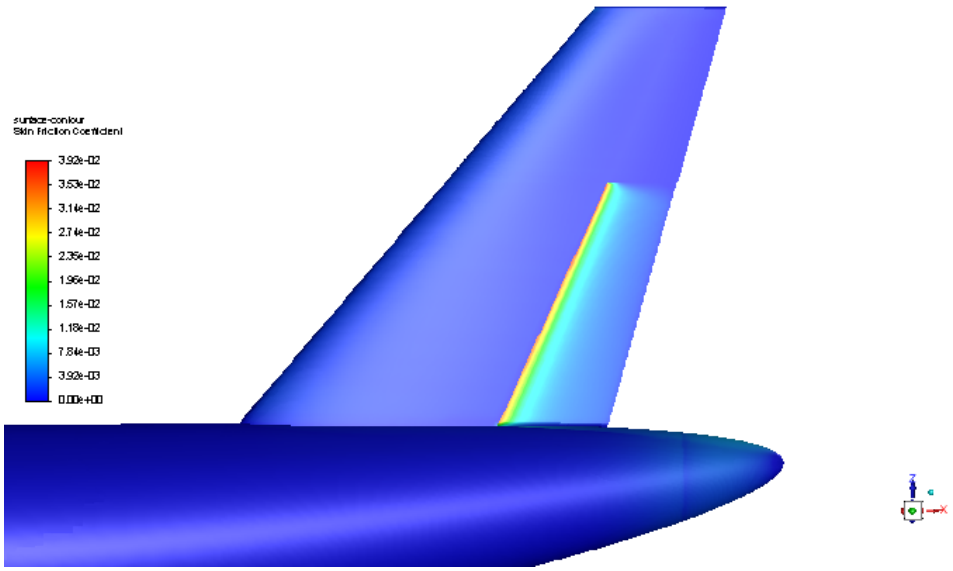

(c) Blown Fan-on

Figure 8.8: Effect of the fan and the wake blowing system on the local surface skin friction coefficients

As can be seen from the table, the wake blowing mechanism only has an increment of less than 4 drag counts as compared to the base case and will not be of much importance for the overall aircraft drag of order of 10e2. The fan addition of the other hand will definitely play an influential role as can be seen by a jump of over 33 drag counts and therefore, needs to be investigated further. To give an idea for the absolute force values, the base case was found to have a drag force of 3182N which is increased to a value of 4892N for the final blown fan-on case.

Since, this study is aimed only to give an indicative idea of the effect of the fan and the blowing system on the drag, a proper thrust drag book-keeping method has not been employed. Thus, the contribution of the thrust of the fan was not considered and neither was the contribution of any other drag component like for example, pumping drag. The current drag values are solely based on the effects of the surface skin friction and the flow pressure around the geometry.

8.6. EFFECT ON MASS FLOW RATE REQUIRED

A lot of discussion has been focused towards the requirements for the wake blowing system in terms of mass flow rate. This is because the mass flow requirements will pose some major design complications for the induction of the wake blowing system. The reason behind this is that the wake blowing system will need considerable amounts of mass flow , as given in Table 8.2. The engine bleed alone, will not be able to suffice these requirements. The typical engine bleed for the modern turbofan engine varies from 0.25Kg/s to around 3-4Kg/s depending on the engine and the extraction point in the compressor[83–87]. These values were found for different modern turbofan engines with different bypass ratios. It is possible to have mass flow rates larger than this but are not recommended due to the loss in thrust and gain in thrust specific fuel consumption. The typical mass flow rate values usually vary from 2-10% of primary flow. As the bypass ratio of turbofan engines increases, this leads to a further lower availability of bleed air. Moreover, this bleed air already finds its uses in systems such as cabin ventilation and thermal management. Thus, an even lower amount of air would be spared for the blowing system. From what can be inferred from the current study, a mass flow rate of at least 1.8Kg/s would be required to achieve proper wake filling in fan-on configuration. This value goes beyond 2Kg/s if a better quality of wake filling and propeller inflow uniformity is desired. Taking out this air from the engine bleed can seriously effect the performance of the engine and is therefore, not a solution. The most logical solution seems to be an addition of a small compressor in the fuselage tail or if possible, the empennage itself. This, however, comes with a lot of logistic and design issues which would need to be tacked. Therefore, another area which definitely needs to be investigated is the possibility of employing a differential blowing mechanism where the mass flow along the slot span is controlled based on the requirement such the the whole system is not using the highest mass flow. Another solution can be to divide the blowing slot into parts and blowing on only a few or alternative number of these parts. This will not only conserve the air mass but could possibly also induce a higher amount of mixing of the flow with the boundary layer.

Case	Mass Flow Rate (Kg/s)
$\frac{h_{slot}}{c} = 0.00075$, **Blown**	1.66
$\frac{h_{slot}}{c} = 0.00075$, **Fan On + Blown**	1.82
$\frac{h_{slot}}{c} = 0.001$, **Blown**	1.96
$\frac{h_{slot}}{c} = 0.001$, **Fan On + Blown**	2.20
$\frac{h_{slot}}{c} = 0.00125$, **Blown**	2.26
$\frac{h_{slot}}{c} = 0.00125$, **Fan On + Blown**	2.46

Table 8.2: Mass flow rates of the jet air injected at the blowing slot in Kg/s for optimum blown cases for the fan-on and fan-off configurations for each slot height, $h_{slot}/c = 0.00075, 0.0001, 0.00125$

9

CONCLUSIONS AND RECOMMENDATIONS

During the course of this thesis, a chord-wise wake blowing system was designed and implemented in order to mitigate the effects that the empennage has on the inflow of the aft mounted BLI propeller. The research has been performed with an intent to address the effect of filling the empennage wake, by the method of chord-wise wake blowing, on the non-uniform inflow of the BLI propeller. Some aircraft level implications of installation of the wake blowing system on the empennage of an A320 like aircraft configuration were also investigated. Two aircraft configurations were studied in this work, first, the aircraft without the presence of the BLI propeller, known as the Fan-off configuration and second, the Fan-on configuration, where the aft propeller was added to the aircraft structure as an actuator disk. The wake blowing analysis was carried out for both of these configurations in order to not only analyse the capability of the system in inducing uniformity in the empennage wake, but also to investigate how the blowing system requirements differ in case of fan-on configuration from the fan-off configuration. Some of the major findings and conclusions based on this study will be stated in section 9.1, followed by a few recommendations for further investigation into this topic, in section 9.2. These recommendations which will facilitate a better understanding of the feasibility and applicability of chord-wise blowing mechanisms for PFCs and also suggest improvements to the design presented in the current study.

9.1. CONCLUSIONS

The chord-wise wake blowing system was found to be a successful tool for achieving uniform flow in the empennage wake, in both, the fan-off and fan-on cases. The level of uniformity achieved was affected by the blowing system design parameters like the non-dimensionalized blowing slot height(h_{slot}/c) and the blowing momentum coefficient(C_μ), which determines the velocity of the jet air added through the blowing slot. Out of the three slot heights investigated, h_{slot}/c = 0.00075, 0.001 and 0.00125, the medium slot height of h_{slot}/c = 0.001 showed the best wake filling capability, based on the wake uniformity coefficient(W criterion). For this slot height, the most uniform empennage wake velocity profiles were achieved for blowing momentum coefficients of C_μ = 0.0095 for the fan-off configuration and C_μ = 0.012 for the fan-on configuration. The corresponding W criterion values were 0.999 and 0.997 which means that a wake uniformity of 99.9% and 99.7% was achieved using chord-wise wake blowing. Moreover, the data gathered from these cases can be used to make an extrapolation for future design investigation into the wake blowing mechanism which would be instrumental in finding out the optimum blowing coefficient for a given slot height and vice-verse. However, since all three slot heights were able to produce uniform wake velocity profiles with the deviation of W criterion from the optimum of less than 1%, the final design parameters for the blowing system is more likely to be governed by other system considerations like required air mass flow rate or addition to aircraft drag.

At the same time it should be kept in mind that a number of factors worked in a favourable manner to yield such high level of uniformity. First among these is the choice of chord-wise location of the blowing slot over the empennage surface. For the case of the current work, a chord wise location of 0.7c was chosen, where c is the local chord of an empennage cross-section. This value was chosen because it provided 30% of the aft empennage for the mixing of the high momentum jet flow with the low momentum empennage boundary layer. Another fixed parameter which played a role in the uniformity of the achieved wake profile, is the distance

of the propeller behind the empennage. Due to the tail strike considerations, the distance that can be kept between the empennage and the aft propeller is limited. However, it was found out that choosing a propeller location 1m behind the empennage-fuselage junction, provided sufficient distance for the blown flow to mix with the wake and lead to a uniform wake velocity profile.

IMPLICATIONS FOR BLI PROPELLER

The primary aim of the wake blowing mechanism was to achieve a uniform wake velocity profile leading to a uniform dynamic pressure loading for the aft propeller. This has been achieved for most part of the propeller disk. The blowing of the wake is able to overcome the deficit in the dynamic pressure loading present in the wake of the empennage. A jump of 0.4-0.5, depending on the radial location, was achieved in the value of the dynamic pressure coefficient, bringing the net dynamic pressure coefficient closer to the desired value of 1. There is, however, a small segment of upper fuselage region where the non-uniformity seems to exist. This corresponds to the region where the blown jet flow energizes even the upper fuselage boundary layer due to the slot orientation and blown flow angle. This is an added effect of the wake blowing system where, the fuselage section behind the empennage has an energized boundary layer leading to a non-uniformity at the propeller hub. But, since the non-uniformity at the propeller hub would largely be encountered by the blade root sections, it is likely that the adverse contribution of this non-uniformity would be low enough to not be of concern. It was also concluded that a spanwise uniformly blown wake might not lead to an ideal disk loading since it has been optimised for a 0.75R radial location and does not have the same filling effect at other radial locations due to the difference in the absolute wake width and the also the difference in the absolute distance from the empennage trailing edge.

Another important quantity which could influence the propeller specifications and design is the inflow angles that the propeller blades will experience at different circumferential locations. The blowing system was found to have a negative impact on the inflow angles that would be experienced by the propeller behind the empennage near the root. An increase in blade angle of up to $\pm 6^{\circ}$ was attained at the hub location on the upper fuselage. Again, as the effect is more confined to the hub location, it is likely that this negative contribution in terms of the high inflow angles is less relevant for blade design and propeller performance.

AIRCRAFT LEVEL IMPLICATIONS

Although the objective behind the addition of a wake blowing system is focused towards mitigating the adverse effects of empennage on the aft propeller inflow, the implications of the blowing system itself on the aircraft in general, cannot be ignore. One of the effects of the wake blowing system is over the aircraft drag. The blowing system operating in the most optimum fan-on configuration of $h_{slot}/c = 0.001$ and $C_{\mu} = 0.012$, achieved within the confines of the design space explored in this study, leads to an addition of about 3 drag counts to the overall drag of the aircraft geometry. This addition is rather small and is seen as an increase in viscous drag.

One of the requirements for operating the wake blowing system proposed in this study, is an input of high speed air inflow. Mass flow rate of 1.82Kg/s to 2.46Kg/s would be required for the optimum blowing configuration, depending on the chosen slot height. This requirement will not be satisfied with the typical engine bleed values for turbofan engines. Therefore, a practical implementation of the wake blowing system in an aircraft empennage would require alternative methods for providing the required air mass flow rates.

9.2. RECOMMENDATIONS FOR FUTURE WORK

The current study established a case for efficiency of chord-wise wake blowing technique in filling the wake of an empennage and mitigating its adverse effects over aft mounted BLI propeller inflow. However, still some research needs to be done to establish a practical viability of the system to be implemented in PFCs. Some recommendations based on the findings and conclusions of the current research are as follows:

- The current research leaves some desire for data on the propulsive efficiency and noise performance of the BLI propeller in presence of the chord-wise wake blowing system, both numerical and experimental. Although, filling the wake has been proven to have a positive impact on the noise performance of

a BLI propeller, it would be prudent to have some quantifiable data regarding the effect that a chord-wise blowing system will have on propeller performance. Although, detailed studies would required a propeller blade design subjective to the APPU concept in order to be more beneficial for the project, some preliminary studies, even on low fidelity models, would add to the knowledge.

- The logical next step would be to investigate the working of the chord-wise wake blowing system in cases of non-zero angles for the aircraft angle of attack, side-slip angle and rudder deflection. These, along with a corresponding investigation for cruise operating conditions, will give a comprehensive understanding of the benefits and limitations of introducing a wake blowing system in an aircraft over all flight phases.
- Present study involved an asymmetric fuselage which lead to a non-circular hub for the BLI propeller. A design iteration would be required to modify the aft fuselage to have a circular propeller hub. This will eliminate any additional affect that the non-circular hub would have had on the currently obtained values for dynamic pressure loading and inflow angles.
- The results obtained for the wake filling effect of the blowing system, although promising, were based on a fixed slot location. Even though the choice of the slot location was made after a thorough literature study, it would be interesting to explore other chord-wise locations where the slot can be places, especially the rudder hinge location.
- From the current study, one major obstacle to be addressed before the chord-wise wake blowing system can be practically implemented in an aircraft, is the requirement of a high air mass flow rate for the system to work as defined in this thesis. Also, it is likely that the engine bleed will not be able to contribute towards this required mass flow. Therefore, alternative sources need to be found for the air supply. One possibility is of introducing a compressor, especially for the wake blowing system, either in the empennage itself or at some other location in the aft fuselage. Also, efforts should be made to find ways by which the mass flow rate requirement of the blowing system itself, can be reduced. A few suggestions to achieve a reduction in the required mass flow rate which can be investigated in succession to this thesis are as follows:
  - One possible way of reducing the mass flow rate requirement of the system would be to optimise the spanwise length of the vertical tail over which the air is being blown. This means that the outboard edge needs to end closer to the point where the blown flow no longer effects the wake profile within the BLI propeller streamtube. But also, the inboard edge of the wake blowing slot, ie. the start of the slot, does not have to be at the empennage-fuselage junction. The results depict that the inboard slot does not contribute to the wake filling due to the blown air direction being perpendicular to the slot surface. The inboard slot is majorly responsible for the additional upper fuselage boundary layer filling and therefore is not beneficial for the BLI propeller. Therefore, the slot could start at a location away from the junction, thus reducing the required mass flow rate.
  - Another option, which could be helpful, is of applying differential blowing momentum coefficients, instead of a uniform blowing momentum coefficient. This means that different blowing coefficients will be used at different spanwise location of the slot in order to match the wake filling requirements at the correspondingly effected radial locations of the propeller inflow plane behind the empennage. This idea develops from the fact that wake deficit experienced at the propeller inflow is not uniform, but slightly lower at the root and the tip. This means a lower blowing coefficient can be employed in the regions of the slot influencing the root and tip of the propeller blade location behind the empennage, which will not only reduce the required mass flow rate but also provide a more radially uniform inflow profile.
  - Lastly, gaps can be introduced in the blowing slot surface so as not to have a continuous jet air requirement over the whole surface but have specified slots in the surface where air will be blown. These can be located at uniform or variable distance from each other based on the requirement, as long as they still provide the required mixing effect between the high momentum blown flow and the low momentum boundary layer.

Apart from the aforementioned recommendations for the blowing slot mechanism and BLI propeller integration into an aircraft, some suggestions can also be made on improving the CFD model and technique

used in this thesis. Although, the current CFD model yield seemingly successful results, investigation needs to be made on whether these results can be improved by employing some of the following recommendations for further analysis:

- A thorough mesh dependency study was conducted in the current research. Still, the meshing technique employed for the study can be improved. Some ways to achieve that are as follows:
  - The current mesh is pre-dominantly unstructured, apart form the surfaces and the blowing slot cavity of the empennage which were meshed structurally. Instead, a hybrid or completely structured mesh could be used to improve the computational efficiency. A structured mesh could be created using ICEM meshing. A hybrid mesh could be constructed which would be easier than the former since the hexahedral cells would be used in the outer domain volume whereas the mesh near geometry would still be unstructured.
  - The blowing slot cavity can be further refined to a point where a y^+ value of 1 could be used over the overall geometry without causing a large volume jump from the blowing slot mesh cells to the prism layer cells. This would improve the resolution of the boundary layer which could result in some changes in the wake profiles or even in the drag contributions of the blowing system.
  - Better techniques for improving the mesh near and downstream of the blowing slot should be investigated. It might also be beneficial to explore meshing software other than Ansys Mechanical or ICEM.
- Different transition turbulence models should also be investigated to analyse their effect on the predicted empennage boundary layer and wake.
- Lastly, other CFD software can be used if they prove to be more efficient for complex flows involving boundary layer and wake. Also, open source software like OpenFOAM could be used to reduce dependency on commercial software like Ansys Fluent.

A

MEAN AERODYNAMIC CHORD(MAC)

By definition, mean aerodynamic chord(MAC) is the average chord length of a tapered and swept wing, or for the current case, the empennage which consists of the vertical stabilizer.

The MAC is an important aerodynamic parameter which is commonly used in aerodynamic and stability calculations in aircraft design [88]. The magnitude of aerodynamic moment does not change with the change in the angle of attach of a typical low speed airfoil, like the NACA0010 used in the current study, when the aerodynamic force is applied over the quarter chord location from the leading edge. This location is generally referred to as the aerodynamic center(AC) of the airfoil. In case of a rectangular lifting surface, the AC for the whole wing is at the same 1/4 chord as the airfoil AC. However, if the wing planform changes to a trapezium, as in case of the VTP used in the current study, the AC has to be averaged over the whole planform to yield what is known as the MAC.
Since MAC can be assumed as an average chord of the of the lifting surface, a chord-weighted average formulation, as given in Equation A.1, can be used:

$$MAC = \frac{2}{3}\int_0^{b/2} c^2 dy \tag{A.1}$$

where, S is the surface area, b is the span, and c is chord length.

However, for a linearly tapered trapezoidal surface, as in the current case, Equation A.1 boils down to Equation A.2

$$MAC = \frac{2}{3} c_r \frac{1+\lambda+\lambda^2}{1+\lambda} \tag{A.2}$$

where , c_r is the root chord, λ is the taper ratio defines as $\frac{c_r}{C_t}$, c_t being the tip chord.

Now, to determine the span wise location of the MAC, a simple technique as described in Figure A.1 can be employed for linearly tapered swept wings. More precise formulas are available in the literature[88] and can be used in case of more complex planforms.

further understanding on the applications of MAC, reader is referred to US FAA Aircraft Weight and Balance Handbook[89]

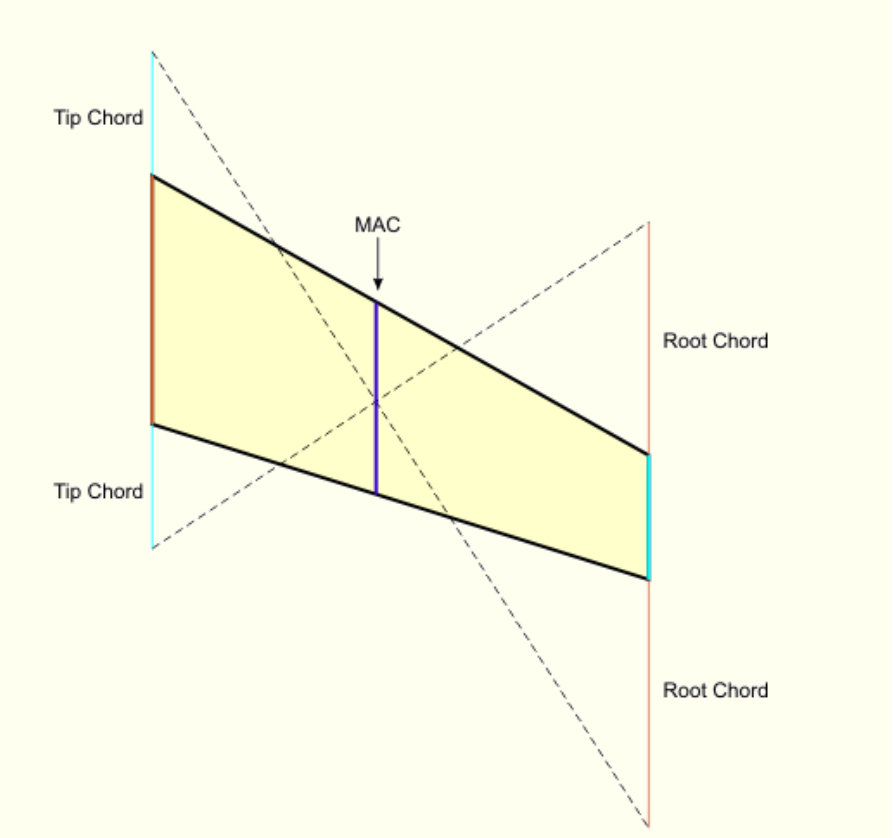

Figure A.1: Graphical representation of a method for approximating the spanwise location of the MAC[18]

B

Calculation for Fan Pressure Jump

The implementation of the fan using the fan boundary condition in fluent, needs a pressure jump formulation for it to work. For the case of this thesis, this pressure jump was assumed to be constant over the whole fan plane.

The initial in-house propeller considerations yielded a requirement of $8.2kN/m^2$ for the effective disk loading of the propeller in order to provide the required break away static thrust for an A320 like aircraft that would be the target range of aircraft for the APPU concept. The other relevant propeller parameters that the proposed APPU propulsor might have for the take-off condition are, RPM of the propeller which was taken to be 1500(=25rps) and the thrust coefficient(C_T) which was taken to be 0.58. The value of thrust coefficient is in the upper regime of typical propeller thrust coefficients[90, 91] but is not unheard off. The take-off velocity was taken as 79.831m/s corresponding to take-off Mach 0.23 found for A320[15]

The corresponding thrust can be obtained using Equation B.1

$$Thrust(T) = C_T \rho n^2 D^4 \tag{B.1}$$

where,
C_T is the thrust coefficient, ρ is the air density, n is the angular velocity of the propeller in rps and D is the propeller diameter.

The pressure jump across the fan disc can be given by Equation B.2

$$\Delta P = \frac{T}{A} \tag{B.2}$$

$$\Delta P = \frac{C_T \rho n^2 D^4}{A} \tag{B.3}$$

For a propeller diameter of 3.8m, the pressure jump across the propeller becomes:

$$\Delta P = \frac{0.58 \cdot 1.225 \cdot 25^2 \cdot 3.8^4}{\pi \cdot \frac{3.8^2}{4}} \tag{B.4}$$

$$\Delta P = 8194 N/m^2 = 8194 Pa \approx 8.2 kN/m^2 \tag{B.5}$$

C

TOP, FRONT AND SIDE VIEWS OF THE EMPENNAGE-FUSELAGE GEOMETRY

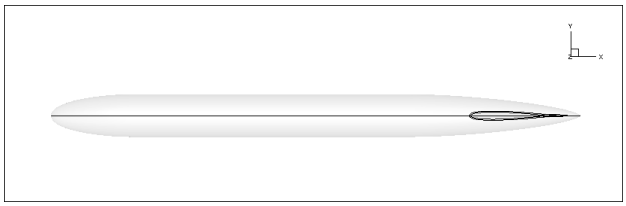

(a)

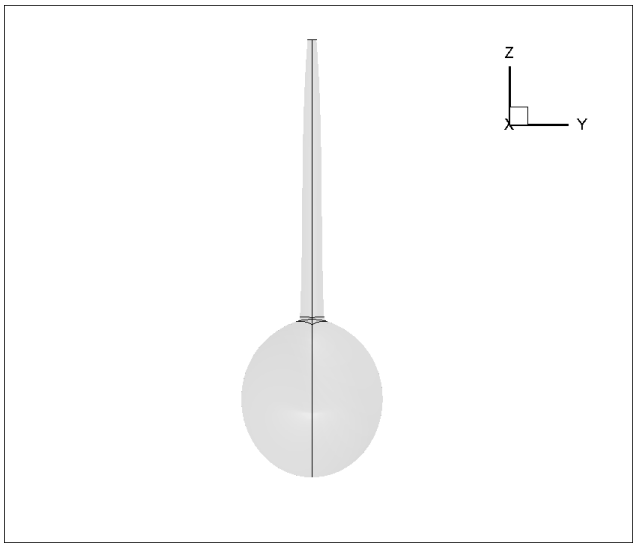

(b)

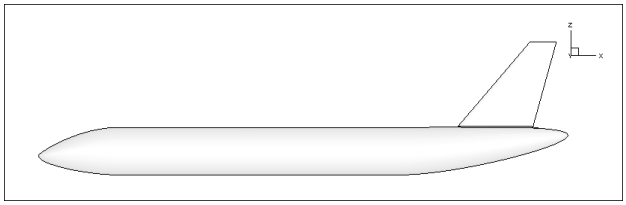

(c)

Figure C.1: (a)Top, (b)Front and (c)Side views of the final empennage-fuselage geometry used for the the mesh and the simulations

D

Additional Plots for Flow and Flow Properties

In this appendix, some additional flow visualisations and flow properties will be shown. Firstly, Figure D.1 shows the visualisation of the flow over the aircraft surfaces and the symmetry plane located at the geometry central cross section, in terms of streamlines.

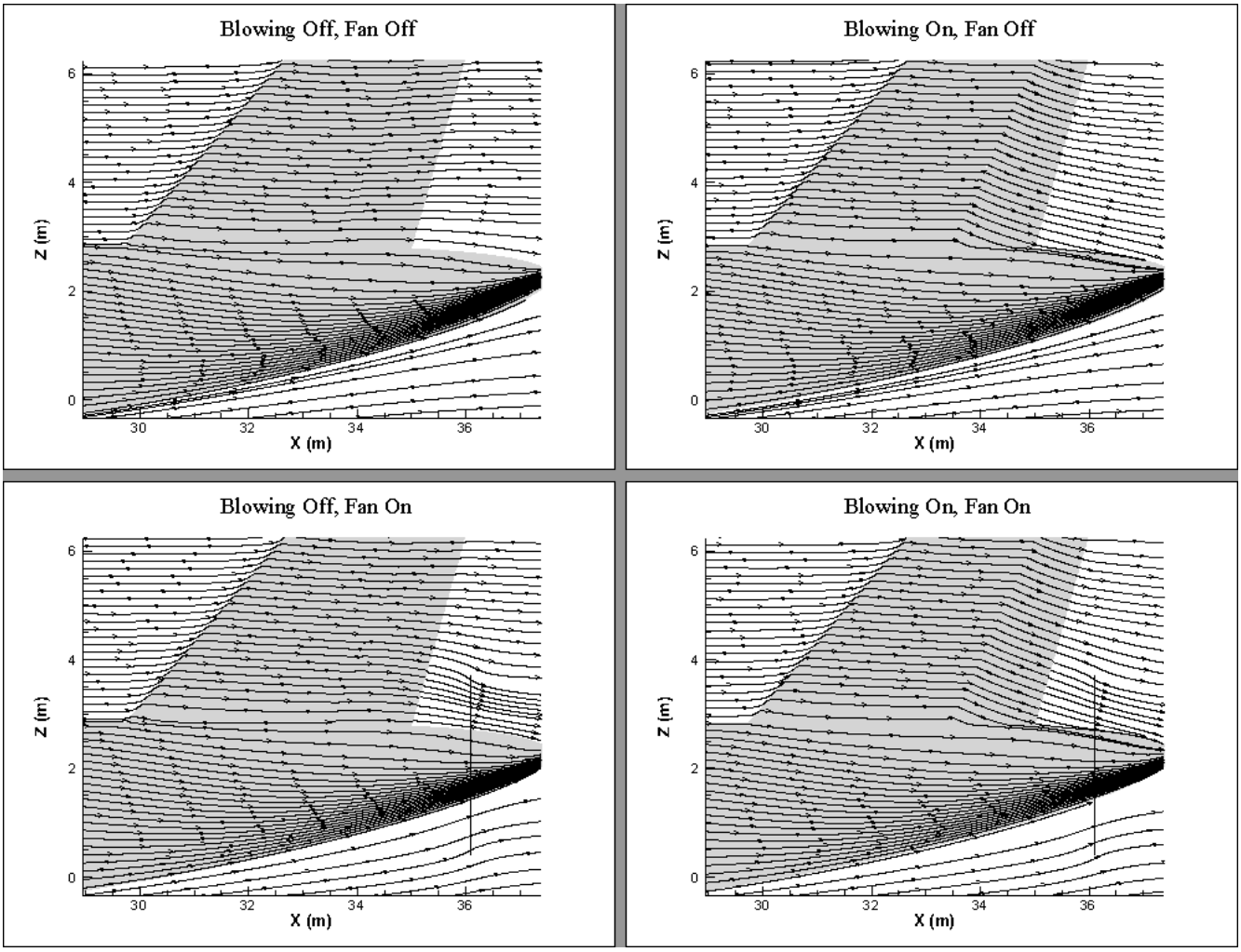

Figure D.1: Flow streamlines over the aircraft surfaces and the symmetry plane of the geometry for the blown and unblown cases for fan-off and fan-on configuration

This plot helps in understanding how the flow is effect by the blowing system and the fan. Since the jet flow at the blowing slot is directed perpendicular to the surface it can be seen that this leads to the flow being forced downwards towards the fuselage. It can be seen that this leads to the congestion of the streamlines on the upper fuselage surface behind the empennage. It is possible that this is a region where some vortices are present due to the high velocity jet blown flow interacting with the upper fuselage surface. Similarly, the streamlines also show the effect of the fan on the flow leaving the empennage. Due to the presence of the fan behind the empennage, the flow engulfed in the propeller streamtube can be seen to converge towards the propeller. Although this effect is less pronounced in the presence of the wake blowing system due to the flow already being directed in the direction of the propeller, some effect on the periphery of the propeller disk can still be seen.

Next, Figure D.2 shows the total pressure coefficient plots. The figure shows a more global effect of the wake blowing system and the propeller. The coefficient is calculated in the same manner as described in section 6.3. A value of 0 refers to a fully recovered total pressure value or, in other words, the total pressure has reached the freestream value. A value of -1 represents the case with full complete loss of total pressure. The total pressure behind the empennage in the blown cases is recovered to the freestream values as was expected. The jump in the total pressure coefficient across the fan disk is consistent with the pressure jump values prescribed in the fluent fan boundary condition. A similar contour plot for the velocity magnitude is shown in Figure D.3

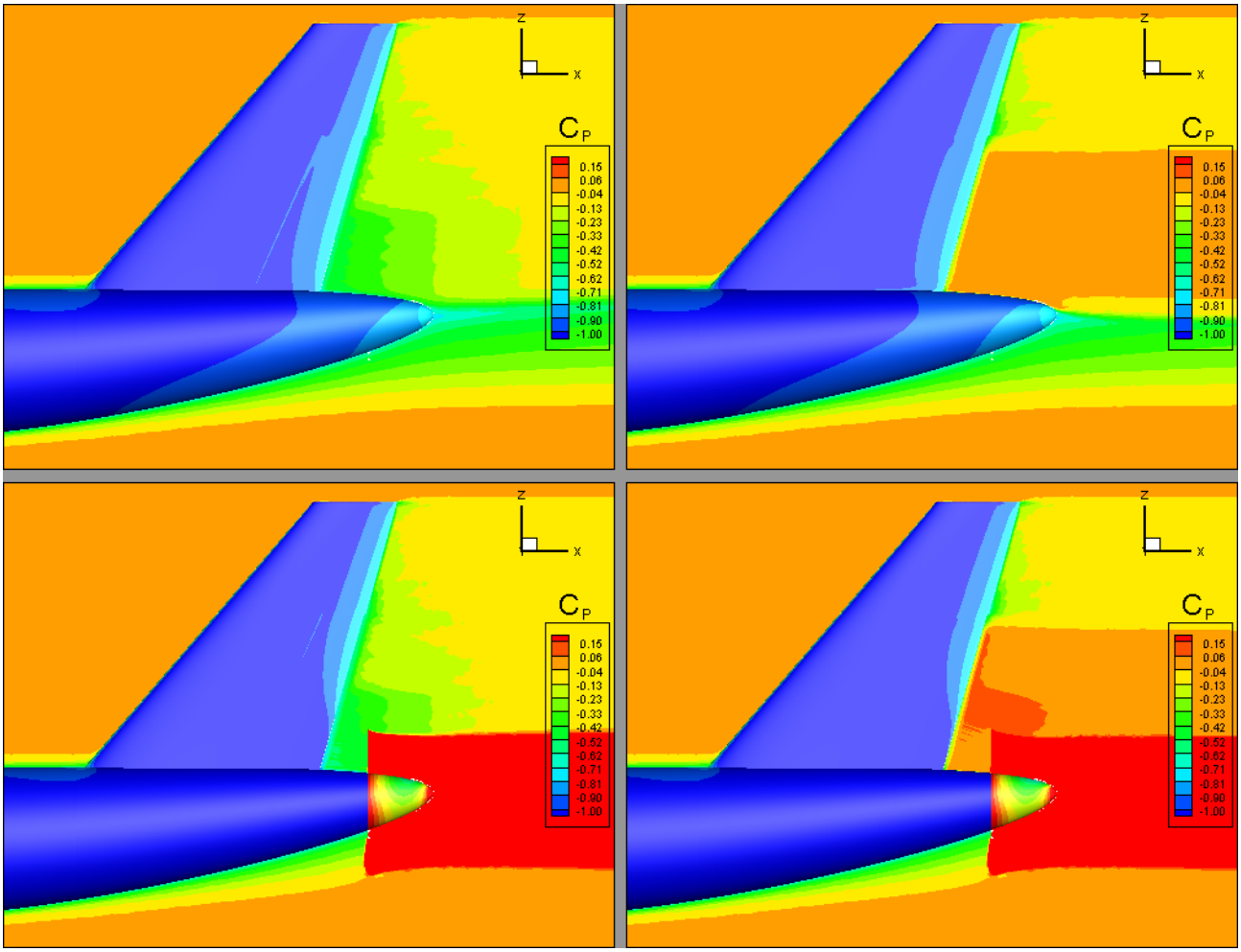

Figure D.2: Total pressure coefficient contours for the blown(Right) and unblown(left) cases for the fan-off(top) and fan-on(bottom) configurations

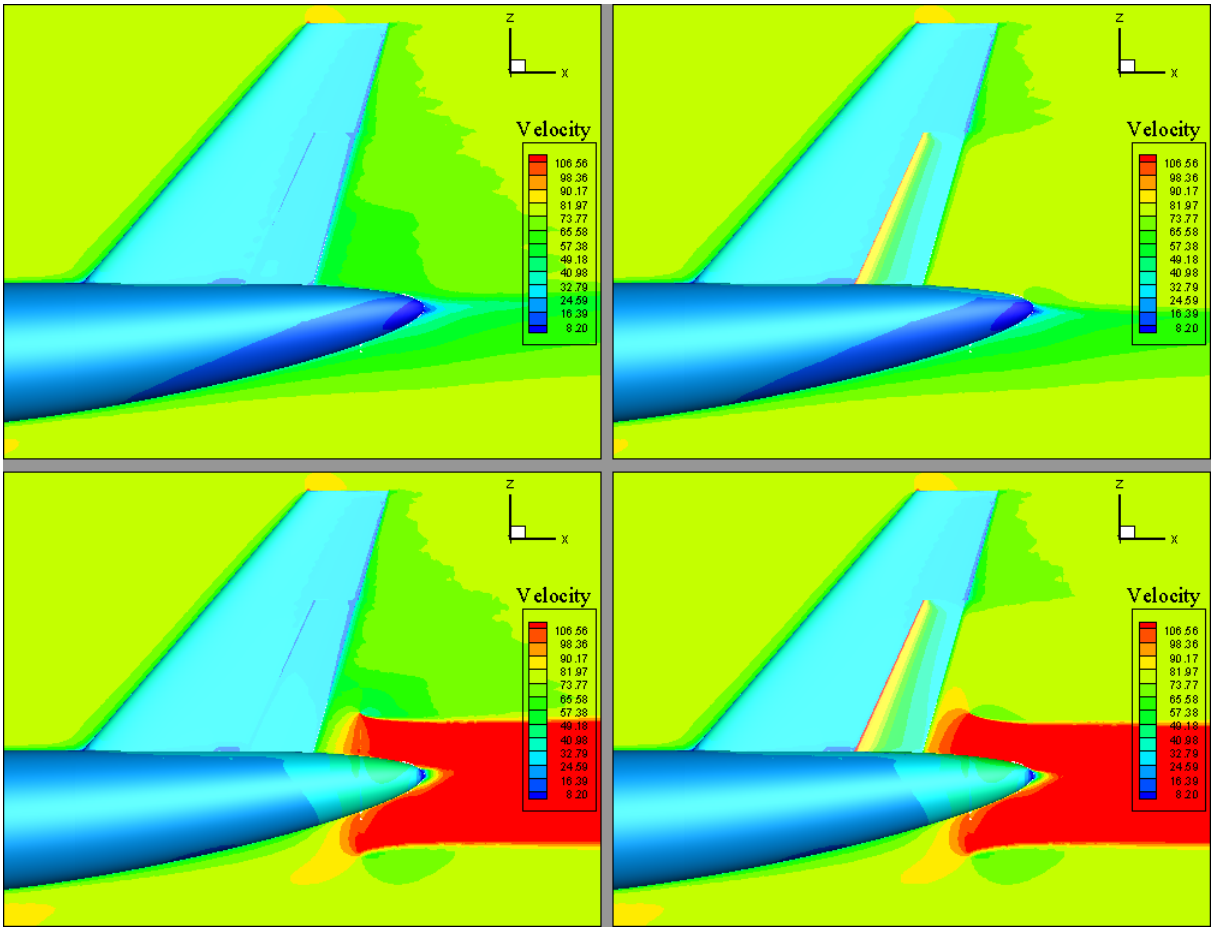

(a)

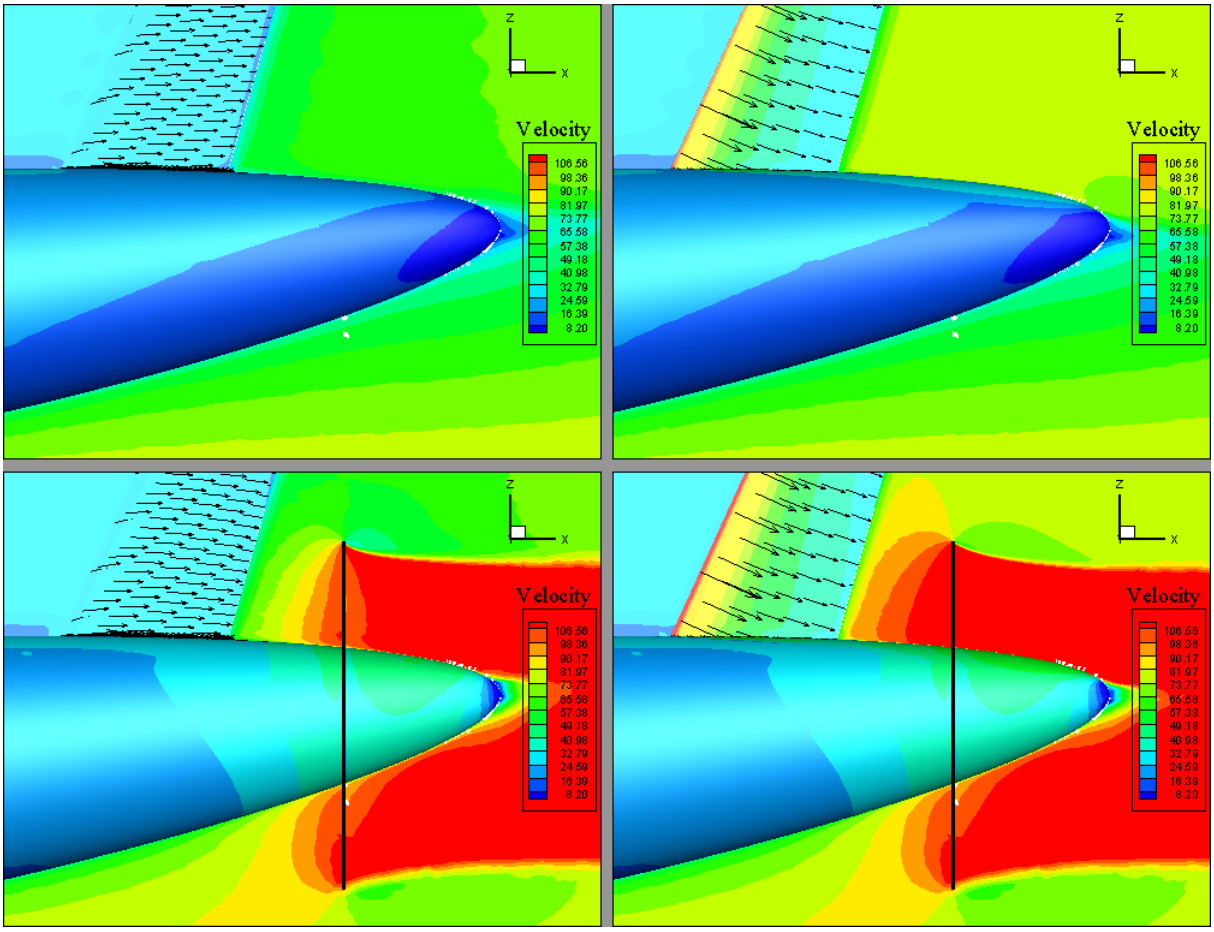

(b)

Figure D.3: Velocity magnitude contours for the blown(Right) and unblown(left) cases for the fan-off(top) and fan-on(bottom) configurations shown in a more (a)global and (b)zoomed in views

In Figure D.3, the first set of figures shows a more zoomed out view of the whole aft geometry, the second set of figures focuses on the blowing slot, empennage wake and the propeller inflow. Along with the velocity magnitude contours, the figures also show how the velocity vectors are influenced over the aft part of the empennage due to the presence of the added jet flow. The effect of the no-slip wall friction in reducing the flow speed of the jet air can be seen from the contours over the aft empennage. The suction effect of the fluent fan boundary condition is evident from the increased flow speeds in the propeller streamtube. Also, the combined effect of the wake blowing mechanism and the propeller suction effect can be seen in terms of an ever higher velocity of the in between the empennage trailing edge and the propeller in the blown fan-on case.

Figure D.3 shows the vortices in the flow using iso-surfaces of Lambda-2 criterion in the first two plots and of vorticity in the next two plots. Here, the definition for the lambda-2 criterion has been adopted form Jeong[92]. Lambda-2 criterion was developed in order to define the vortices that originate in a flow in terms of the eigenvalues of the symmetric tensor $S^2 + \Omega^2$; here S and Ω were defined as the symmetric and anti-symmetric parts of the velocity gradient tensor ∇u. It was shown that the criterion can capture the high Reynolds number flow in the low pressure regions in the plane that is perpendicular to the vortex axis. It is also able to define the vortex cores at low Reynolds number. However, it should be noted that the lambda-2 criterion was designed for incompressible flows. Therefore, iso-surface plots for the vorticity are also presented to support the observations made from these plots. In all four plots the iso-surfaces have been colored with the total pressure coefficient.

The horse shoe vortex can be seen to originate from the empennage-fuselage leading edge junction and progresses towards a location behind the empennage for the unblow fan-off cases. The effect of the addition of the propeller on this vortex is that it is reduced in size as can be seen from the two lambda-2 plots, plotted for a value of $-4.2s^{-2}$. For the case of with the addition of wake blowing for both the configurations, the horse shoe vortex encounters another vortex which stems from the interaction of the high speed jet flow with the fuselage surface. It is again evident that the propeller has a positive effect in reducing the magnitude of these vortices as well. Also, it can be seen that the vortical structures that stem due to the presence of the wake blowing mechanism, propagate to the fuselage tail cone end and detach from the surface.

Another observation is that the vortices that originate behind the empennage trailing edge line, are more prominent with the addition of the wake blowing system. This can be majorly attributed to the higher velocity jet flow which now leaves the empennage trailing edge.

The vorticity iso-surface plots complement these observations. The first iso plot is for a vorticity value of $83s^{-1}$ while the second one is for a value of $208s^{-1}$. The difference in magnitude between the two plots highlights the fact that the horse shoe vortex and the vortex due to the blowing system are less dominant when compared to the vortices that will stem from the edges of the propeller disk.

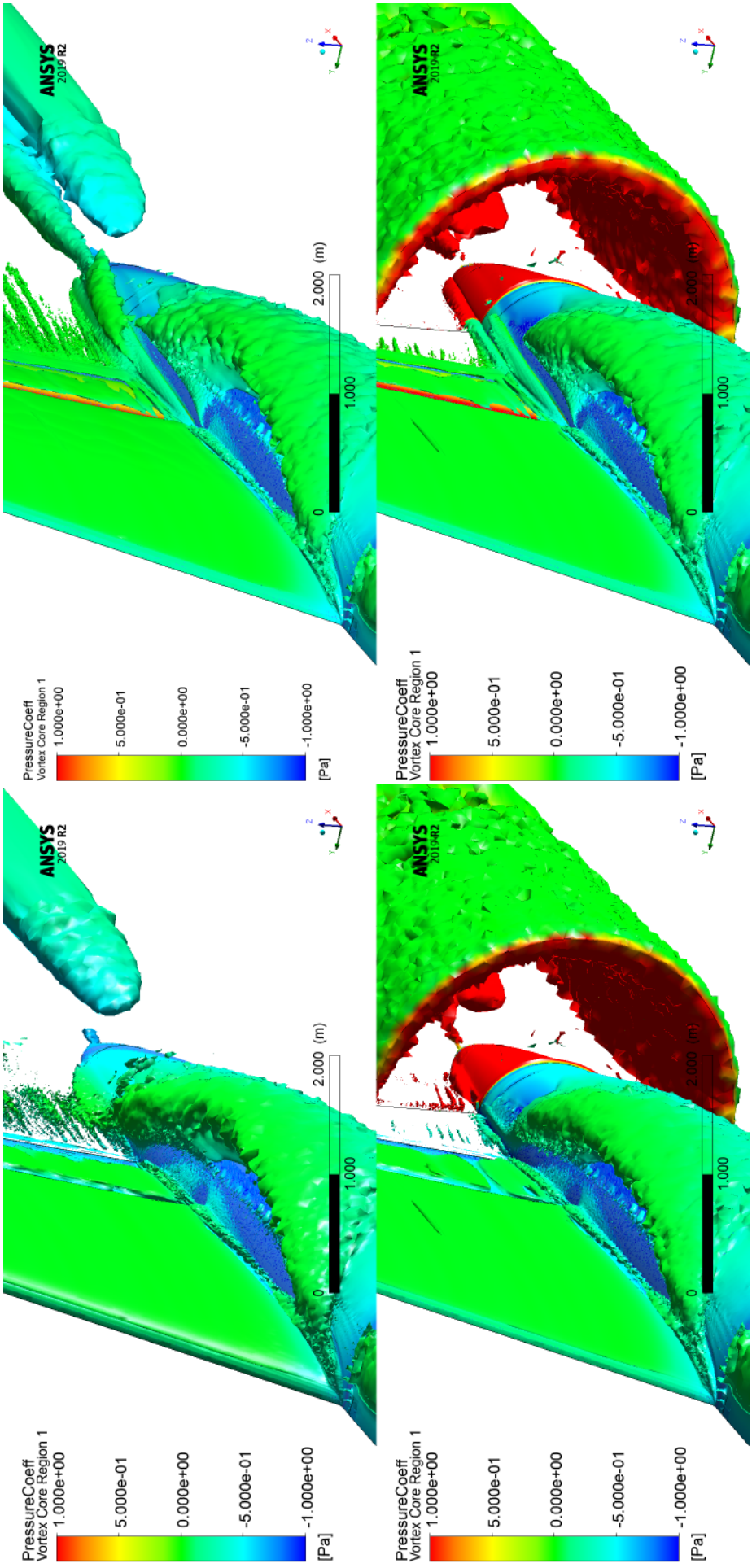

(a) Lambda 2 criterion - iso view

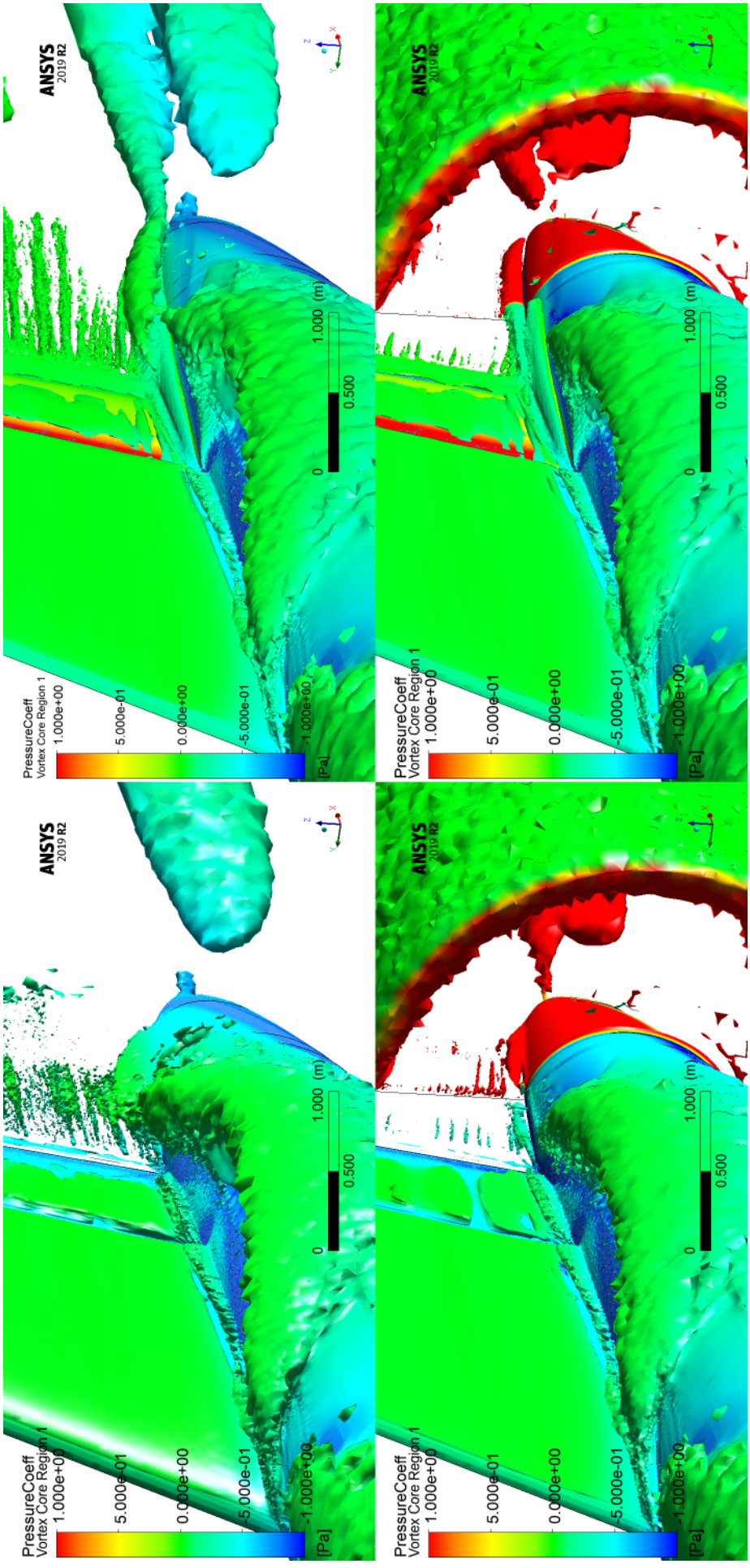

(b) Lambda 2 criterion - a more lateral view

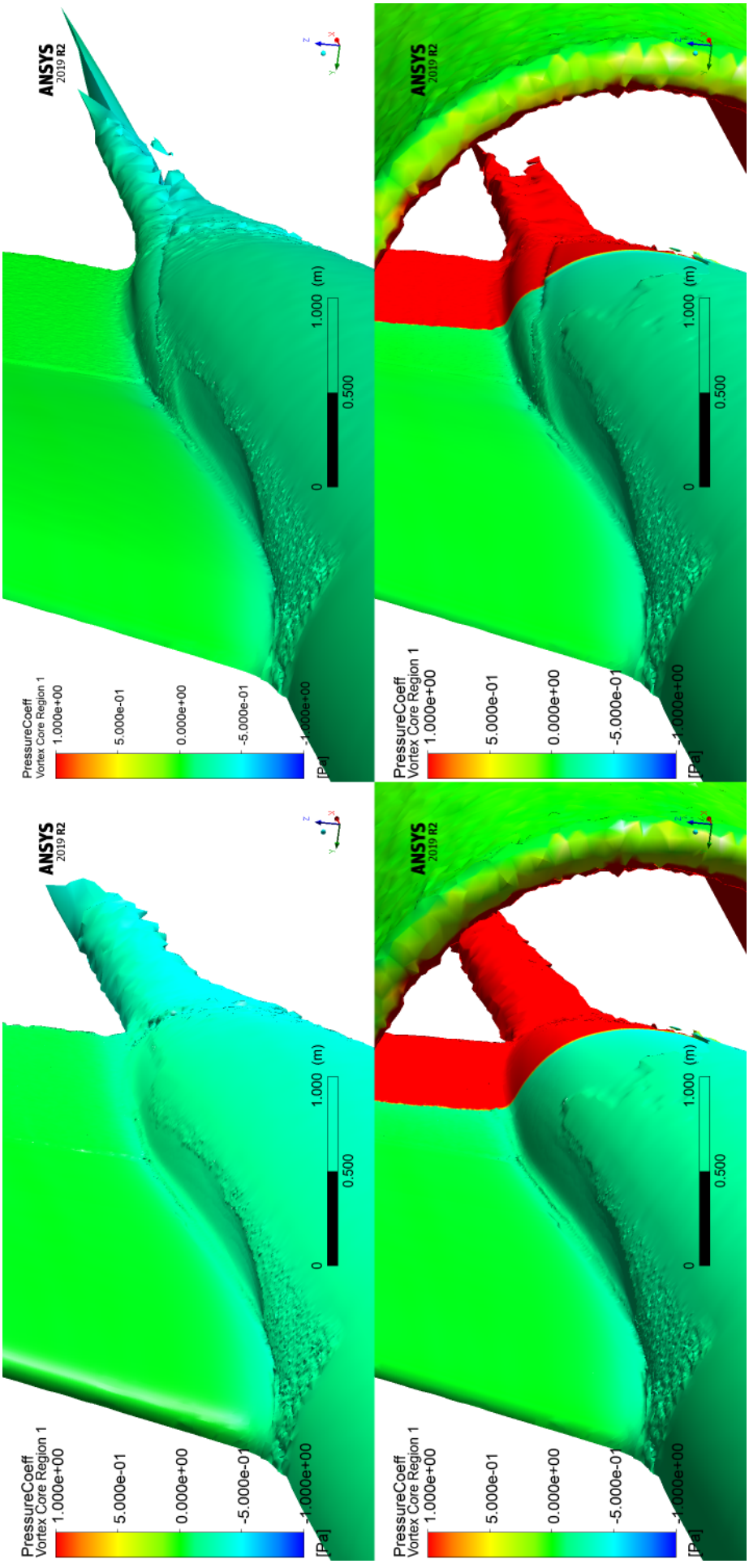

(c) Iso surface with vorticity magnitude of $83s^{-1}$

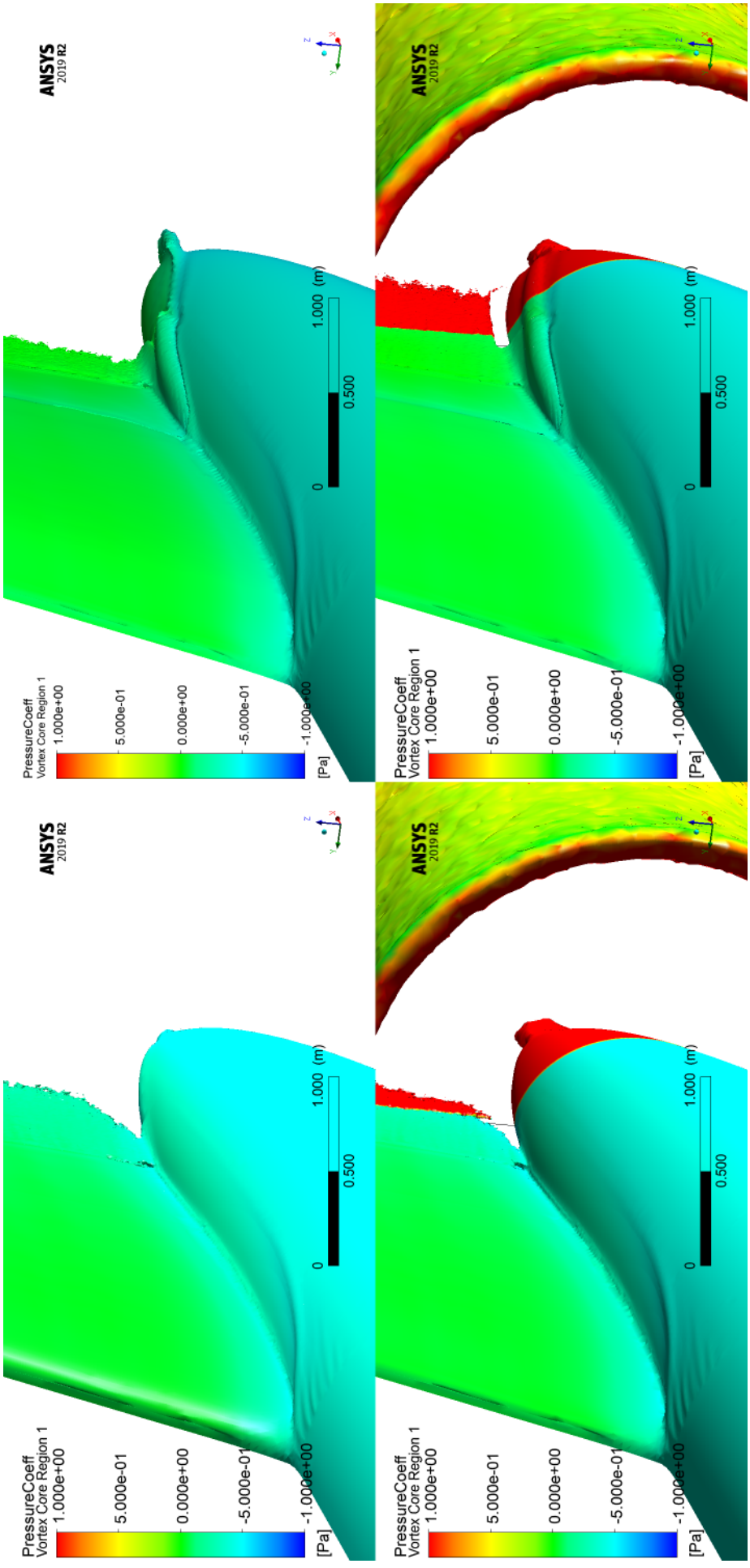

(d) Iso surface with vorticity magnitude of $208 s^{-1}$

Figure D.3: Lambda 2(a) and vorticity(b,c) iso surfaces depicting the vortices in the flow with the contours colored by pressure coefficient for the blown(Right) and unblown(left) cases for the fan-off(top) and fan-on(bottom) configurations in each figure.

Boundary Layer Plots

In this section a few empennage and fuselage plots are shown based on some preliminary post processing. All the plots have been taken for the most optimum blowing coefficient for the slot height of $h_{slot}/c = 0.001$

Figure D.4 shows the progression of the boundary layer over the empennage surface at a 0.75R radial location. Four chord-wise location, x/c = 0.6, 0.7, 0.8 and 0.9, were investigated for the unblown and blown cases of the fan-off and fan-on configurations. The increase in the boundary layer height with a higher chord-wise coordinate, is evident from the plots. The presence of the propeller reduces the boundary layer height, which was expected due to a larger pressure gradient in the boundary layer induces by the propeller. Also, the difference in the local velocities, to which the boundary layer velocities settle to, is also reduced. The effect of the wake blowing mechanism is also interesting. The effect on the blown jet flow over the empennage boundary layer can be seen in terms of the velocity overshoot for the x/c = 0.8 and 0.9 locations. It can also be observed that the overshoot is less in magnitude for x/c=0.9 because the flow losses its momentum as it progresses over the empennage surface and also because the high momentum jet flow has already started mixing with the boundary layer which can be seen from the reduction in the secondary minima when going from x/c=0.8(yellow line) to x/c=0.9(magenta line).

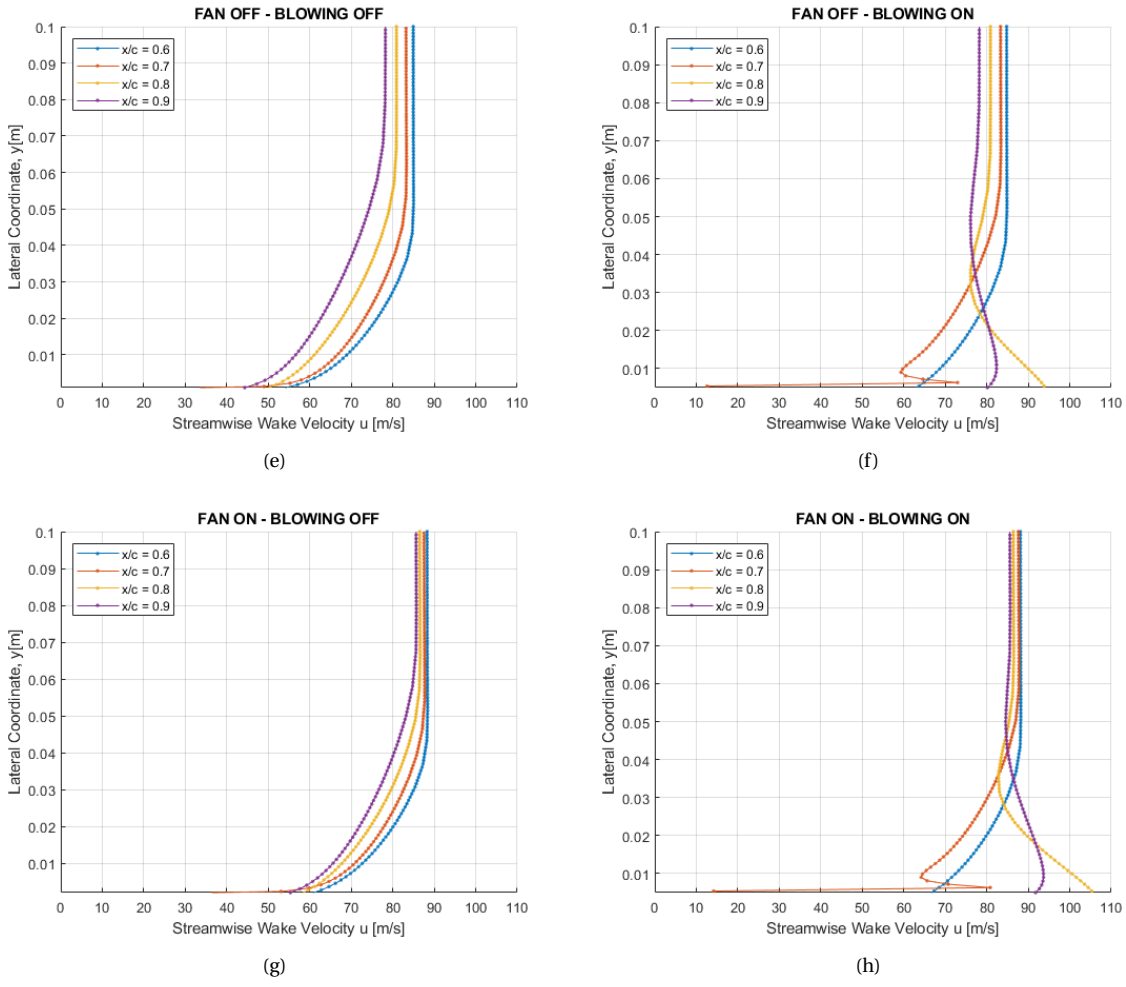

Figure D.4: Boundary layer development over the empennage at 0.75R radial location for different chord-wise locations for the blown(Right) and unblown(left) cases for the fan-off(top) and fan-on(bottom) configurations

It is clear that the blown flow does not have any effect of the boundary layer profile at the location x/c=0.6. The behaviour of the profile at the location x/c=0.7, needs explanation. It can be speculated that the blown flow speeds up the flow just upstream of the jet location due to a small shear induces pressure difference.

This is observed as a very sharp and small spike in the boundary layer very close to the surface.

Figure D.5 shows the boundary layer profiles for the 4 cases at a chord-wise location of 0.8c over the empennage surface in order to compare the effect of the wake blowing mechanism and the propeller on the boundary layer profile at a particular location. A shift in the boundary layer plots is observed due to the presence of the propeller as discussed for the boundary layer progression plots. It should be noted that the blown profiles show, not only the velocity overshoot due to the added high momentum flow, but also the secondary minima which persists, showing that the slot does not blow over the whole boundary layer. Another observation which can be made from these plots is that of the development of a new primary minima. Due to the no-slip empennage wall, the velocity of the flow is zero at the wall. This induces a gradient in the flow velocity adjacent to it which leads to the formation of the boundary layer. Now, even though the aft-empennage surface is blown, the velocity at the wall is still zero. This leads to the development of a new viscous sub-region which leads to the rise in the new primary minima.

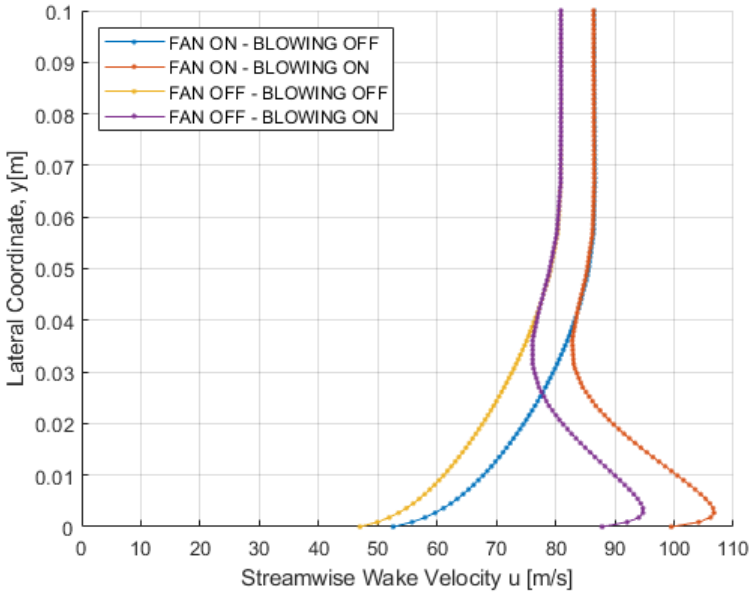

Figure D.5: Empennage Boundary layer comparison for for the blown and unblown cases for the fan-off and fan-on configurations at a single location downstream of the slot at 0.8c

Figure D.6 shows the boundary layer profiles over the fuselage surface at four locations between the empennage trailing edge junction and the propeller. Plots are shown for the unblown and blown cases for the fan-off and fan-on configurations. The axial locations x_1, x_2, x_3, x_4 are the same as described in chapter 7 but are normalised with vertical tail root chord. The lateral coordinate is normalised with the MAC like in the wake velocity plots.

The addition of the fan has an opposite effect as was observed for the empennage boundary profiles. The profiles for the fan-on configurations have a larger velocity jump between the profiles at progressing axial locations. This can be attributed to a more direct influence of the pressure gradient, due to the suction effect caused by the propeller disc, which becomes stronger towards the the propeller disk. The inclusion of the blowing mechanism has two effects. Firstly it reduces the mean velocity difference between the profiles and secondly, it has a flow straightening effect due to the addition of a span-wise addition of a high speed uniform velocity flow. This also reduces the effective fuselage boundary layer height. Figure D.7 shows the comparison for the BL profiles for the four cases at specified axial locations of 0.5m and 0.25m ahead of the propeller. One major observation is the reduction in BL height with the addition of the propeller. The BL at a location 0.25m ahead of the propeller reduces from around 12cm(y/c=0.025) to approximately, 4.8cm(y/c=0.01). These plots can be used to derive more precise BL height calculations for the empennage and fuselage BL, in future, as and when desired.

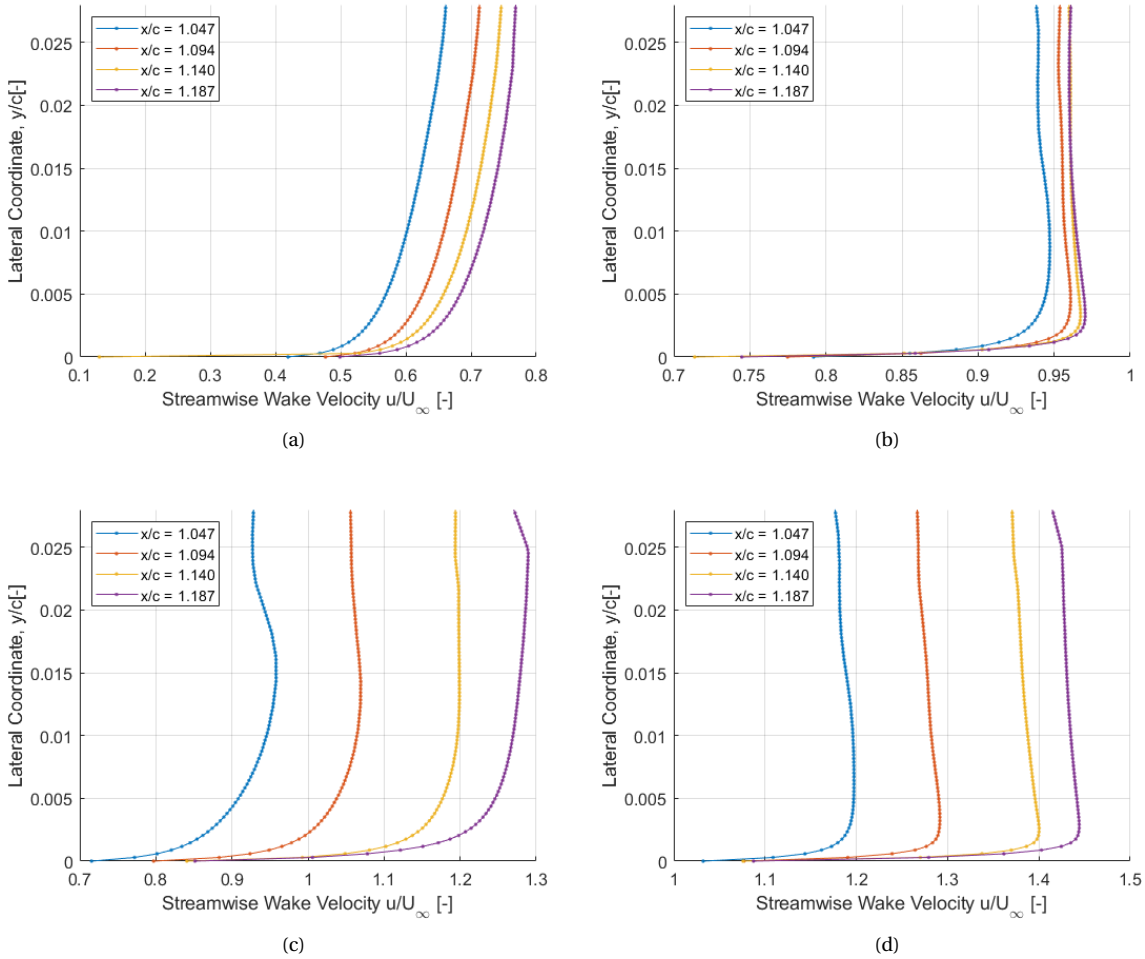

Figure D.6: Boundary layer development over the fuselage at different axial locations between the empennage-fuselage trailing edge junction and the propeller inflow plane for the blown(Right) and unblown(left) cases for the fan-off(top) and fan-on(bottom) configurations

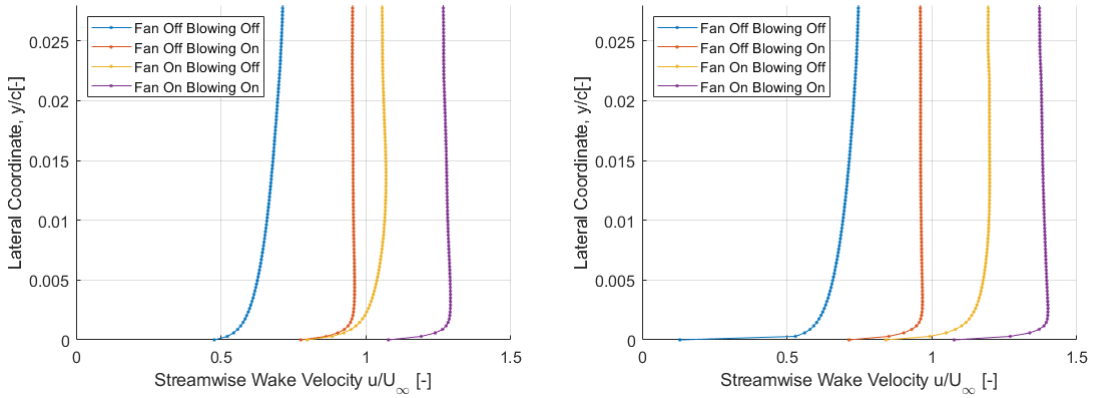

(a) Axial location 0.5m from empennage trailing edge junction(0.5m from propeller plane as well)

(b) Axial location 0.75m from empennage trailing edge junction(0.25m from propeller plane)

Figure D.7: Empennage Boundary layer comparison for for the blown and unblown cases for the fan-off and fan-on configurations at two axial locations between the empennage-fuselage trailing edge junction and the propeller plane

E

Code for Lift and Drag Coefficients based on Emperical Formulae

The calculations in the code are based on the emperical formulations from Torenbeek[80] and Raymer[81].

Description: The current program is designed to calculate the aircraft level lift and drag coefficient based on a basic set of inputs. Contributions from components such as wing, fuselage, empennage, nacelles and landing gear are included.

Prerequisites: The program requires python software and a corresponding compiler like PyCharm. An Anaconda environment is suggested for package management and deployment. Following python libraries need to be installed for the program to work: numpy, matplotlib and configparser.

Running the code: 1)Open "Input.txt" in the "Input" folder and assign the values to the parameters. More information on parameter description and input file format can be found in "InputFormatDescription.txt" 2)Open and run "Main.py" in the "SourceCode" folder.

Author Sparsh Garg

Main.py

```
import configparser
from AircraftModel import AircraftModel as AM
from Compare import *

def main():
    # Read the input files
    config = configparser.ConfigParser()
    config.read('..\Input\Input.txt')
    # Get sections from the input file
    config.sections()
    config2 = configparser.ConfigParser()
    config2.read('..\Input\Input2.txt')
    config2.sections()

    # Create instances of the parent class
    AM1 = AM(config)
    AM2 = AM(config2)

    # Write the output file
    AM1.write_output()
    print("Writing output file")

    # Plots comparing differnt models
    CL_compare(AM1,AM2)
```

```
    # Completion message
    print("Program completed")

# Improve robustness: Use os.chdir() to access all input.txt files and automate using a reading f

if __name__ == '__main__':
    main()
```

AIRCRAFTMODEL.PY

```
import configparser
import numpy as np
from matplotlib import pyplot as plt
from Wing import Wing
from Fuselage import Fuselage
from Empennage import Empennage
from Nacelles import Nacelles
from LandingGear import LandingGear as LG

class AircraftModel(object):
    # Parent class: instances initiated

    def __init__(self, config):
        # Extracting variable from input files
        # Config sections passed to corresponding classed and class objects are initiated
        self.wing = Wing(config['Wing'])
        self.fuselage = Fuselage(config['Fuselage'])
        self.empennage = Empennage(config['Empennage'])
        # Import required variables from global "Default" section
        self.Cfe = float(config['DEFAULT']['C_fe'])
        self.Sref = float(config['DEFAULT']['Sref'])

    # Function to calculate the aircraft level lift coefficient
    def LiftCoeff(self):
        # Call the 'calc' function of Wing class to get the lift curve slope
        self.CLalpha = self.wing.CLalpha_calc()
        # Calculate the CL at 0 AoA
        self.CL0aoa = self.CLalpha * -self.wing.Alpha0
        # Calculate CL
        self.CL = self.CLalpha*(self.wing.Alpha-self.wing.Alpha0)
        return self.CL

    # Function to plot and save CL vs AoA curve
    def CLCurve(self):
        # Get stall AoA
        self.AlphaMax= self.wing.alphamax()
        # Initiate lists to append aoa and CL values
        self.aoa = []
        self.CLlist = []
        for i in np.arange(int(self.wing.Alpha0)-1, self.AlphaMax+0.1):
            CL = self.CLalpha*(i-self.wing.Alpha0)
            self.aoa.append(i)
            self.CLlist.append(CL)
        CLplot = plt.figure(1)
        plt.plot(self.aoa,self.CLlist)
        plt.xlabel('Angle of Attack [deg]')
```

```
    plt.ylabel('Coefficient of Lift [-]')
    plt.grid()
    plt.axhline(0, color='black')
    plt.axvline(0, color='black')
    # plt.show()
    plt.savefig('..\Output\CLvsAoA.png')
    plt.close()
    # print(self.aoa,self.CLlist)


# Function to calculate the aircraft level drag coefficient
def DragCoeff(self):
    self.CD = self.wing.k*(self.LiftCoeff()**2) + self.CD0_cntr()
    # print(self.CD)
    return self.CD

# Function to plot and save CD vs AoA curve
def CDCurve(self):
    self.AlphaMax= self.wing.alphamax()
    self.aoa = []
    self.CDlist = []
    for i in np.arange(int(self.wing.Alpha0)-1, self.AlphaMax+0.1):
        CL = self.CLalpha*(i-self.wing.Alpha0)
        CD = self.wing.k * (CL ** 2) + self.CD0_cntr()
        self.aoa.append(i)
        self.CDlist.append(CD)
    CDplot = plt.figure(2)
    plt.plot(self.aoa,self.CDlist)
    plt.xlabel('Angle of Attack [deg]')
    plt.ylabel('Coefficient of Drag [-]')
    plt.grid()
    plt.axhline(0, color='black')
    plt.axvline(0, color='black')
    # plt.show()
    plt.savefig('..\Output\CDvsAoA.png')
    plt.close()
    # print(self.aoa,self.CDlist)


# Function to retrieve and add component contribution to CD0 to return the aircraft CD0
def CD0_cntr(self):
    # Retrieve wetted area of each component
    Sw_fuselage = self.fuselage.Sw_calc()
    Sw_wing = self.wing.Sw_calc()
    Sw_empennage = self.empennage.Sw_calc()
    Sw_nacelles = Nacelles().Sw_calc()
    Sw = Sw_fuselage+Sw_wing+Sw_empennage+Sw_nacelles
    # Calc. CD0 contribution of landing gear
    CD0_LG = LG().Sw_calc()/self.Sref
    # sum all the contributions
    self.CD0 = CD0_LG + self.Cfe*(Sw/self.Sref)
    return self.CD0

# Function to plot CL vs aoa for different models together and compare
def CLCurve_Comp(self,model):
    AlphaMax= self.wing.alphamax()
```

```
        CLalpha = self.wing.CLalpha_calc()
        aoa = []
        CLlist = []
        for i in np.arange(int(self.wing.Alpha0)-1, AlphaMax+0.1):
            CL = CLalpha*(i-self.wing.Alpha0)
            aoa.append(i)
            CLlist.append(CL)
        plt.plot(aoa,CLlist, label=model)


    # Function to write the output file
    def write_output(self):
        cl = self.LiftCoeff()
        self.CLCurve()
        cd = self.DragCoeff()
        self.CDCurve()
        outfile = open('..\Output\Output.txt', 'w')
        outfile.write('Parameter Values\n\n'+'CL_AOA0='+"\t"+str(self.CL0aoa)+'\n' + 'CL_Alpha='+
        outfile.write("------------------------------------------------------------------------
        outfile.write("\n\n{0:20},{1:20},{2:10}\n\n".format("CL", "CD", "AoA"))
        for (i,j,k) in zip(self.CLlist,self.CDlist,self.aoa):
            outfile.write("{0:20},{1:20},{2:10}\n".format(i,j,k))
        config = configparser.ConfigParser()
        config['DEFAULT'] = {'CL_AOA0': self.CL0aoa,'CL_Alpha': self.CLalpha,'CD0': self.CD0, 'Al
        config['CL, CD, AoA'] = {'CL': self.CLlist,'CD': self.CDlist, 'AoA': self.aoa}
        with open('..\Output\Output_cfg.txt', 'w') as configfile: config.write(configfile)



if __name__ == '__main__':
    import configparser
    # Make a stand alone script if needed
```

EMPENNAGE.PY

```
from numpy import *

class Empennage(object):
    # Child Class: Composition relation

    def __init__(self, input):
        # Extracting variable from corresponding input file section
        self.vt_sweep = float(input['vt_sweep'])
        self.vt_area = float(input['vt_area'])
        self.vt_span = float(input['vt_span'])
        self.vt_taper = float(input['vt_taper'])
        self.ht_sweep = float(input['ht_sweep'])
        self.ht_area = float(input['ht_area'])
        self.ht_span = float(input['ht_span'])
        self.ht_taper = float(input['ht_taper'])
        self.t_r = 0.14
        self.t_t = 0.08
        self.t_ratio = self.t_t / self.t_r
        # some variables are hard-coded

    # Function to calculate the wetted area for CD0 calculations
```

```
    def Sw_calc(self):
        Sw_vt = 2*self.vt_area*(1+(0.25*self.t_r)*((1+self.t_ratio*self.vt_taper)/(1+self.vt_taper)))
        Sw_ht = 2 * self.ht_area * (1 + (0.25 * self.t_r) * ((1 + self.t_ratio * self.ht_taper) / (1 +
        Sw = Sw_vt+Sw_ht
        return Sw


if __name__ == '__main__':
    import configparser
    # Make a stand alone script if needed
```

FUSELAGE.PY

```
from numpy import *

class Fuselage(object):
    # Child Class: Composition relation

    def __init__(self, input):
        # Extracting variable from corresponding input file section
        self.len = float(input['length'])
        self.dia = float(input['diameter'])

    # Function to calculate the wetted area for CD0 calculations
    def Sw_calc(self):
        self.FR = self.len/self.dia
        Sw = pi*self.len*self.dia*((1-(2/self.FR))**(2/3))*(1+(1/(self.FR**2)))
        return Sw


if __name__ == '__main__':
    import configparser
    # Make a stand alone script if needed
```

LANDINGGEAR.PY

```
from numpy import *

class LandingGear(object):
    # Aggregate Class

    def __init__(self):
        # Specify the required variables
        self.C_wheel = 0.25
        self.A_nosewheel = 0.5
        self.A_mainwheel = 0.6
        self.C_strut = 0.3
        self.A_strut = 3*0.32
        self.C_bogey = 1.2
        self.A_bogey = 0.18
        self.n_nose = 2
        self.n_main = 4
        self.n_strut = 3
        self.n_bogey = 22

    # Function to calculate the wetted area for CD0 calculations
    def Sw_calc(self):
```

```
        D = (self.n_nose*self.A_nosewheel*self.C_wheel)+(self.n_main*self.A_mainwheel*self.C_whee
        return D


if __name__ == '__main__':
    import configparser
    # Make a stand alone script if needed
```

NACELLES.PY

```
from numpy import *

class Nacelles(object):
    # Aggregate Class
    def __init__(self):
        # Specify the required variables
        self.Dn =2.3
        self.Dhl =1.6
        self.l1 =0.93
        self.ln =2.5
        self.lg =1.5
        self.lp =0.2
        self.Dp =0.5
        self.Deg =1.2
        self.Dg =1.9
        self.Def =2.1

    # Function to calculate the wetted area for CD0 calculations
    def Sw_calc(self):
        Sw_fancowl = self.ln*self.Dn*(2+(0.35*self.l1/self.ln)+(0.8*(self.l1/self.ln)*(self.Dhl/s
        Sw_gasgen = pi*self.lg*self.Dg*(1-((1/3)*(1-self.Deg/self.Dg)*(1-0.18*((self.Dg/self.lg)*
        Sw_plug = 0.7*pi*self.lp*self.Dp
        Sw = Sw_fancowl+Sw_gasgen+Sw_plug
        return Sw


if __name__ == '__main__':
    import configparser
    # Make a stand alone script if needed
```

WING.PY

```
from numpy import *


class Wing(object):
    # Child Class: Composition relation

    def __init__(self, input):
        # Extracting variable from corresponding input file section
        self.sweep = float(input['sweep'])
        self.area = float(input['area'])
        self.span = float(input['span'])
        self.e = float(input['e'])
        self.a = 0.1097
        self.Alpha0 = float(input['alpha0'])
        self.Alpha = float(input['alpha_guess'])
```

```
        self.AlphaMax = float(input['alpha_max'])
        self.taper = float(input['taper'])
        self.t_r = 0.14
        self.t_t = 0.08
        self.t_ratio = self.t_t/self.t_r
        self.AR = (self.span ** 2) / self.area
        self.k = 1 / (pi * self.AR * self.e)
        # some variables are hard-coded


    # Function to calculate the lift curve slope of the wing
    def CLalpha_calc(self):

        self.CLalpha = self.a / (1 + ((57.3 * self.a) / (pi * self.AR * self.e)))
        return self.CLalpha

    def alphamax(self):
        return self.AlphaMax

    # Function to calculate the wetted area for CD0 calculations
    def Sw_calc(self):
        S_exp = 5.9*3.95
        Sw = 2*S_exp*(1+(0.25*self.t_r)*((1+self.t_ratio*self.taper)/(1+self.taper)))
        return Sw




if __name__ == '__main__':
    import configparser
    # Make a stand alone script if needed
```

COMPARE.PY

```
from matplotlib import pyplot as plt
from AircraftModel import *

def CL_compare(AM1,AM2):
    # Function to plot CL vs AoA plots for different models

    plt.figure()
    plt.legend()
    AM1.CLCurve_Comp('Model1')
    AM2.CLCurve_Comp('Model2')
    plt.legend()
    plt.xlabel('Angle of Attack [deg]')
    plt.ylabel('Coefficient of Lift [-]')
    plt.grid()
    plt.axhline(0, color='black')
    plt.axvline(0, color='black')
    plt.savefig('..\Output\CLvsAoA_comp.png')
    plt.close()



# Add other comparision functions for eg. CD_compare() or DragPolar_compare()
```

INPUT.TXT

```
[DEFAULT]
e = 0.85
alpha_guess = 23
C_fe = 0.003
Sref = 122

[Wing]
sweep = 25
area = 122
span = 35
alpha0 = -1.2
alpha_max = 23
taper = 0.24

[Fuselage]
length = 37.57
diameter = 3.95

[Empennage]
vt_sweep = 34
vt_area = 21.5
vt_span = 6.2
vt_taper = 0.303
ht_sweep = 29
ht_area = 31
ht_span = 12.45
ht_taper = 0.256
```

OUTPUT.TXT

```
Parameter Values

CL_AOA0= 0.10664017156760984
CL_Alpha= 0.08886680963967487
CD0= 0.06737956235615397
Alpha= 23.0
CL_aircraft= 2.150576793280132
CD_aircraft= 0.23986993231602272
-----------------------------------------------------------------------------------------------------------

CL                   ,CD                   ,AoA

-0.07109344771173991, 0.06756806354591956,      -2.0
 0.01777336192793497, 0.06739134368051432,      -1.0
 0.10664017156760984, 0.06780369003312653,       0.0
 0.19550698120728474, 0.06880510260375619,       1.0
 0.28437379084695963,  0.0703955813924033,       2.0
  0.3732406004866345, 0.07257512639906785,       3.0
 0.46210741012630935, 0.07534373762374985,       4.0
  0.5509742197659843,  0.0787014150664493,       5.0
  0.6398410294056591, 0.08264815872716619,       6.0
  0.7287078390453339, 0.08718396860590052,       7.0
  0.8175746486850087, 0.09230884470265231,       8.0
  0.9064414583246837, 0.09802278701742155,       9.0
  0.9953082679643586, 0.10432579555020824,      10.0
```

```
1.0841750776040333, 0.11121787030101235,      11.0
1.1730418872437083, 0.11869901126983393,      12.0
1.2619086968833833, 0.12676921845667297,      13.0
 1.350775506523058, 0.13542849186152942,      14.0
 1.439642316162733, 0.14467683148440336,      15.0
1.5285091258024077, 0.15451423732529468,      16.0
1.6173759354420827,  0.1649407093842035,      17.0
1.7062427450817574, 0.17595624766112972,      18.0
1.7951095547214324, 0.18756085215607346,      19.0
1.8839763643611072, 0.19975452286903458,      20.0
1.9728431740007821,  0.2125372598000132,      21.0
 2.061709983640457, 0.22590906294900925,      22.0
 2.150576793280132, 0.23986993231602272,      23.0
```

BIBLIOGRAPHY

[1] The CleanEra Team, *Cleanera: a collection of research projects for sustainable aviation,* IOS Press (2015).

[2] G. A. C. (DLR) and the Georgia Institute of Technology, *Iata technological roadmap,* IATA (4th edition, 2013).

[3] *Advanced Propulsion and Power Unit(APPU) website,* (2019), https://www.tudelft.nl/lr/appu.

[4] S. A. Pandya, A. Uranga, A. Espitia, , and A. Huang, *Boundary layer ingestion benefit of the d8 transport aircraft,* 52nd Aerospace Sciences Meeting, AIAA, Maryland **2014-0907** (2014).

[5] B. Mccormick, S. Aljabri, S. Jumper, and Z. Martinovic, *The analysis of propellers including interaction effects,* (1979), 10.4271/790576.

[6] P. Lv and A. Gangoli Rao, *Conceptual analysis of boundary layer ingestion towards aircraft propulsion integration,* (2013).

[7] C. Soares, *10 - performance, performance testing, and performance optimization,* in *Gas Turbines*, edited by C. Soares (Butterworth-Heinemann, Burlington, 2008) pp. 387–470.

[8] J. Ricouard, E. Julliard, M. Omais, V. Regnier, S. Baralon, and A. Parry, *Installation effects on contra-rotating open rotor noise.* 16th AIAA/CEAS Aeroacoustics Conference, Stockholm, Sweden (2010).

[9] T. Sinnige and L. Veldhuis, *Pylon trailing edge blowing effects on the performance and noise production of a pusher propeller.* 52nd Aerospace Sciences Meeting, AIAA SciTech, National harbor, Maryland, USA (2014).

[10] D. Ragniz, G. Eitelberg, T. Sinnige, K. Lynchy, and L. Veldhuis, *Aerodynamic and aeroacoustic effects of pylon trailing edge blowing on pusher propeller installation.* 21st AIAA/CEAS Aeroacoustics Conference, Dallas, TX (2015).

[11] E. B. Jr., J. G.L. Gentry, and M. Takallu, *Effect of pylon wake with and without pylon blowing on propeller thrust.* NASA Technical Memorandum (NASA-TM-4162) (1990).

[12] T. Sinnige, *The effects of pylon blowing on pusher propeller performance and noise emissions,* MSc Thesis, Faculty of Aerospace Engineering, Delft University of Technology (2013).

[13] A. Chelius, N. Nasr, B. Rodriguez, and S. Canard-Caruana, *Blowing strategies of pylon- propeller configuration for noise reduction using numerical approach.* 6th AIAA Flow Control Conference, New Orleans, LA, USA (2012).

[14] A. Jindal, T. Sinnige, S. J. Hulshoff, and L. L. M. Veldhuis, *Numerical analysis of pylon-blowing systems for pusher-propeller applications,* 35th AIAA Applied Aerodynamics Conference (2017).

[15] AIRBUS, *Aircraft characteristics airport and maintenance planning,* Technical Data Support and Services **Rev. 2020** (1985), https://www.airbus.com/sites/g/files/jlcbta136/files/2021-11/Airbus-Commercial-Aircraft-AC-A320.pdf.

[16] A. Jindal, *Pylon wake control using steady blowing: A numerical study,* MSc Thesis, Faculty of Aerospace Engineering, Delft University of Technology (2016).

[17] F. White, *Fluid Mechanics*, McGraw-Hill series in mechanical engineering (McGraw Hill, 2011).

[18] P. Sforza, *Commercial Airplane Design Principles* (Butterworth-Heinemann, Boston, 2014) pp. 119–212.

[19] P. S. Lloyd Jenkinson and D. Rhodes, *Civil jet aircraft design database,* AIAA Educational Series (1999), https://doi.org/10.2514/4.473500.

[20] B. Owen and D. Lee, *Aviation emissions,* Encyclopaedia of Aerospace Engg., John Wiley & Sons (2010).

[21] *Cop26 goals - un climate change conference uk 2021,* (Accessed November 2021), https://ukcop26.org/cop26-goals/.

[22] *Paris agreement to the united nations framework convention on climate change,* T.I.A.S. No. 16-1104 (2015).

[23] ACARE, *Advisory council for aviation research and innovation in europe website,* (Accessed on October 2020), https://www.acare4europe.org/.

[24] H. M. Clyde, *Wind-tunnel test of a 1/20-scale airship model with stern propellers.* Technical report, National Aeronautics and Space Administration, Virginia (1962).

[25] A. Plas, *Performance of a boundary layer ingesting propulsion system.* PhD thesis, Massachusetts Institute of Technology (2006).

[26] L. Smith, *Wake ingestion propulsion benefit,* 27th AIAA/SAE/ASME/ASEE Jt. Propulsion Conference , 11 (1991).

[27] *An energy mix combined with a novel engine concept to make aviation much more sustainable,* (2020), https://www.tudelft.nl/en/2020/lr/an-energy-mix-combined-with-a-novel-engine-concept-to-make-aviation-much-more-sustainable/gid=1pid=1.

[28] B. Shivashankara, D. Johnson, and R. Cuthbertson, *Installation effects on counter rotating propeller noise.* 13th AIAA Aeroacoustics Conference, Tallahassee, FL, USA (1990).

[29] M. Omas, J. Ricouard, E. Julliard, and V. Regnier, *Installation effects on contra-rotating open rotor noise.* 16th AIAA/CEAS Aeroacoustics Conference (AIAA 2010-3795), Stockholm, Sweden (2010).

[30] A. Stuermer and J. Yin, *Aerodynamic and aeroacoustic installation effects for pusher-configuration cror propulsion systems.* 28th AIAA Applied Aerodynamics Conference (AIAA-2010-4235), Chicago, Illinois, USA (2010), https://doi.org/10.2514/6.2010-4235.

[31] N. Peake and A. B. Parry, *Modern challenges facing turbomachinery aeroacoustics.* Annual Review of Fluid Mechanics **44(No.:1)**, 227 (2012).

[32] P. Block, *Experimental study of the effects of installation on single- and counter-rotation propeller noise,* NASA-TP-2541 (1986).

[33] P. Block, *Pusher propeller noise directivity and trends.* 10th AIAA Aeroacoustics Conference, Seattle, WA, USA (1986).

[34] D. Elliott, *Initial investigations of the acoustics of a counter-rotating open rotor model with historical baseline blades in a low-speed wind tunnel,* NASA-TM-2012-217258 (2012).

[35] S. Funke, L. Kim, , and H. Siller, *Microphone-array measurements of a model scale contra-rotating open rotor in a reverberant open wind-tunnel.* 17th AIAA/CEAS Aeroacoustics Conference (32nd AIAA Aeroacoustics Conference), Portland, OR, USA, (2011).

[36] A. Breeze, T. Wood, K. Ramakrishnan, U. Paliath, J. Wojno, T. Goerig, A. Opalski, S. A. Khalid, D. Lurie, and J. Barrett5, *Faa cleen program open rotor aeroacoustic technology non-proprietary report,* DOT/FAA/AEE/2014-03 [Accessed 14 July 2020].

[37] P. Bevilaqua and C. Yam, *Propulsive efficiency of wake ingestion,* Journal of Propulsion and Power **36**, 1 (2020), https://doi.org/10.2514/1.B37695.

[38] N. Cumpsty and A. Heyes, *Selection of Fan Pressure Ratio, Specific Thrust and Bypass Ratio* (2018) pp. 82–98.

[39] G. Wislicenus and L. Smith, *Hydraulic Jet Propulsion and Incipient Cavitation,* Tech. Rep. (Internal Flow Research Report 1-6, Part A, Johns Hopkins C. Mcrlr. Eng. Dept, 1952).

[40] G. F. Wislicenus, *Hydrodynamics and propulsion of submerged bodies,* ARS Journal **30**, 1140 (1960).

[41] W. S. Gearhart and R. E. Henderson, *Selection of a propulsor for a submersible system,* Journal of Aircraft **3**, 84 (1966).

[42] E. P. Bruce, W. Gearhart, J. Ross, and A. Treaster, *The design of pumpjets for hydrodynamic propulsion,* Fluid Mech., Acoustics, and Design of Turbomachinery, Pt. 2 (1974).

[43] A. Betz, *Introduction to the theory of flow machines.* Pergamon Press (1966).

[44] M. Drela, *Power balance in aerodynamic flows.* 27th AIAA Applied Aerodynamics Conference, San Antonio (2009).

[45] W. Douglass, *Propulsive efficiency with boundary-layer ingestion,* McDonnell Douglas Report **1600**, J0860 (1970).

[46] R. T. Kawai, D. M. Friedman, and L. Serrano, *Blended wing body (bwb) boundary layer ingestion (bli) inlet configuration and system studies,* (2006).

[47] L. W. Hardin, G. T. amd O. P. Sharma, and N. Glenn, *Aircraft system study of boundary layer ingesting propulsion,* (2012).

[48] A. Uranga, M. Drela, E. M. Greitzer, N. A. Titchener, M. K. Lieu, N. M. Siu, A. C.Huang, G. M. Gatlin, J. A. Hannon, , and N. Langley, *Preliminary experimental assessment of the boundary layer ingestion benefit for the d8 aircraft,* , 1–25 (2014).

[49] T. Hartuc., *Boundary layer ingestion theoretical and experimental research.* MSc Thesis, Delft University of Technology (2015).

[50] B. Blumenthal, M. Maughmer, and S. Schmitz, *Computational investigation of a boundary-layer-ingestion propulsion system,* Journal of Aircraft **Vol. 55, No. 3** (2018).

[51] C. Rohrback and F. Metzer, *The prop-fan - a new look in propulsors.* 11th AIAA/SAE Propulsion Conference, Anaheim, CA, USA (1975).

[52] M. Bowels and V. Dawson, *The advanced turboprop project: Radical innovation in a conservative environment.* Engineering Science to Bid Science: The NACA and NASA Collier Trophy Research Project Winners. Washington, D.C.: National Aeronautics and Space Administration (1998).

[53] *Toward future flight,* Spinoff magazine, NASA , pp.30 (1987).

[54] S. Lauret, *Safran and'green engines'-the future of civil aviation,* Vayu Aerospace and Defence Review , 120 (2015).

[55] P. Lv, A. G. Rao, D. Ragni, and L. Veldhuis, *Performance analysis of boundary layer ingestion for aircraft design,* Journal of Aircraft **Volume 53, issue 5**, 1517 (2016).

[56] O. Sitges, *Cfd analysis of a blowing pylon system for the apian propeller in pusher configuration.* 5th CESA Air and Space Conference , 156 (2015).

[57] Ansys, *Ansys Fluent 2019R3,* (2019), commertial Software.

[58] NASA, *Open VSP ,* (2012), open-source parametric aircraft geometry design tool, http://openvsp.org.

[59] Dassault Systems, *Catia-V5,* (2019), CAD Software, http://www.3ds.com.

[60] M. van Sluis and B. DellaCorte, *Final pfc aircraft aerodynamic design and performance,* Centreline **D3.03** (2020).

[61] G. A. . H. M. Habermann, A.L., *Numerical investigation of the effects of fuselage upsweep in a propulsive fuselage concept.* CEAS Aeronaut J **12**, 173–189 (2021).

[62] H. Versteeg and W. Malalasekera, *An introduction to computational fluid dynamics - the finite volumemethod,* Pearson Education Limited, 2nd edition (2007).

[63] J. D. Anderson, *Fundamentals of aerodynamics* (1985).

[64] J. Wendt, J. Jr, J. Degroote, G. Degrez, E. Dick, R. Grundmann, and J. Vierendeels, *Computational Fluid Dynamics: An Introduction* (2009) pp. 1–332.

[65] P. Wang and X.-S. Bai, *Large eddy simulation of turbulent premixed flames using level-set g-equation,* Proceedings of the Combustion Institute **30**, 583 (2005).

[66] H. Andersson and M. Lygren., *Les of open rotor-stator flow.* International Journal of Heat and Fluid Flow **27(4):551557** (2006).

[67] L. Davidson, *Fluid mechanics, turbulent flow and turbulence modeling.* Lecture notes, Chalmers University of Technology (2014).

[68] O. Reynolds, *On the dynamical theory of incompressible viscous fluids and the determination of the criterion,* Philosophical Transactions of the Royal Society of London **186**, 123 (1895).

[69] M. van Sluis, *A numerical investigation into the aerodynamic characteristics of aerocity,* MSc Thesis, Faculty of Aerospace Engineering, Delft University of Technology (2017).

[70] J. Boussinesq, *Essai sur la theorie des eaux courantes,* Mèmoires présèntes par divers savants a l'Acádemie des Sciences **23**, 1 (1877).

[71] P. Spalart and S. Allmaras, *A one-equation turbulence model for aerodynamic flows,* AIAA **AIAA-92-0439** (January 1992).

[72] Ansys, *Fluent theory guide,* **R3**, Sec. 4.2 (Rev. 2019).

[73] S. C. J. Dacles-Mariani, G.G. Zilliac and P. Bradshaw, *Numerical/experimental study of a wingtip vortex in the near field,* AIAA Journal **33(9)**, 1561 (1995).

[74] W. K. Anderson and D. L. Bonhaus, *An implicit upwind algorithm for computing turbulent flows on unstructured grids,* Computers & Fluids **23**, 1 (1994).

[75] Ansys, *Spaceclaim documentation, ansys help 19.1,* **R3** (Rev. 2019).

[76] Ansys, *Mechanical user's guide,* **R3** (Rev. 2019).

[77] *CFD Online Y+ Estimation Tool,* http://www.cfd-online.com/Tools/yplus.php.

[78] M. Drela, *Xfoil,* (2013), open-source Software.

[79] J. Sun, J. Hoekstra, and J. Ellerbroek, *Aircraft drag polar estimation based on a stochastic hierarchical model,* (2018).

[80] E. Torenbeek, *Synthesis of subsonic airplane design,* (1982), 10.1007/978-94-017-3202-4.

[81] D. Raymer, *Aircraft design: A conceptual approach, sixth edition,* (2018).

[82] V. Kornilov, *Combined blowing/suction flow control on low-speed airfoils,* Flow, Turbulence and Combustion **106** (2021), 10.1007/s10494-020-00157-7.

[83] EASA, *Cfm international cfm56-2/3, easa type-certificate data sheet,* (2008), https://www.easa.europa.eu/downloads/7691/en.

[84] A. Evans, *The effects of compressor seventh-stage bleed air extraction on performance of the f100-pw-220 afterburning turbofan engine,* (1991).

[85] A. Yuhas and R. Ray, *Effects of bleed air extraction of thrust levels on the f404-ge-400 turbofan engine,* (1992), 10.2514/6.1992-3092.

[86] R. Slingerland and S. Zandstra, *Bleed air versus electric power off-takes from a turbofan gas turbine over the flight cycle,* (2007), 10.2514/6.2007-7848.

[87] J. Mattingly and W. Heiser, *Performance estimation of the mixed flow, afterburning, cooled, two-spool turbofan engine with bleed and power extraction,* (1986), 10.2514/6.1986-1757.

[88] T. Vogeltanz, *Application for calculation of mean aerodynamic chord of arbitrary wing planform.* AIP Conference Proceedings 1738, 120018 (2016), https://doi.org/10.1063/1.4951901.

[89] J. Duncan, *Aircraft Weight and Balance Handbook* (Oklahoma: US Department of Transporation, 2007).

[90] B. McCormick, S. Aljabri, S. Jumper, and Z. Martinovic, *The analysis of propellers including interaction effects,* (1979), 10.4271/790576.

[91] T. Sinnige, T. Stokkermans, N. van Arnhem, and L. Veldhuis, *Aerodynamic performance of a wingtip-mounted tractor propeller configuration in windmilling and energy-harvesting conditions,* (2019), 10.2514/6.2019-3033.

[92] J. Jeong and F. Hussain, *On the identification of a vortex,* J. Fluid Mech. **332**, 339 (1995).